Future Changes in Convective Precipitation and Severe Weather Environment in Western Canada and the Central U.S. Plains

by

Jennifer Bruneau

A Thesis submitted to the Faculty of Graduate Studies of the University of Manitoba in partial fulfillment of the requirements of the degree of

MASTER OF SCIENCE

Department of Environment and Geography

University of Manitoba

Winnipeg

Abstract

Thunderstorms are a common atmospheric phenomenon in North America that may yield extreme weather like hail, tornadoes, heavy rain, and lightning and can thus have significant societal and economic impacts. As global mean surface temperature has increased, regional climate models (RCMs) have been used to examine the relationship between thunderstorms and global climate change. This thesis examined this relationship using precipitation and severe weather parameter data from three model pairings produced by the North American Regional Climate Change Assessment Program (NARCCAP) over a domain divided into five ecoregions that encompass western Canada and the central U.S. Plains. Over parts of western Canada, the pairings show statistically significant increases in convective precipitation and CAPE, suggesting increased frequency and/or intensity of thunderstorms over this region. In the central U.S. Plains, the results were more mixed, suggesting future increases in severe thunderstorms and/or increased potential for severe thunderstorms over certain regions whereas others suggested an increase in non-severe thunderstorms due to decreases in wind shear.

Acknowledgements

First and foremost, I would like to thank my advisor Dr. John Hanesiak for his guidance, advice, and support in the completion of my master's thesis and for giving me the opportunity to conduct and learn about research. Further, I would like to thank my committee members, Dr. Ron Stewart, for his advice and helpful suggestions, and Dr. Julian Brimelow, for his invaluable contributions to this research and help with Python.

Next, I would like to thank NARCCAP for making the precipitation data used in this research available. NARCCAP is funded by the National Science Foundation (NSF), the U.S. Department of Energy (DoE), the National Oceanic and Atmospheric Administration (NOAA), and the U.S. Environmental Protection Agency Office of Research and Development (EPA). I would also like to thank CCRN for providing the financial support for this research.

Many thanks go to Kyle Ziolkowksi for his advice as I learned to code in Python and to Scott Kehler for helping me write Python scripts.

I would also like to express gratitude to Dr. John Iacozza for his advice and guidance on how to interpret and conduct the statistical tests performed in this research. Further, the use of the Grex super-computing facility at the University of Manitoba and the technical support of the WestGrid staff have been invaluable in running these tests.

Many thanks go to William Burrows of Environment and Climate Change Canada for producing the severe weather parameter datasets used in this research.

Last, and certainly not least, I would like to thank my family for their patience, guidance, help, and support throughout my master's program.

Table of Contents

List of Figures

List of Tables

Chapter 1 Introduction

1.1 Background

According to the Intergovernmental Panel on Climate Change (IPCC) (2013), there is certainty that the global mean surface temperature has increased since the late 19th century, with "[e]ach of the past three decades [being] successively warmer at the Earth's surface than all the previous decades in the instrumental record, and the first decade of the 21st century [being] the warmest" (p. 161). This has primarily been due to an increase of greenhouse gases from anthropogenic sources, a trend that is anticipated to continue should levels of fossil fuel usage remain the same (Brooks, 2013). Climate variability has important consequences for extreme weather like convective storms, which is the primary focus of this thesis.

Convective precipitation includes any precipitation resulting from convective processes, which are processes that involve the transport of heat through buoyant updrafts ("Convection", n.d.). In this research, we focus our attention on thunderstorms, as they are a common source of convective precipitation in the warm season across our domain. There are numerous types of thunderstorms, including short-lived single-cell thunderstorms, mesoscale convective systems, and supercell thunderstorms (Stull, 2015). Any of these types may produce precipitation; however, because of the spatial resolution of the climate models used in this research and the use of 30-year climatological averages of convective and total precipitation, it is impossible to determine what type of thunderstorm has produced precipitation. Thus, we use convective precipitation as a proxy for the occurrence of any type of thunderstorm.

It is generally considered that the three environmental conditions required to form a thunderstorm are: low-level humidity, instability, and a triggering mechanism to cause lifting (Stull, 2015). A fourth ingredient is needed to contribute to severe thunderstorms: vertical wind

shear. Warmer temperatures “will create more evaporation, greater amounts of low-level moisture, and more instability (IPCC, 2007)” (as cited in Lee, 2012, p. 326). Since moisture and instability are important ingredients in the development of convective weather, a potential result of increased global mean surface temperature is an increase in the number and/or severity of convective weather events. Indeed, there have been projected future increases in the potential for thunderstorm environments resulting from anthropogenic climate change (Gensini, Ramseyer, & Mote, 2014; Wehner, 2013).

Thunderstorms are a common atmospheric phenomenon in many parts of the world, including North America. Such storms can produce extreme weather and pose a significant threat to society; this extreme weather can include damaging surface winds, hail, tornadoes, lightning, and heavy rainfall (Trapp et al., 2007) and can result in flooding, erosion, and property damage (Mahoney, Alexander, Scott, & Barsugli, 2013). It is important to establish the relationship between global climate change and thunderstorms as thunderstorms can have significant societal and economic impacts. From a social perspective, thunderstorms have impacts ranging from loss of livelihood to loss of life and from an economic standpoint are the impacts of agricultural loss and damage to buildings and vehicles (Sanderson et al., 2014). Further, understanding how climate change may affect thunderstorms is important to help inform the decision-making process for government officials, planners, and the public in regard to climate change mitigation and adaptation (Sobolowski & Pavelsky, 2012).

Despite the significant impacts of thunderstorms, there has been limited research into the relationship between global climate and thunderstorms (Brooks, 2013) and, as a result, the IPCC (2013) has low confidence for trends in small-scale severe weather events – something they attribute to insufficient studies and data quality. Further, the Committee on Extreme Weather

Events and Climate Change Attribution (CEWECCA) (2016) has assessed both the level of understanding of the effect of climate change on various event types and the level of scientific confidence that exists in the current capabilities for attributing specific events to anthropogenic climate change. Their findings indicate that the level of confidence and understanding for thunderstorms is the lowest out of all event types (see Fig. 1.1).

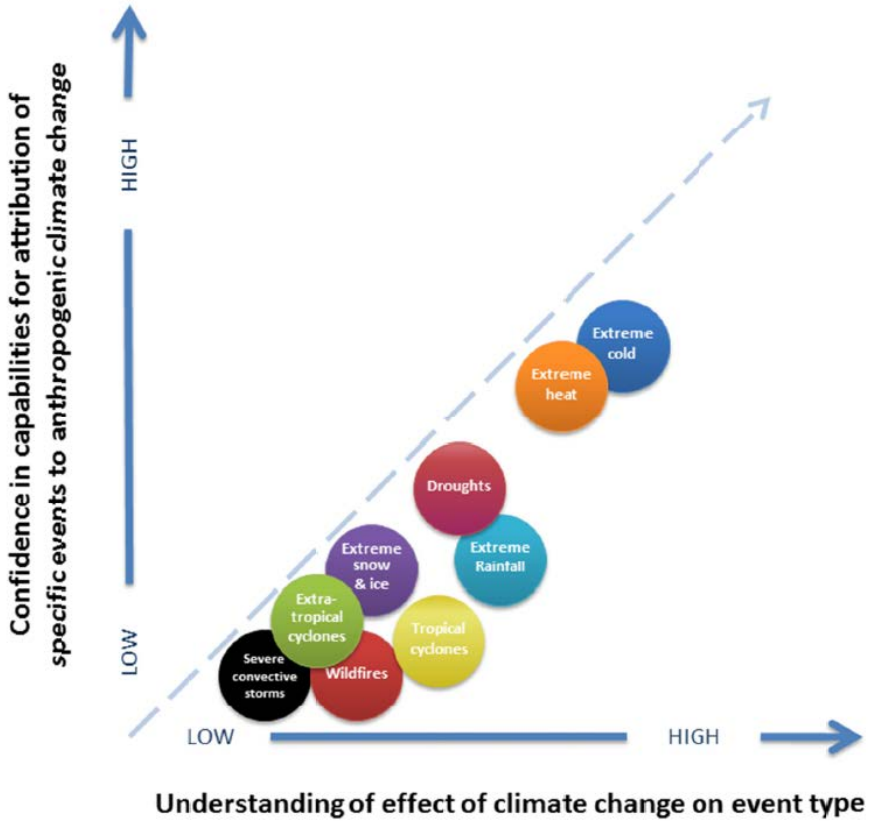

Figure 1.1 Assessment of the state of science attribution for different weather event types. Republished with permission of The National Academies Press, from Attribution of Extreme Weather Events in the Context of Climate Change, Committee on Extreme Weather Events and Climate Change Attribution, 2016; permission conveyed through Copyright Clearance Center, Inc.

In comparison to other extreme weather events (e.g. hurricanes), thunderstorms are small on both spatial and temporal scales (CEWECCA, 2016). This is a major issue when researchers attempt to study thunderstorms in relation to global climate: because of the scale of convective

weather processes (~10 km (Stull, 2015)) there are limitations resulting from an overall lack of reliable data due to inadequate observational records as well as the coarse resolution of global climate models (GCMs; 100 to 500 km (Stull, 2015)) and their subsequent inability to resolve these processes (Brooks, 2013). Observational data on thunderstorms are typically inadequate because surface meteorological observing stations are too dispersed to measure important convective weather parameters for all severe weather events that occur (IPCC, 2013). Hail and tornadoes, specifically, are highly localized phenomena and are not well resolved by systems of meteorological observing stations (CEWECCA, 2016). Records of these phenomena are largely based on eyewitness reports made by amateur observers; as such, they are dependent on observer availability and a reporting system and are thus subject to human error (Brooks, Lee, & Craven, 2003; CEWECCA, 2016) (e.g. the severity of a tornado could be miscategorised).

With a higher resolution than their global counterparts (on the order of tens of kilometres), regional climate models (RCMs) allow for improved resolution of topography and better simulation of mesoscale atmospheric processes (Khaliq, Sushama, Monette, & Wheater, 2015; Mladjic et al., 2011). To improve the coarse resolution of GCMs, a common approach has been to run a dynamical RCM using GCM outer boundary forcing to improve spatial resolution; this approach is referred to as dynamic downscaling (Mearns et al., 2013). Specifically, RCMs have been found to better simulate precipitation extremes than GCMs (Alexander, Scott, Mahoney, & Barsugli, 2013; Bukovsky, McCrary, Seth, & Mearns, 2017). The concept of the "added value" of dynamic downscaling is defined as "a measure of the extent to which the downscaled climate is closer to the observations than the model from which the boundary conditions were obtained (Flato et al., 2013)" (Curry et al., 2016, p. 365). In other words, RCM

simulations should offer improved representation (relative to observational data) of the climate when compared to their driving GCM.

Numerous studies have examined the added value of RCMs in simulating the climatology of precipitation. Lucas-Picher et al. (2012) examined precipitation over Greenland, finding that with increased resolution their RCM better captured the spatial variability of the region than the low-resolution driving model. Similarly, Torma, Giorgi, and Coppola (2015) found RCMs added valuable information in the simulation of precipitation over the European Alps, a region characterized by complex topography. Wang, Swati, Stein, and Kotamarthi (2015) found a 12 km resolution RCM displayed better agreement with observational data in simulating small-scale spatial variations over the United States in total monthly precipitation than the reanalysis data used to drive their model. Paeth and Mannig (2013), using an RCM with 0.5° spatial resolution nested within a GCM, found the RCM simulations of precipitation trends over the Mediterranean Basin to be more consistent with observations than the driving GCM. To summarize, RCMs have proven to perform well in downscaling GCMs to tens of kilometers and to add value to their driving GCMs in the representation of resolution-dependent variables like precipitation; further, they have been shown to consistently account for synoptic-scale processes like mesoscale cyclones, particularly in regions with complex topography (Curry et al., 2016; Paeth & Mannig, 2013; Wang et al., 2015).

A number of recent studies have found RCM output to be reliable when modeling past and future thunderstorm environments; further, recent research has indicated that these environments may potentially become more conducive to severe thunderstorms under the influence of future climate change (Gensini et al., 2014; Trapp et al., 2007; Van Klooster & Roebber, 2009). Trapp et al. (2007) used the product of convective available potential energy

(CAPE) and 0 to 6 km vertical wind shear to discriminate between significant and non-significant severe thunderstorm environments; their findings indicate future decreases in shear and dramatic increases in CAPE resulting in an overall increase in the number of days on which conditions would support the development of thunderstorms in the late 21st century. Similarly, Van Klooster and Roebber (2009) found a decrease in shear and increase in CAPE that could result in increased potential in the first half of the 21st century for severe thunderstorms east of the Rocky Mountains. Using an RCM with a 50 km spatial resolution and the product of CAPE and 0 to 6 km wind shear, Gensini et al. (2014) found there to be an increase in the number of days with environments favourable for thunderstorms over the Great Lakes, Northeast United States, and Southeast Canada between 2041 and 2065.

Many studies assessing the relationship between anthropogenic global warming and thunderstorms have used RCM projections; however, it is impossible for the RCMs currently available to adequately simulate thunderstorms, so most of these studies focus on examining large-scale environmental variables that are associated with thunderstorm activity – variables such as CAPE and wind shear – instead of simulating thunderstorms themselves; this is referred to as statistical downscaling (Lee, 2012; CEWECCA, 2016). As stated by Kapsch, Kunz, Vitolo, and Economou (2012), “if a relationship exists between appropriate convective parameters and severe weather occurrence, it can be expected that changes in the parameter values also impact the intensity and/or number of thunderstorms” (p. 2). Essentially, these parameters act to represent the conditions necessary to support the formation of severe thunderstorms.

A number of international programs have examined uncertainties in simulations of future climate on regional scales using an ensemble framework and by embedding RCMs within GCMs to obtain more detail over a particular domain (Mearns et al., 2013). One such program is the

North American Regional Climate Change Assessment Program (NARCCAP). The primary scientific motivation of NARCCAP is to explore uncertainty in regional projections of future climate change that result from using multiple GCMs to drive multiple RCMs (Mearns et al., 2009). The other motivation "is to provide the climate impacts and adaptation community with high- resolution regional climate change scenarios that can be used for studies of the societal impacts of climate change and possible adaptation strategies" (Mearns et al., 2009, p. 311). To accomplish this, NARCCAP provides six RCM simulations for which four GCMs provide the boundary conditions. These simulations are provided for a common time period and domain and have the same spatial and temporal resolution (Mearns et al., 2013). Simulations from three NARCCAP RCM-GCM pairings form the primary data source for this research.

1.2 Objectives

Given the importance of precipitation, the first objective of this thesis is to characterize total and convective precipitation produced by three different RCM-GCM model pairings in order to characterize future changes in the climatology of these variables over the domain of interest. In performing this analysis, it can be assessed whether or not total precipitation will increase over the domain in the future as well as what portion of this increase can be attributed to precipitation from convective weather, and if this percentage will increase under the influence of a changing climate. A future increase in convective precipitation would indicate an increase in the frequency and/or intensity of convective weather events and subsequently the environments favourable for such weather.

As stated previously, despite increased resolution from their global counterparts, the RCM projections made available by NARCCAP (with a spatial resolution of 50 km) are still unable to resolve finer-scale convective weather phenomena; however, the NARCCAP model

output can be used to ascertain the favourable environmental conditions for thunderstorm occurrence over a certain area (Walawender, Kielar, & Ustrnul, 2015). As such, it is important to examine these environments and the variables used to describe them (e.g. CAPE, wind shear, etc.). According to Christenson et al. (2013) (as cited in Bukovsky et al., 2017) RCM projections of future climate change are considered to be more credible when the primary drivers of the change are adequately simulated and projected by the RCM. Since it is important to examine future change in convective and total precipitation, as this can have societal and economic impacts, it is important to investigate the key drivers of changes in precipitation, the parameters that describe them, how well-simulated these parameters are, and how they may change in a future climate. Thus, the second objective of this work is to examine a number of severe weather parameters calculated using the output from three NARCCAP model pairings in order to characterize future changes in the severe weather environment. In this way, it can be determined which variables are influencing changes in convective precipitation over the domain. Thus, to summarize, the objectives of this thesis are to:

1) Characterize the future change in convective and total precipitation over western Canada and the central U.S. Plains, and
2) Characterize the future change in severe weather environment over western Canada and the central U.S. Plains.

Chapter 2 Data and Methods

2.1 NARCCAP

The primary data source for this research is the North American Regional Climate Change Assessment Program (NARCCAP). NARCCAP provides data for a variety of atmospheric variables for two 30-year periods: a current period ranging from 1971 to 2000 and a future period from 2041 to 2070. The data are provided at a 50 km spatial resolution and 3-hour temporal resolution, resulting in 8 time steps per day. For this research, the data for total precipitation and convective precipitation were downloaded from NARCCAP (http://www.narccap.ucar.edu/index.html) in NetCDF format. The precipitation data come in the form of an instantaneous flux, in units of $kg/m^2/s$, which is averaged over the previous 3 hours; however, the data were converted to total mm of precipitation in the Python routines used to analyze the data. The total and convective precipitation data were analyzed using Python routines whereby all of the time steps were summed over monthly (March – August) and seasonal timescales (MAM and JJA). The World Meteorological Organization (WMO) (2018) defines climatological standard normals as averages of climatological data computed over a 30-year period. Climate normals have increasingly been used as predictors of future climate at a given location (WMO, 2018). As such, we calculate averages of the monthly and seasonal sums of precipitation over each of the 30-year periods. In order to evaluate changes between future and current climate for each of the variables, the 30-year averaged dataset calculated for the current period was subtracted from that for the future period and then plotted. In addition to these plots, we calculated average daily totals across each of the five ecoregions (shown in Section 2.2) for the current and future periods. We then plotted them as histograms in order to examine how the frequency distribution has shifted from current to future.

NARCCAP uses six RCMs to simulate climate. These are the Canadian RCM (CRCM), the Met Office Hadley Centre's Regional Model 3 (HadRM3), the National Center for Atmospheric Research (NCAR)/Pennsylvania State University Mesoscale Model 5 (MM5), the NCAR Weather Research and Forecasting (WRF) model, the Abdus Salam International Centre for Theoretical Physics' Regional Climate Model Version 3 (ICTP RegCM3), and the Experimental Climate Prediction Center Regional Spectral Model (RSM). The four GCMs used by NARCCAP are the Canadian Climate Centre (CGCM3), the Geophysical Fluid Dynamics Laboratory (GFDL) CM2.1, the Hadley Centre HadCM3, and NCAR's CCSM3 (Mearns et al., 2009). As a result of funding limitations, the simulations for all 24 RCM-GCM pairings could not be performed. Instead, a statistical design framework was developed whereby each GCM provided the boundary conditions for three RCMs and each RCM used boundary conditions from two different GCMs; this yielded a total of 12 RCM-GCM simulations (Mearns et al., 2009).

The IPCC (2000) has developed climate change emission scenarios that are meant to be used in the analysis of possible climate change and its impacts. Demographic and socio-economic developments as well as changes in technology play a role in determining the complex dynamic systems that produce future greenhouse gas emissions (IPCC, 2000). Greenhouse gas emissions in the future are uncertain so each emissions scenario developed by the IPCC represents different ways future emissions may unfold (IPCC, 2000). The emissions scenario used by NARCCAP for the future period is the A2 emissions scenario from the IPCC's Special Report on Emissions Scenarios. In this scenario, the population reaches over 10 and 15 billion by the middle and end of the 21st century, respectively (IPCC, 2000). Cumulative carbon dioxide (CO_2) emissions are projected to be approximately 600 and 1850 GtC by the middle and end of the 21st century, respectively, and CO_2 concentrations are expected to reach approximately 575

parts per million (ppm) and 870 ppm by the middle and end of the 21st century, respectively (IPCC, 2000). Overall, this scenario is considered to be at the higher end of the emissions scenarios. It was selected by NARCCAP because a higher-emission scenario was considered to provide more information than a lower-emission one from an adaptation and mitigation viewpoint (Sobolowski & Pavelsky, 2012) and it is thought that if society can adapt to a world with high emissions then it can adapt to one with a less extreme increase in emissions (Gensini et al., 2014).

The three NARCCAP model pairings selected for this research are based on the selection of models by Brimelow, Burrows, and Hanesiak (2017). Their identification of the model pairings was a two-step process. The first step was to exclude the model pairings that ranked lowest for reproducing the current climate over North America based on the results of Elguindi and Grundstein (2013) (as cited in Brimelow et al., 2017). HRM3-HadCM3 was selected because it ranked the highest in these results; GFDL-ECP2 and CGCM3-RegCM3 ranked the lowest and were excluded from further analysis. For the second step, the HAILCAST model (Brimelow, Reuter, & Poolman, 2002) was run in conjunction with the remaining models for a 5-year period at the end of the 20th century. Based on the results of mean number of severe hail days for March through September, the three final model pairings were selected and CRCM3-CCSM3, CRCM3-CGCM3, and WRFG-CGCM3 were eliminated based on their inability to reproduce spatial patterns in precipitation and hail climatologies. Thus, this research uses three model pairings based on the results of Brimelow et al. (2017): MM5-HadCM3, MM5-CCSM, and HRM3-HadCM3.

2.2 Domain

The spatial domain of the NARCCAP simulations includes northern Mexico, the lower 48 contiguous United States, and Canada up to 60°N; however, the domain of this research is only a subset of this larger area, extending from 35°N to about 60°N and from the Rocky Mountains to as far east as Iowa. This smaller domain of interest is further broken down into five ecoregions: Northwest Boreal Forest (NWF), Canadian Prairies (CAP), United States Prairies (USP), Southern Great Plains (SGP), and Colorado Rockies and High Plains (CHP). The boundaries of these ecoregions are based on those outlined by Brimelow et al. (2017) which were initially based on the United States' Environmental Protection Agency's Level 1 Ecoregions of North America. To reflect the progression of thunderstorm activity throughout the spring and summer months over the Great Plains ecoregion, it was subdivided into three separate ecoregions: at 41°N, it was divided to form SGP to the south and USP to the north and at 49°N to define the northern boundary of USP and the southern boundary of CAP (Brimelow et al., 2017). SGP was further cropped for the purposes of this research at 35°N to form its southern boundary. Finally, the eastern boundary of CHP was ascertained using the 1100 m height contour (Brimelow et al., 2017). The boundary of the domain and of the five ecoregions is shown in Fig. 2.1.

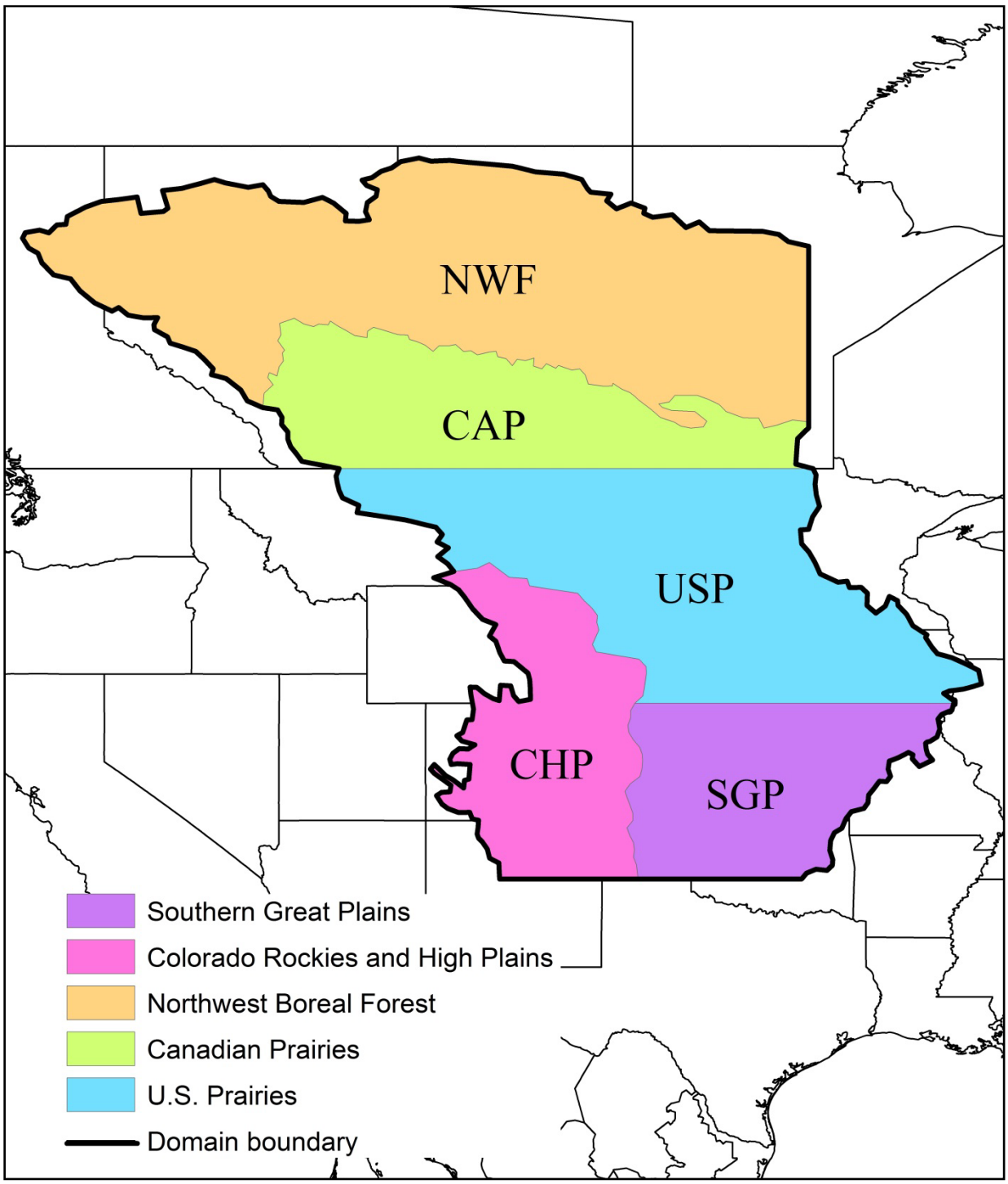

Figure 2.1 Domain boundary and the boundaries of the five ecoregions used in this research.

2.3 Severe weather parameters

In addition to examining changes in convective and total precipitation, this research aims to examine future changes in severe weather environments. The data from the three NARCCAP model pairings allows for the calculation of a variety of severe weather parameters; a total of ten are used in this research and are listed in Table 2.1.

Table 2.1 Full name, abbreviation, and units of severe weather parameters used in this research

Severe Weather Parameter	Abbreviation	Unit
Surface dewpoint temperature	SurfDewpoint	K
Mixed-layer surface dewpoint temperature	MLDewpoint	K
Surface-based CAPE	SBCAPE	J/kg
Most unstable CAPE	MUCAPE	J/kg
50 mb mixed-layer CAPE	MLCAPE	J/kg
50 mb mixed-layer convective inhibition	MLCIN	J/kg
Bulk wind difference (surface to 6 km)	BWD0to6km	m/s
Bulk wind difference (surface to 1 km)	BWD0to1km	m/s
Supercell Composite Parameter	SCP	Unitless
Significant Tornado Parameter	STP	Unitless

These particular variables were not produced by NARCCAP but rather were produced using FORTRAN. NARCCAP provides two-dimensional data, like the precipitation data discussed in Section 2.1, and three-dimensional data. The atmospheric fields available from NARCCAP are three-dimensional and are provided every 25 mb from 1050 mb up to 700 mb and every 50 mb from 650 mb to 50 mb. For example, these atmospheric fields include the zonal and meridional wind components from which BWD0to1km and BWD0to6km were calculated. The FORTRAN code read in the necessary variables from NARCCAP needed to calculate each parameter and produced files in ASCII format containing every parameter for each month in

each year. The parameters were calculated for the same current and future time periods as for the total and convective precipitation data but were only calculated for the 2100 UTC and 0000 UTC time-steps: times of the day when peak daytime heating has the greatest probability of resulting in severe thunderstorms (Stull, 2015).

Examination of the statistical distributions of the severe weather parameters at a selection of gridpoints for the current period revealed that they were strongly skewed, making the median a better measure of central tendency than the mean for these datasets. The climatological medians for the 30-year periods were calculated using a Python routine. In contrast to the total and convective precipitation data directly available from NARCCAP where the datasets were complete, there were numerous instances of missing data in the severe weather parameter datasets. Where data were missing at any given gridpoint, it was stipulated in the Python routine that the median was to be calculated using only the years where there were available data at that gridpoint. Finally, the medians were calculated excluding zeros (i.e. the days where nothing occurred); this would remove the unwanted effect of very small changes on the medians calculated for the current and future periods.

Since the RCMs used in this research have too coarse a spatial resolution to directly resolve thunderstorms, we instead examine proxies that represent the environmental conditions necessary for the formation of a thunderstorm. The first of these environmental conditions is instability which is most commonly described using convective available potential energy (CAPE). The latent heat released when water vapour condenses in a storm is what gives it its buoyancy and subsequently its energy; CAPE is a measure of this energy (Stull, 2015). In this research, we use three different methods of calculating CAPE: surface-based CAPE (SBCAPE), mixed-layer CAPE (MLCAPE), and most unstable CAPE (MUCAPE). SBCAPE was calculated

using the surface temperature and the surface dewpoint temperature. MLCAPE was calculated using the average air and dewpoint temperature in the lowest 50 mb of the atmospheric column. Lastly, MUCAPE was calculated by measuring CAPE for air parcels beginning from various heights in the lowest 300 mb of the atmosphere and selecting the level that yielded the highest CAPE values.

2.3.1 Composite Parameters

In addition to the singular parameters we use to describe moisture, instability, and vertical wind shear, this thesis examines two composite parameters that incorporate these individual parameters. Researchers have created composite parameters by assessing the relative importance of moisture, instability, and vertical wind shear parameters to the forecasting of supercell thunderstorms and tornadoes (Thompson, Edwards, & Hart, 2002). The first composite parameter we examine is the Supercell Composite Parameter (SCP). The SCP was created by forecasters at the Storm Prediction Center (SPC) in Norman, Oklahoma in order to identify environments conducive to the formation of supercells (Thompson, Edwards, Hart, Elmore, & Markowski, 2003). In the formulation of SCP that we examine, MUCAPE, 0 to 3 km storm-relative helicity, and Bulk Richardson Number (BRN) shear are normalized to approximate supercell threshold values and then combined into a single, dimensionless parameter (Thompson et al., 2003):

(1) $\text{SCP} = (\text{MUCAPE}/1000\ \text{J/kg}) \times (\text{SRH0to3km}/100\ \text{m}^2/\text{s}^2) \times (\text{BRN shear}/40\ \text{m}^2/\text{s}^2)$

SRH0to3km is the storm-relative helicity for the 0 – 3 km layer and BRN shear is the bulk-Richardson-number shear. BRN shear is the ratio of instability in the mid- to upper-troposphere to wind shear in the lower troposphere; thus, it is useful for discriminating between environments conducive to supercell thunderstorms and those that are not (Stull, 2015).

Similarly, SRH0to3km is useful in the forecasting of mesocyclones (the defining characteristic of supercell thunderstorms) and tornadoes (Stull, 2015).

The second composite parameter examined is the Significant Tornado Parameter (STP). It is used to aid forecasters in differentiating between tornadic and non-tornadic supercells. Similar to SCP, environmental ingredients that seem to favor supercell thunderstorms with tornadoes have been identified in a number of studies and then combined into this one dimensionless parameter (Thompson et al., 2002; Thompson et al., 2003). In this calculation, CAPE and lifted condensation level (LCL) height based on the lowest 100 mb mean parcel, 0 to 1 km SRH, and 0 to 6 km BWD are normalized to approximate threshold values for supercells and significant tornadoes (Thompson et al., 2003). The equation used here mimics that of Thompson et al. (2003) except that it uses the surface-based CAPE and LCL parameters:

$$\text{STP} = (\text{SBCAPE}/1500\ \text{J/kg}) \times ((2000 - \text{SBLCL})/1000\ \text{m}) \times (\text{SRH0to1km}/150\ \text{m}^2/\text{s}^2) \times (\text{BWD0to6km}/20\ \text{m/s}) \quad (2)$$

SRH0to1km is the storm-relative helicity for the 0 – 1 km layer and is calculated relative to right-moving thunderstorms. SBLCL is the surface-based lifting condensation level. If SBLCL is less than 1000 m, this term is normalized to 1.0 and if it is greater than 2000 m it is normalized to 0. Further, if BWD0to6km is greater than 30 m/s it is normalized to 1.5 and if it is less than 12.5 m/s it is normalized to 0.

It is important to note that both SCP and STP and the approximate threshold values used to normalize their components were developed based on soundings obtained across the United States (Thompson et al., 2003). In particular, the approximate threshold values of CAPE are not necessarily appropriate for Canada since CAPE is directly related to surface temperature and surface temperature decreases with increasing latitude.

2.4 Statistical significance

The difference between the future and current periods for the precipitation and severe weather parameter data were tested for statistical significance at the 95% confidence level using the Wilcoxon rank sum test. This test is a non-parametric test; thus, it does not require the data under examination to have a normal distribution. Both the precipitation and severe weather parameter data were tested for normality using the Shapiro-Wilkes test. For every variable, the distributions for at least a portion of the gridpoints in the domain were found to be non-normal, thus requiring the use of a non-parametric statistical test.

The Wilcoxon rank sum test is used to compare two independent random sample rank sums for difference and has three assumptions: that the samples being compared are independent random samples, that both population distributions have the same shape, and that the data is either measured at the ordinal scale or downgraded from the interval/ratio scale (Chapman McGrew Jr. & Monroe, 2009); the data used in this research meets all of these assumptions. The Wilcoxon rank sum test uses the ranks of observations to measure the magnitude of the differences in the ranked positions between two datasets; in this research, the two datasets are the current and future time periods. These two datasets are combined and placed in a single ranked set. They are then considered independently and the sum of ranks is calculated for each (Chapman McGrew Jr. & Monroe, 2009).

2.5 Model agreement

For the purpose of examining spatial differences in precipitation change between the model pairings, plots of model agreement were produced. These plots show the agreement between two and three model pairings on positive and negative change. Since the MM5 and HRM3 RCMs have different grid dimensions and grid projections, the HRM3 RCM precipitation

data had to be regridded to the MM5 grid dimension and projection. The MM5 grid was selected as the reference grid since the MM5 RCM is used to downscale two different driving GCMs whereas the HRM3 RCM is only used to downscale one driving GCM. To interpolate the HRM3 grid to the MM5 grid, a nearest neighbour interpolation approach in Python was used whereby the HRM3 precipitation data was interpolated to the MM5 grid using the latitude and longitude from both RCMs as input.

Chapter 3 Results – Precipitation

3.1 Spring

In MAM, MM5-HadCM3 (Fig. 3.1a) shows statistically significant increases in total precipitation over most of CAP, northern and western Alberta, western Manitoba, and eastern Saskatchewan in NWF. There are small areas of significant increase in USP and significant decrease in CHP and SGP. These increases in total precipitation are not matched by significant increases in convective precipitation (Fig. 3.2a), except for northern Alberta. Similarly, there are only small areas of significant increase in convective precipitation over the rest of NWF and in the other four ecoregions.

In contrast to MM5-HadCM3, MM5-CCSM (Fig. 3.1b) shows primarily insignificant increases in total precipitation over all five ecoregions, excluding an area of significant increase in southeastern USP and northeastern SGP. There are small areas of decrease in central NWF and along the boundary between CHP and SGP, and on the western boundary of CHP. In convective precipitation (Fig. 3.2b), there are large areas of significant increase over all of the ecoregions except for CHP. It is also apparent that the significant increase in total precipitation in southeastern USP and northeastern SGP is the result of a statistically significant increase in convective precipitation over this area.

HRM3-HadCM3 (Fig. 3.1c) shows statistically significant increases in total precipitation over southern Alberta and central Saskatchewan in CAP and NWF. Apart from this, there are primarily insignificant increases over all five ecoregions. There is also a decrease in total precipitation in the southern part of CHP. The changes in convective precipitation (Fig. 3.2c) in MAM are consistent with the increases in total precipitation, specifically over CAP and the southern part of USP. However, there are not decreases in convective precipitation where there

are decreases in total precipitation except for southern CHP and western SGP. This suggests increased convective precipitation as a percentage of total precipitation and thus, an increase in the frequency and/or intensity of heavy (convective) rainfall events. This variable is quantified in Appendix A where plots for the current and future time periods as well as for the difference between the two time periods are provided.

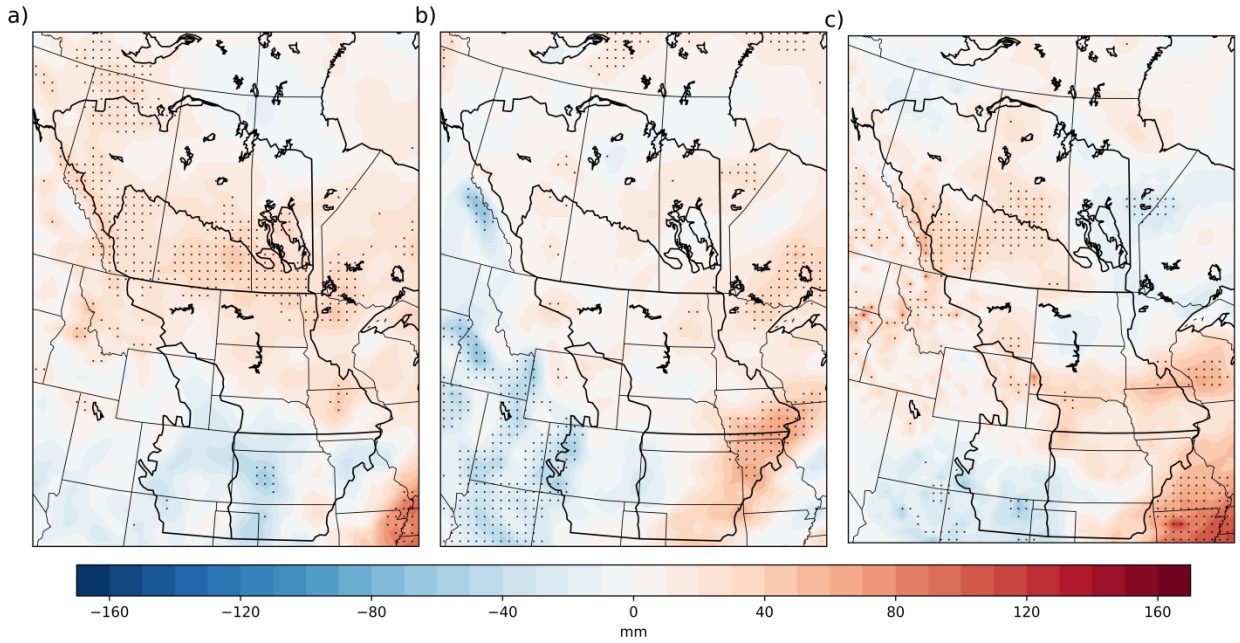

Figure 3.1 (a) Difference (future – current) in average spring (MAM) precipitation for MM5-HadCM3 (b) MM5-CCSM (c) HRM3-HadCM3. Stippling indicates statistical significance at the 95% confidence level.

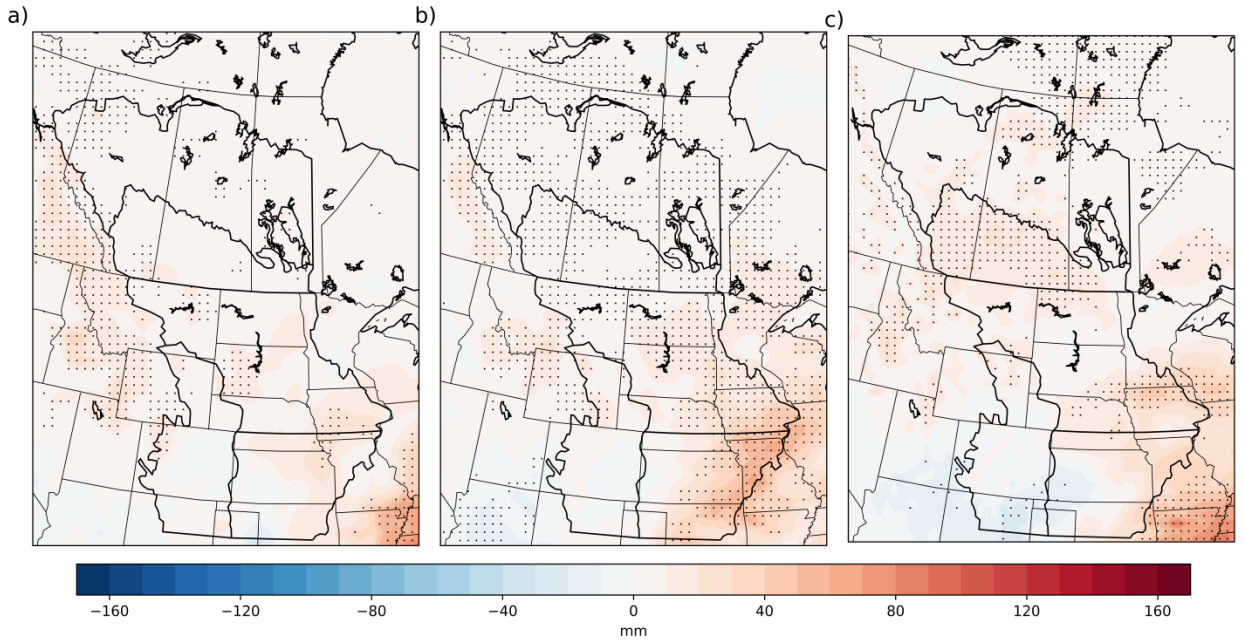

Figure 3.2 (a) Difference (future – current) in average spring (MAM) convective precipitation for MM5-HadCM3 (b) MM5-CCSM (c) HRM3-HadCM3. Stippling indicates statistical significance at the 95% confidence level.

At the monthly scale for MM5-HadCM3, the increases in total precipitation in western Alberta are occurring primarily in March (Fig. 3.3a) and April (3.3b) and in northern Alberta, primarily in May (Fig. 3.3c), and there is a large swath of significant increase over North and South Dakota. Over USP, CHP, and SGP, the result of little to no change at the seasonal scale appears to be the product of monthly increases and decreases balancing out to an insignificant change. For example, there is a significant increase in total precipitation in the northern point of CHP in March but insignificant decreases in this area in April and May; the result of this is an insignificant increase in total precipitation at the seasonal timescale. In contrast, there are very few areas of statistically significant change in convective precipitation in March (Fig. 3.4a) and April (Fig. 3.4b) with most of the significant areas of increase seen at the seasonal timescale being the result of increases occurring in May (Fig. 3.4c).

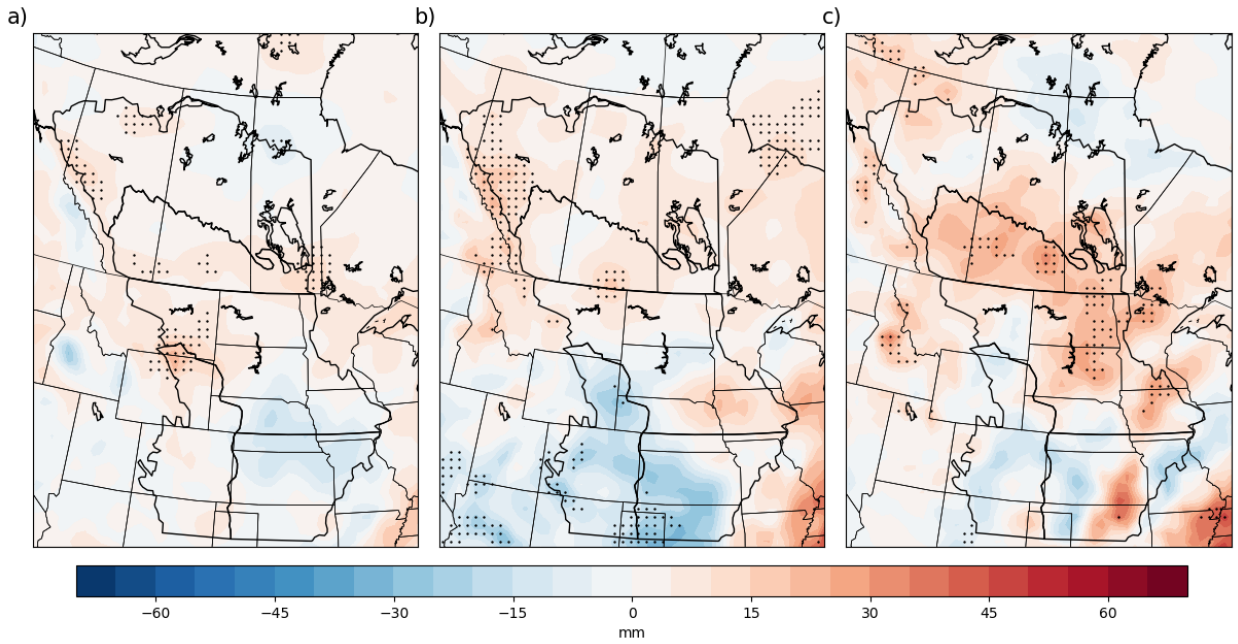

Figure 3.3 Difference (future – current) in average precipitation for MM5-HadCM3 for a) March b) April and c) May. Stippling indicates statistical significance at the 95% confidence level.

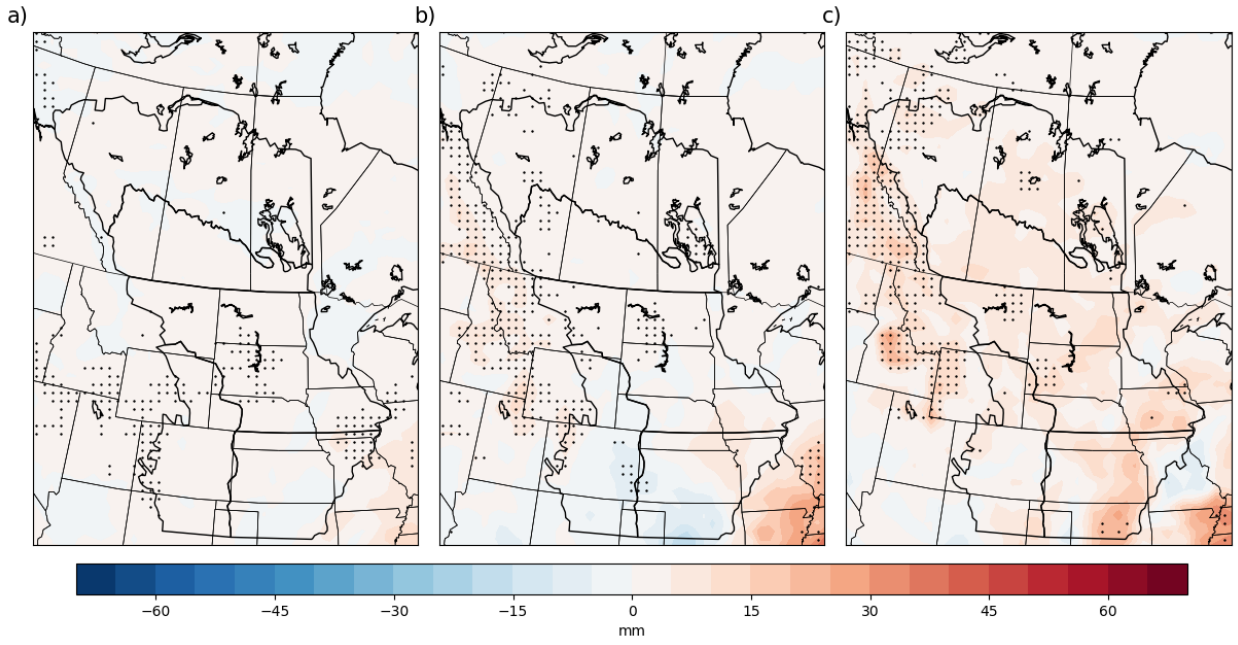

Figure 3.4 Difference (future – current) in average convective precipitation for MM5-HadCM3 for a) March b) April and c) May. Stippling indicates statistical significance at the 95% confidence level.

At the monthly scale for MM5-CCSM, it is apparent that the significant increases seen at the seasonal scale in both convective and total precipitation are the result of a significant increase in May (Fig. 3.5c and Fig. 3.6c). There are also significant increases in May in NWF, eastern USP, and in northern CAP in convective and total precipitation; however, these increases seem to be balanced out by little to no change or decreases in March (Fig. 3.5a and Fig. 3.6a) and April (Fig. 3.5b and Fig. 3.6b), resulting in the May increases not being captured at the seasonal timescale.

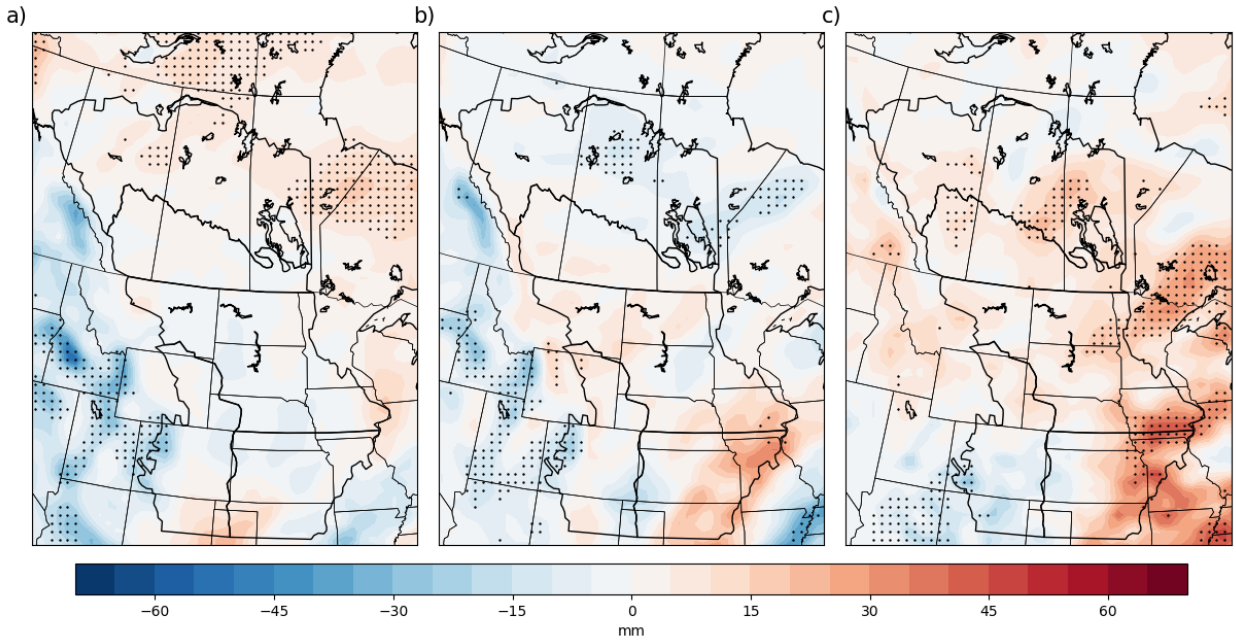

Figure 3.5 Difference (future – current) in average precipitation for MM5-CCSM for a) March b) April and c) May. Stippling indicates statistical significance at the 95% confidence level.

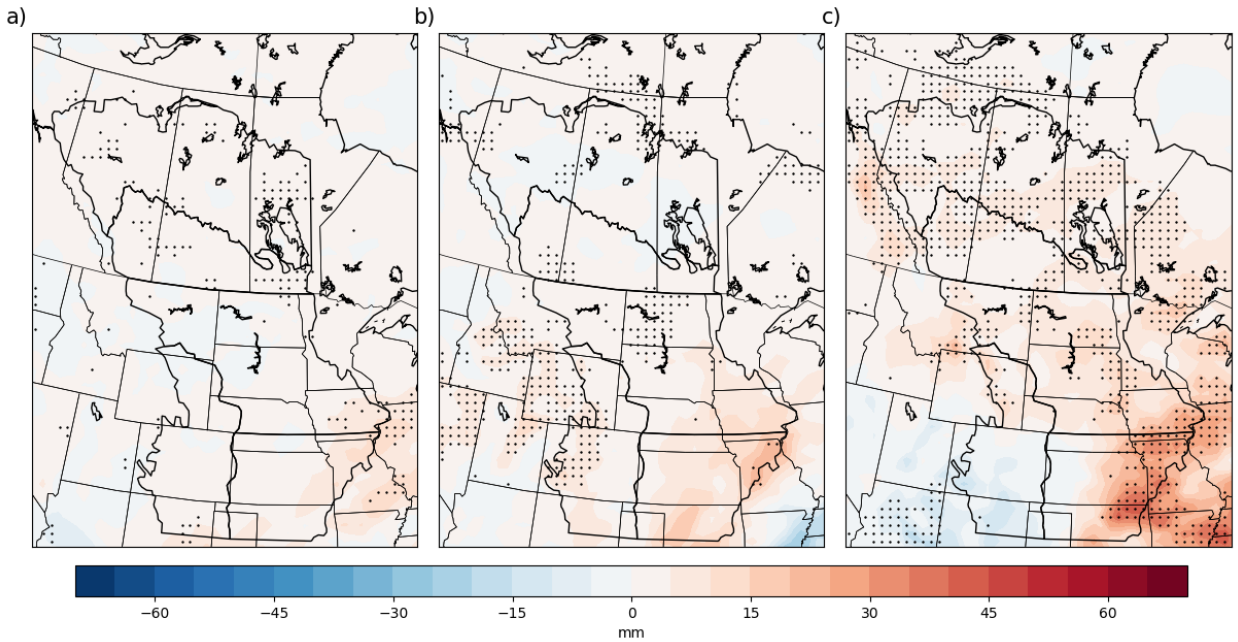

Figure 3.6 Difference (future – current) in average convective precipitation for MM5-CCSM for a) March b) April and c) May. Stippling indicates statistical significance at the 95% confidence level.

At the monthly scale, HRM3-HadCM3 shows little to no statistically significant change in total precipitation in March (Fig. 3.7a) with most of the change seen at the seasonal scale over CAP, southern USP, and the decreases over the boundary between CHP and SGP occurring in April (Fig. 3.7b) and May (Fig. 3.7c). There is a similar pattern in convective precipitation at the monthly scale for HRM3-HadCM3 with significant increases over CAP and southeastern USP in April (Fig. 3.8b) and May (Fig. 3.8c) being reflected at the seasonal scale. Further, there are decreases over the boundary between CHP and SGP. There is an exception for March (Fig. 3.8a) where there is a significant increase in convective precipitation over southeastern SGP that is not reflected at the seasonal scale.

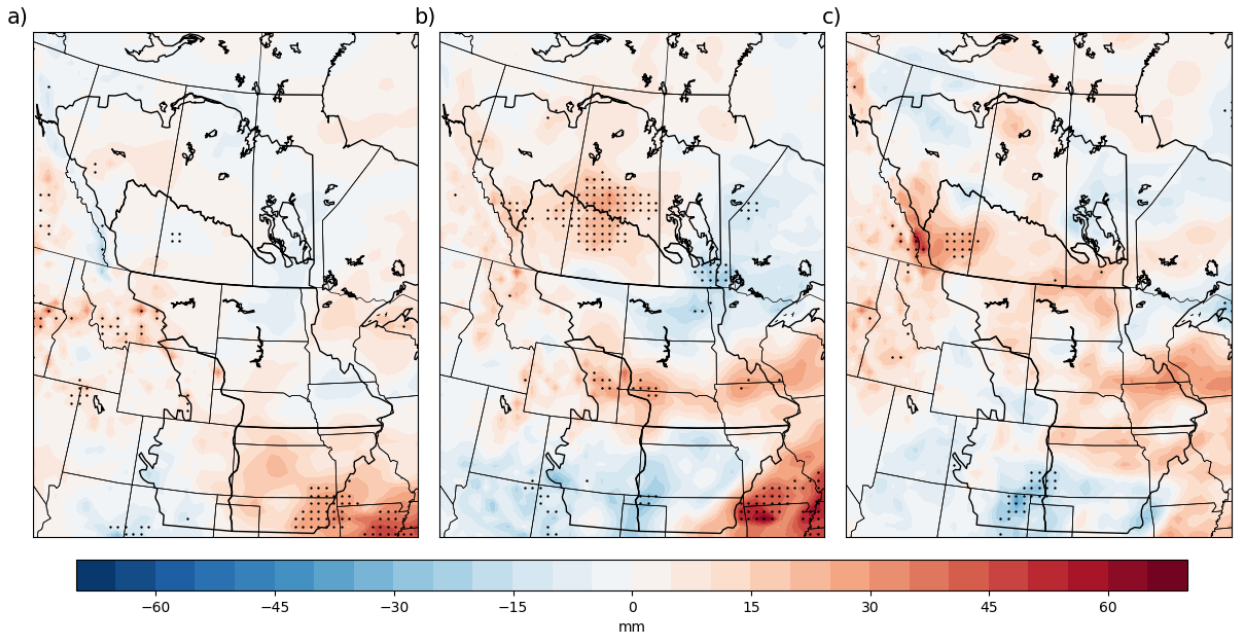

Figure 3.7 Difference (future – current) in average precipitation for HRM3-HadCM3 for a) March b) April and c) May. Stippling indicates statistical significance at the 95% confidence level.

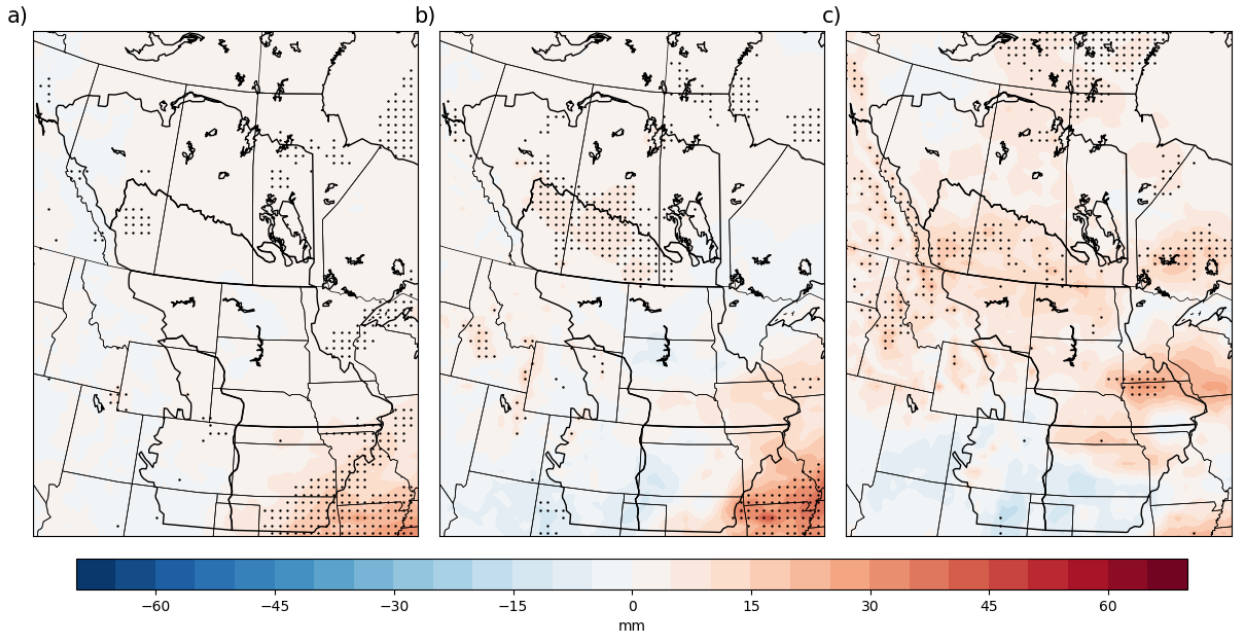

Figure 3.8 Difference (future – current) in average convective precipitation for HRM3-HadCM3 for a) March b) April and c) May. Stippling indicates statistical significance at the 95% confidence level.

3.2 Summer

In JJA, MM5-HadCM3 shows more areas of significant increase in total precipitation than significant decrease (Fig. 3.9a). These areas include the parts of Alberta bound by CAP and NWF, northern and eastern CHP, USP over southwestern North Dakota, and central Manitoba. There is only one notable area of significant decrease over central NWF. Convective precipitation in JJA for MM5-HadCM3 (Fig. 3.10a) is shown to increase significantly over most of Alberta, the western edge of Saskatchewan, and over most of Manitoba that is contained within NWF. There are also statistically significant increases over northern and central CHP and western USP. Unlike for total precipitation, there is no region of decrease in convective precipitation over central NWF.

MM5-CCSM shows similar patterns of change in both convective and total precipitation (Fig. 3.9b and Fig. 3.10b, respectively), though the changes in convective precipitation are of lesser magnitude. There are significant decreases in both variables over southern CHP and SGP. Further, there are significant increases in both over the eastern half of CAP and northern USP. Convective precipitation and total precipitation differ over NWF where there are significant increases over much of the ecoregion in convective precipitation. In contrast, there are only significant increases in total precipitation over central Manitoba and northern Alberta.

HRM3-HadCM3 shows primarily decreases in total precipitation (Fig. 3.9c). Over CHP there are primarily statistically significant decreases. There is a small area of significant increase over central Nebraska, at the border between USP and SGP. Similar to total precipitation, HRM3-HadCM3 shows statistically significant decreases in convective precipitation (Fig. 3.10c) over much of CHP. However, in contrast, there are primarily insignificant increases over much

of the domain but with a significant increase over Nebraska, at the border between USP and SGP.

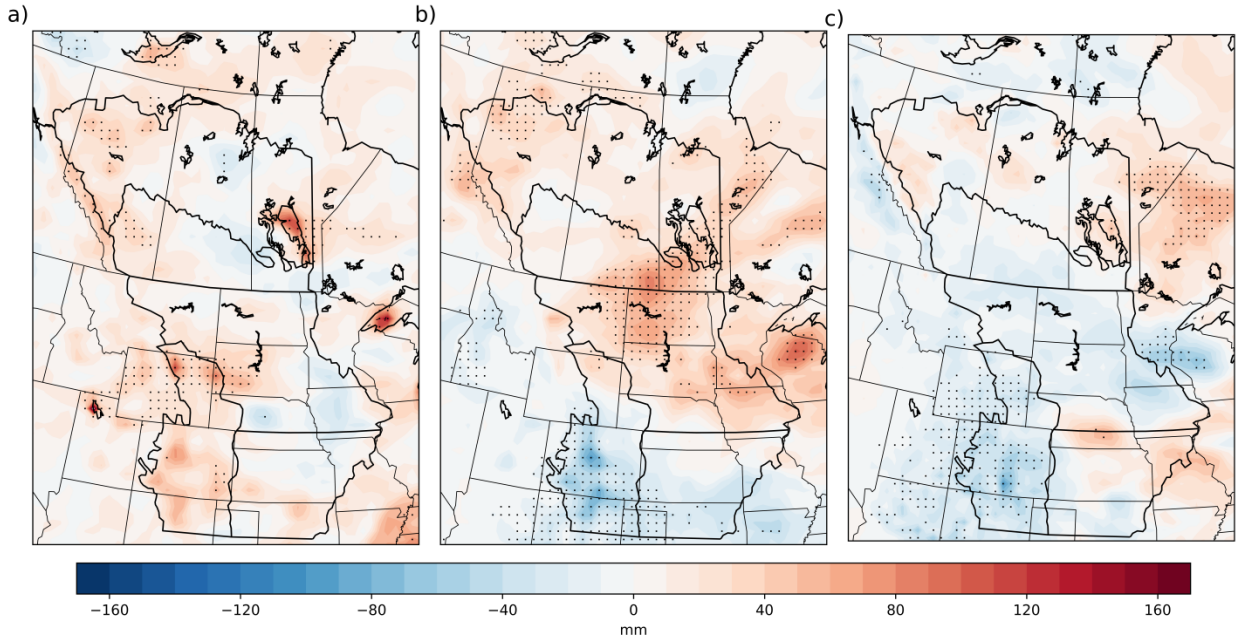

Figure 3.9 Difference (future – current) in average summer (JJA) precipitation for MM5-HadCM3 (b) MM5-CCSM (c) HRM3-HadCM3. Stippling indicates statistical significance at the 95% confidence level.

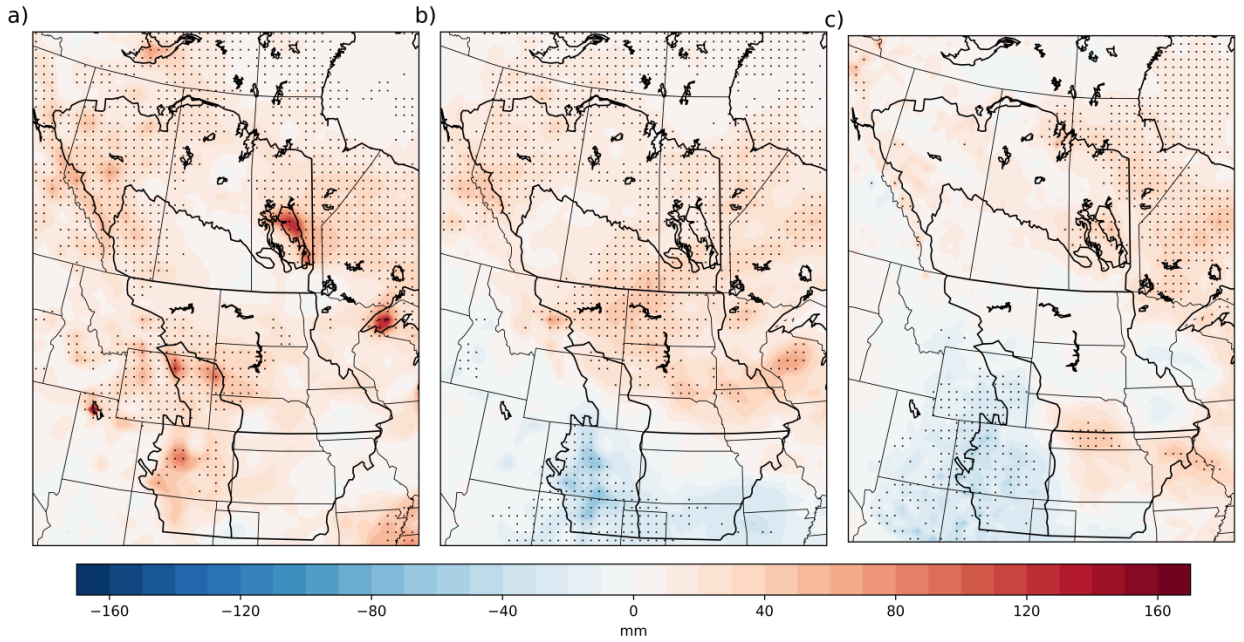

Figure 3.10 Difference (future – current) in average summer (JJA) convective precipitation for MM5-HadCM3 (b) MM5-CCSM (c) HRM3-HadCM3. Stippling indicates statistical significance at the 95% confidence level.

For MM5-HadCM3 at the monthly scale, the statistically significant increases in total precipitation occurring over north CHP at the seasonal scale are the result of significant increases in June (Fig. 3.11a) and July (Fig. 3.11b). Over Alberta, it can be seen that the increases at the seasonal scale are the result of increases in June, July, and August (Fig. 3.11c) over NWF. In contrast, the increase over Alberta contained within CAP is primarily the result of increases in August. For convective precipitation, the significant increase over northern CHP at the seasonal scale is reflected in June (Fig. 3.12a), July (Fig. 3.12b), and August (Fig. 3.12c). Similarly, the increase in convective precipitation in NWF over Alberta is most apparent in June and July and less so in August; this is as opposed to CAP where the increase is more significant from June to August. Finally, the region of significant increase over central CHP seen at the seasonal scale is the result of a localized increase in July.

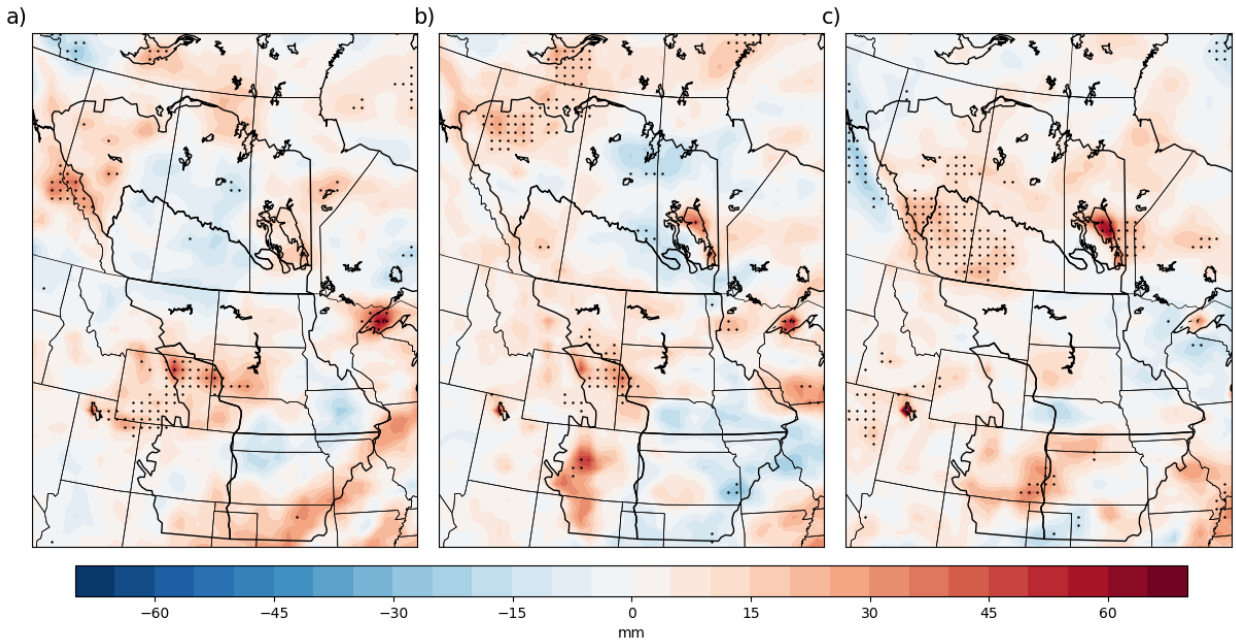

Figure 3.11 Difference (future – current) in average precipitation for MM5-HadCM3 for a) June b) July and c) August. Stippling indicates statistical significance at the 95% confidence level.

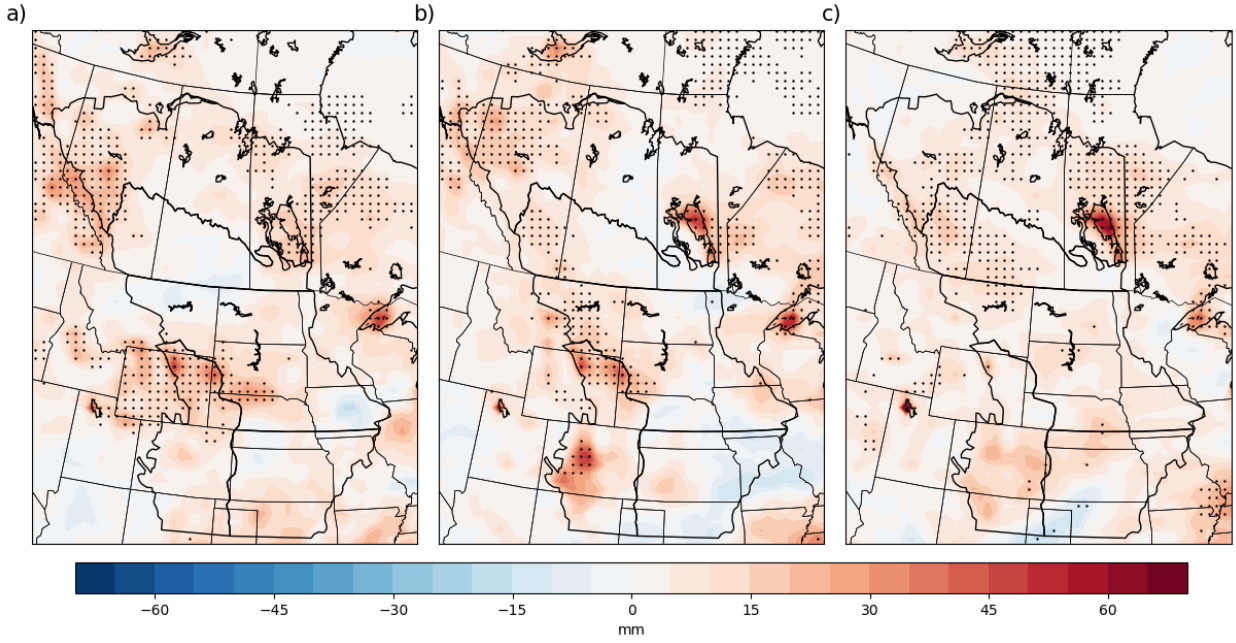

Figure 3.12 Difference (future – current) in average convective precipitation for MM5-HadCM3 for a) June b) July and c) August. Stippling indicates statistical significance at the 95% confidence level.

At the monthly scale, MM5-CCSM shows similar patterns of change in both convective and total precipitation (Fig. 3.13 and Fig. 3.14, respectively) to those at the seasonal scale. In June (Fig. 3.13a and Fig. 3.14a) and July (Fig. 3.13b and Fig. 3.14b), there are statistically significant decreases in both variables in southern CHP. In August (Fig. 3.13c and Fig. 3.14c), there are significant decreases in southern CHP and western SGP. In both variables, the pattern of significant increase over CAP seen at the seasonal scale occurs in July and August whereas over NWF, the significant increases occur primarily in June and August.

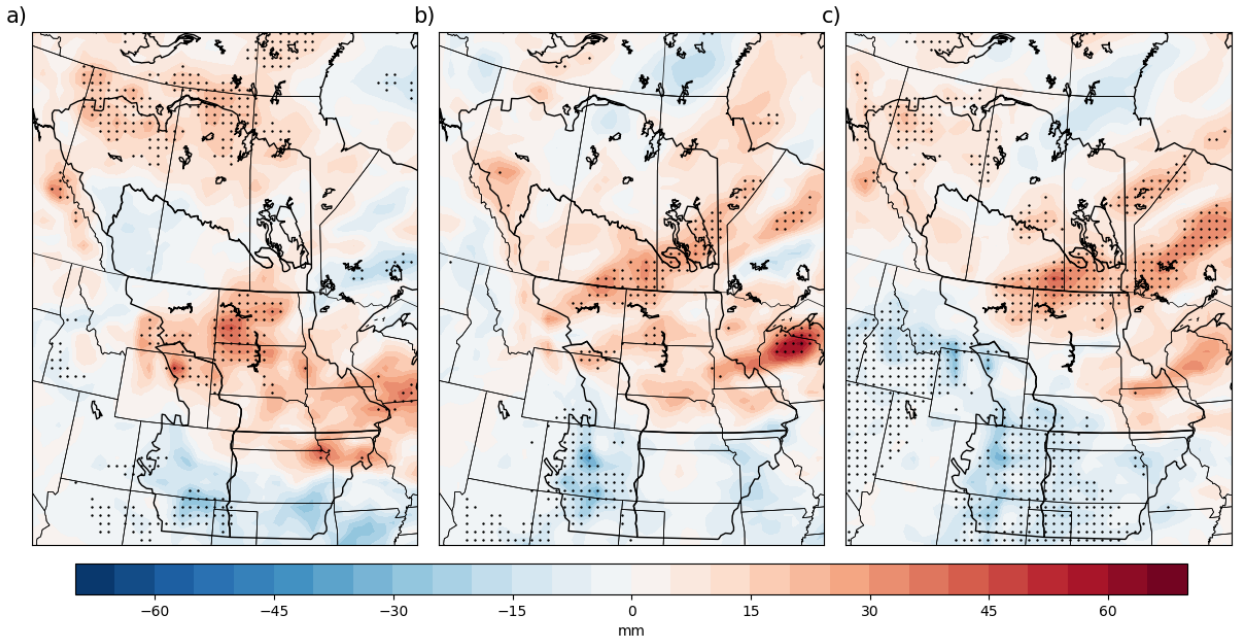

Figure 3.13 Difference (future – current) in average precipitation for MM5-CCSM for a) June b) July and c) August. Stippling indicates statistical significance at the 95% confidence level.

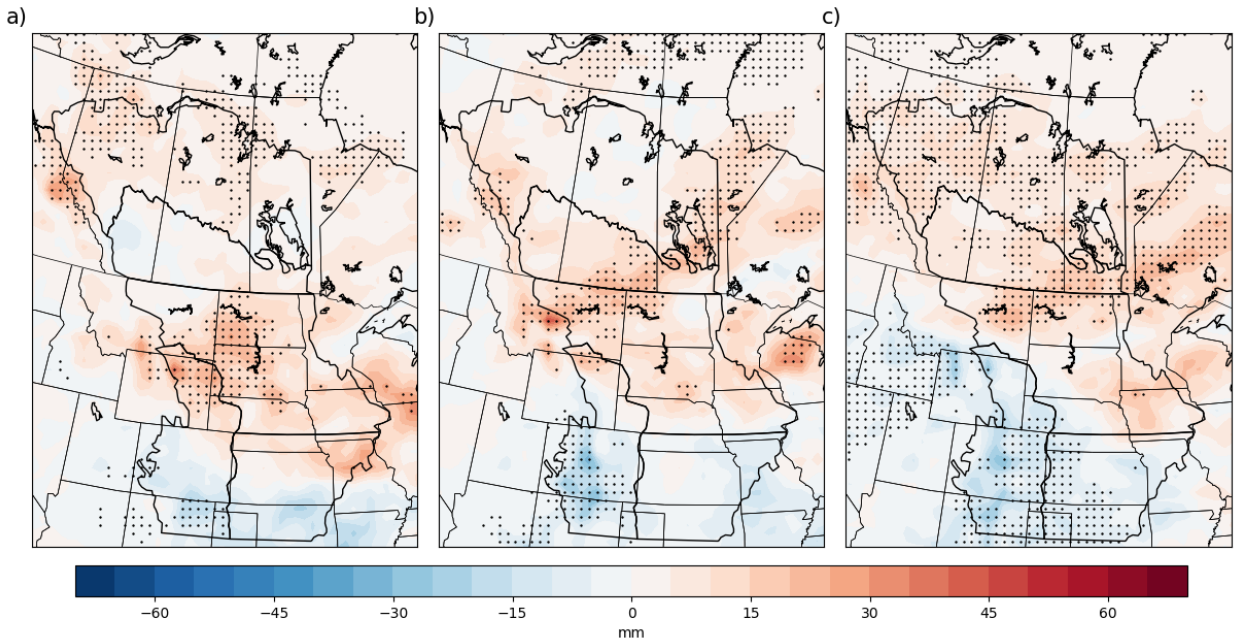

Figure 3.14 Difference (future – current) in average convective precipitation for MM5-CCSM for a) June b) July and c) August. Stippling indicates statistical significance at the 95% confidence level.

At the monthly scale, HRM3-HadCM3 shows patterns of change in June (Fig. 3.15a and Fig. 3.16a), July (Fig. 3.15b and Fig. 3.16b), and August (Fig. 3.15c and Fig. 3.16c) in convective and total precipitation that are similar to those at the seasonal scale, with decreases over CHP and few areas of significant increase. In both variables, the statistically significant decrease over CHP seen at the seasonal scale is primarily the result of significant decreases in July and August. In total precipitation, there is a significant decrease over North Dakota and northern South Dakota that is not reflected at the seasonal scale. Further, the increase in convective and total precipitation seen over central Nebraska at the seasonal scale is present in all three months.

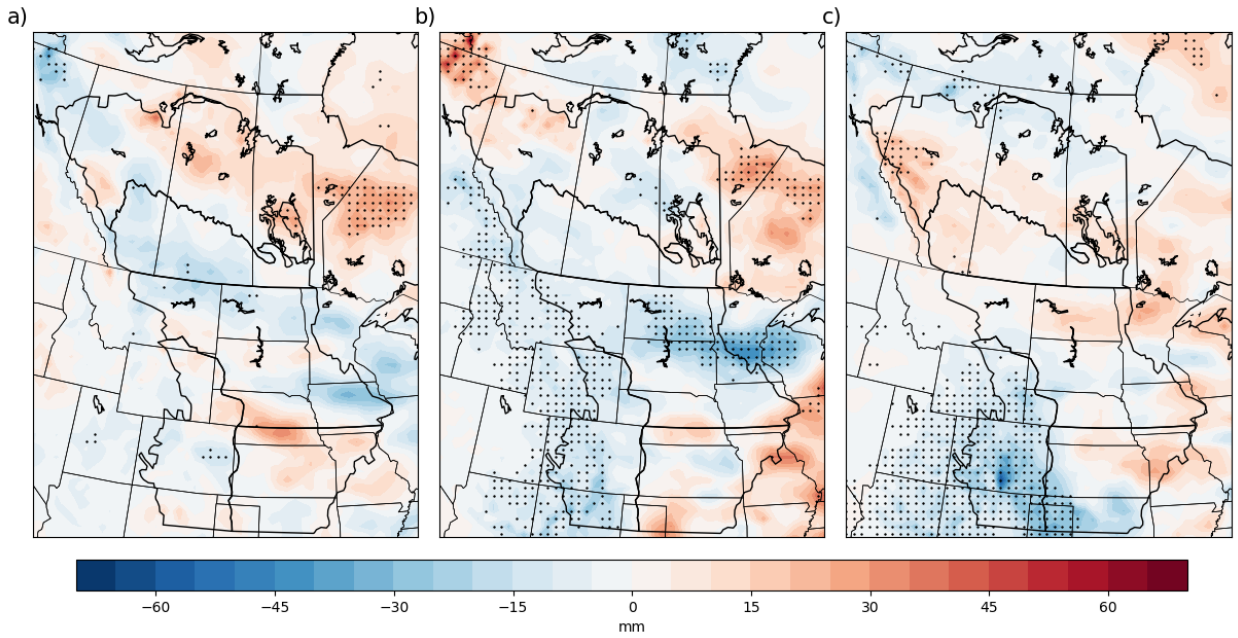

Figure 3.15 Difference (future – current) in average precipitation for HRM3-HadCM3 for a) June b) July and c) August. Stippling indicates statistical significance at the 95% confidence level.

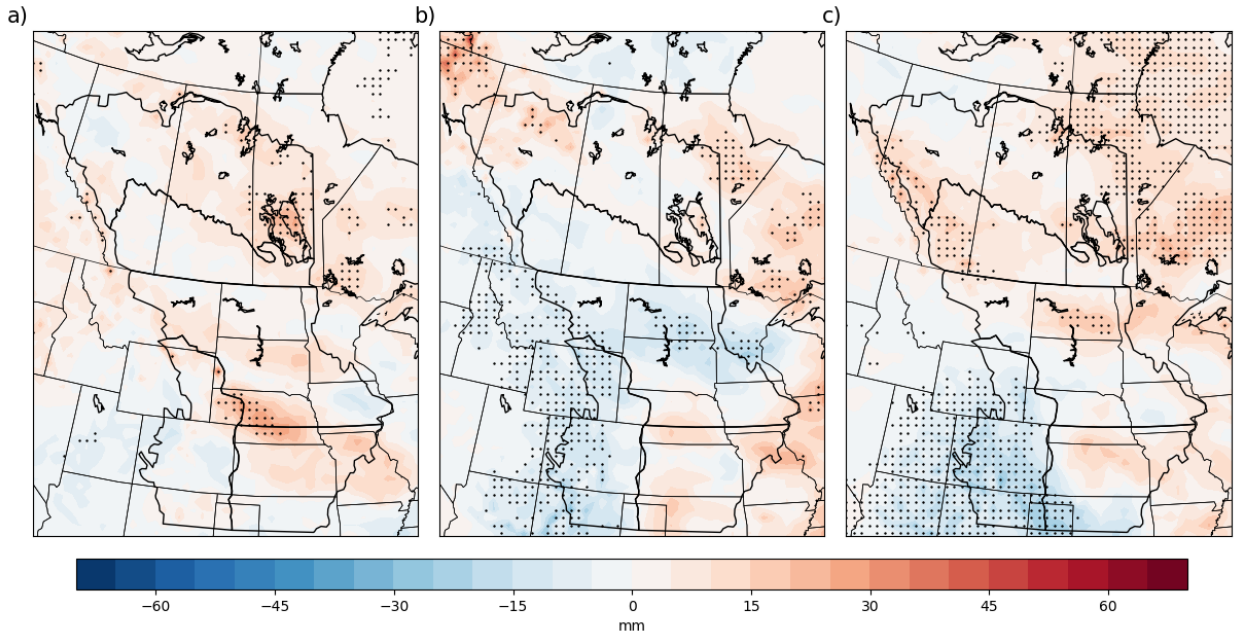

Figure 3.16 Difference (future – current) in average convective precipitation for HRM3-HadCM3 for a) June b) July and c) August. Stippling indicates statistical significance at the 95% confidence level.

3.3 Histograms

In addition to the plots in the previous section, histogram plots were created whereby daily totals were calculated at each gridpoint for the current and future time periods and then the daily totals were averaged across each ecoregion for each 30-year time period. These daily average totals were then plotted as frequency distributions for each month and season in order to illustrate change between the current and future time periods. To test for statistically significant change, the Wilcoxon rank sum test was used and the results are summarized in Tables 3.1, 3.2, and 3.3 for MM5-HadCM3, MM5-CCSM, and HRM3-HadCM3, respectively. An example of the histograms is shown below in Figure 3.17.

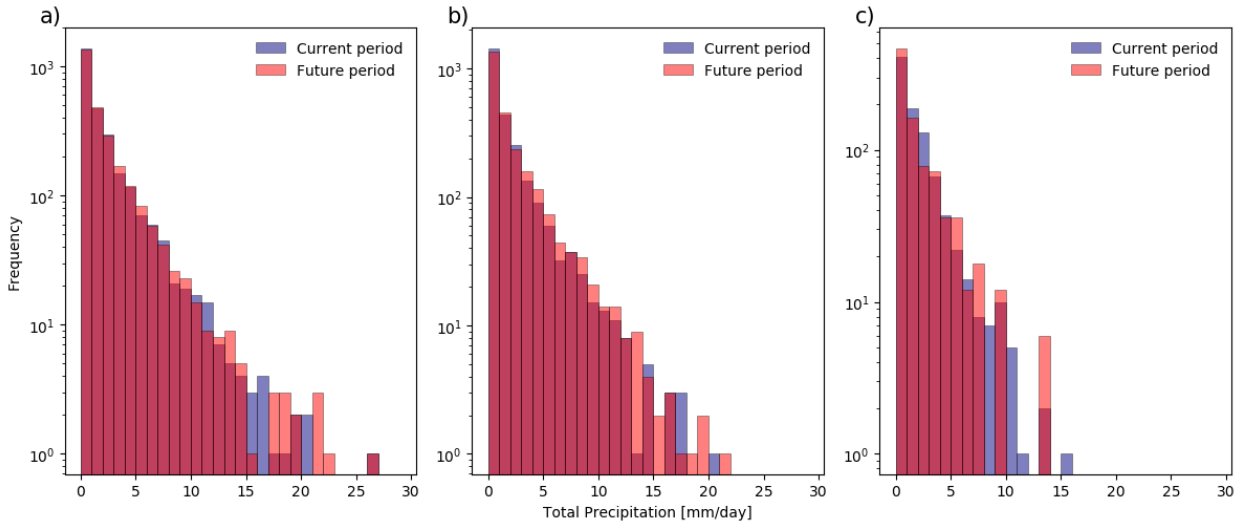

Figure 3.17 Histograms for the CAP ecoregion and JJA time period for a) MM5-HadCM3, b) MM5-CCSM, and c) HRM3-HadCM3.

Table 3.1: Results of Wilcoxon Rank Sums test between frequency distributions of current (1971 – 2000) and future (2041 – 2070) period average daily totals for MM5-HadCM3. Cells highlighted in red represent a statistically significant increase in the future and cells highlighted in blue represent a statistically significant decrease in the future.

MM5-HadCM3																
	March				April				May				MAM			
	pr		prc		pr		prc		pr		prc		pr		prc	
	Z	p-value	Z	p-value	Z	p-value	Z	p-value	Z	p-value	Z	p-value	Z	p-value	Z	p-value
CAP	-1.85E+00	6.46E-02	-3.61E-01	7.18E-01	-1.97E+00	4.84E-02	-3.92E+00	8.79E-05	-3.14E+00	1.69E-03	-2.33E+00	2.00E-02	-4.01E+00	5.96E-05	-2.77E+00	5.57E-03
USP	5.61E-02	9.55E-01	-1.92E+00	5.51E-02	5.00E-01	6.17E-01	-4.42E-01	6.59E-01	-1.11E+00	2.69E-01	-2.49E+00	1.29E-02	-2.79E-01	7.80E-01	-2.11E+00	3.48E-02
SGP	1.31E+00	1.91E-01	-1.88E+00	5.98E-02	2.65E+00	8.16E-03	2.43E+00	1.53E-02	1.27E-01	8.99E-01	-9.42E-01	3.46E-01	2.26E+00	2.37E-02	1.27E-01	8.99E-01
NWF	-6.48E-01	5.17E-01	6.71E-01	5.02E-01	-2.04E+00	4.18E-02	-4.65E+00	3.28E-06	-2.70E+00	6.90E-03	-3.25E+00	1.14E-03	-3.25E+00	1.16E-03	-2.96E+00	3.11E-03
CHP	8.08E-01	4.19E-01	-1.13E+00	2.59E-01	3.59E+00	3.37E-04	-3.04E-01	7.61E-01	7.03E-01	4.82E-01	-1.70E+00	8.99E-02	2.74E+00	6.19E-03	-1.68E+00	9.23E-02
	June				July				August				JJA			
	pr		prc		pr		prc		pr		prc		pr		prc	
	Z	p-value	Z	p-value	Z	p-value	Z	p-value	Z	p-value	Z	p-value	Z	p-value	Z	p-value
CAP	1.38E+00	1.68E-01	3.22E-01	7.48E-01	-9.38E-01	3.48E-01	-1.67E+00	9.44E-02	-1.76E+00	7.85E-02	-2.59E+00	9.57E-03	-8.49E-01	3.96E-01	-2.33E+00	2.00E-02
USP	3.72E-01	7.10E-01	-1.38E+00	1.67E-01	-8.62E-01	3.89E-01	-1.88E+00	6.04E-02	-8.06E-01	4.20E-01	-2.34E+00	1.94E-02	-6.53E-01	5.14E-01	-3.17E+00	1.53E-03
SGP	-3.34E-01	7.39E-01	-4.84E-01	6.29E-01	2.69E+00	7.14E-03	2.19E+00	2.86E-02	-5.57E-01	5.78E-01	-1.27E+00	2.05E-01	1.04E+00	2.98E-01	2.78E-01	7.81E-01
NWF	-4.19E-02	9.67E-01	-3.58E+00	3.42E-04	-8.73E-01	3.83E-01	-3.56E+00	3.71E-04	-2.19E+00	2.86E-02	-4.42E+00	9.71E-06	-1.77E+00	7.69E-02	-6.55E+00	5.81E-11
CHP	-1.49E+00	1.37E-01	-2.66E+00	7.76E-03	-2.95E+00	3.21E-03	-3.46E+00	5.39E-04	-7.46E-01	4.56E-01	-1.57E+00	1.17E-01	-3.03E+00	2.46E-03	-4.46E+00	8.13E-06

Table 3.2: Same as Table 3.1 but for MM5-CCSM.

MM5-CCSM																
	March				April				May				MAM			
	pr		prc		pr		prc		pr		prc		pr		prc	
	Z	p-value	Z	p-value	Z	p-value	Z	p-value	Z	p-value	Z	p-value	Z	p-value	Z	p-value
CAP	2.29E-01	8.19E-01	-2.42E+00	1.56E-02	1.97E+00	4.92E-02	-4.02E+00	5.84E-05	-2.74E+00	6.10E-03	-4.21E+00	2.51E-05	-5.06E-01	6.13E-01	-4.93E+00	8.14E-07
USP	1.24E+00	2.16E-01	-1.59E-02	9.87E-01	1.50E-01	8.81E-01	-3.15E+00	1.62E-03	-3.18E+00	1.46E-03	-1.12E+00	2.65E-01	-1.31E+00	1.89E-01	-1.98E+00	4.79E-02
SGP	-6.97E-02	9.44E-01	-4.94E-01	6.21E-01	1.13E-01	9.10E-01	-4.90E+00	9.74E-07	-3.48E+00	5.01E-04	-1.48E+00	1.38E-01	-1.96E+00	4.95E-02	-3.75E+00	1.79E-04
NWF	-1.49E+00	1.37E-01	-3.82E+00	1.35E-04	4.75E+00	2.04E-06	-1.83E+00	6.68E-02	-2.10E+00	3.58E-02	-6.06E+00	1.33E-09	5.14E-01	6.08E-01	-5.22E+00	1.77E-07
CHP	1.05E+00	2.92E-01	1.75E+00	7.97E-02	1.65E+00	9.95E-02	-1.64E+00	1.01E-01	2.18E+00	2.91E-02	6.25E+00	4.12E-10	2.77E+00	5.61E-03	3.74E+00	1.81E-04
	June				July				August				JJA			
	pr		prc		pr		prc		pr		prc		pr		prc	
	Z	p-value	Z	p-value	Z	p-value	Z	p-value	Z	p-value	Z	p-value	Z	p-value	Z	p-value
CAP	-6.60E-01	5.09E-01	-2.16E-01	8.29E-01	-2.44E+00	1.46E-02	-3.11E+00	1.89E-03	-3.79E+00	1.50E-04	-6.09E+00	1.16E-09	-3.96E+00	7.40E-05	-5.34E+00	9.29E-08
USP	-3.39E+00	7.05E-04	-4.95E+00	7.61E-07	-2.59E+00	9.59E-03	-1.61E+00	1.07E-01	-1.40E+00	1.61E-01	-3.40E+00	6.83E-04	-4.24E+00	2.21E-05	-5.78E+00	7.59E-09
SGP	9.43E-01	3.46E-01	-4.78E-01	6.33E-01	4.67E+00	2.94E-06	3.24E+00	1.18E-03	2.99E+00	2.80E-03	8.03E-01	4.22E-01	4.65E+00	3.32E-06	1.73E+00	8.45E-02
NWF	-3.39E+00	7.02E-04	-4.25E+00	2.11E-05	-1.91E+00	5.66E-02	-4.33E+00	1.49E-05	-3.32E+00	8.96E-04	-5.89E+00	3.91E-09	-4.95E+00	7.34E-07	-8.15E+00	3.58E-16
CHP	1.38E+00	1.66E-01	-2.92E-03	9.98E-01	3.52E+00	4.35E-04	9.85E-01	3.24E-01	6.73E+00	1.69E-11	-1.75E+00	7.94E-02	6.76E+00	1.34E-11	-4.47E-01	6.55E-01

Table 3.3: Same as Table 3.1 but for HRM3-HadCM3.

HRM3-HadCM3																
	March				April				May				MAM			
	pr		prc		pr		prc		pr		prc		pr		prc	
	Z	p-value	Z	p-value	Z	p-value	Z	p-value	Z	p-value	Z	p-value	Z	p-value	Z	p-value
CAP	3.13E-01	7.54E-01	-3.38E+00	7.22E-04	3.38E-01	7.36E-01	-5.38E-01	5.90E-01	-7.67E-01	4.43E-01	-5.41E-01	5.88E-01	3.13E-01	7.54E-01	-3.38E+00	7.22E-04
USP	-5.06E-01	6.13E-01	-5.22E+00	1.75E-07	5.33E-01	5.94E-01	4.86E+00	1.18E-06	5.73E-01	5.67E-01	-1.42E+00	1.54E-01	-5.06E-01	6.13E-01	-5.22E+00	1.75E-07
SGP	-3.02E-01	7.63E-01	-2.28E+00	2.23E-02	8.63E-01	3.88E-01	5.86E+00	4.53E-09	2.45E+00	1.44E-02	1.76E+00	7.86E-02	-3.02E-01	7.63E-01	-2.28E+00	2.23E-02
NWF	1.64E+00	1.01E-01	-1.16E+00	2.44E-01	-4.86E-01	6.27E-01	-3.33E+00	8.63E-04	3.87E-01	6.98E-01	1.88E+00	5.98E-02	1.64E+00	1.01E-01	-1.16E+00	2.44E-01
CHP	3.81E-01	7.03E-01	-1.78E+00	7.46E-02	1.12E+00	2.62E-01	1.99E+00	4.60E-02	2.82E+00	4.86E-03	4.84E+00	1.30E-06	3.81E-01	7.03E-01	-1.78E+00	7.46E-02
	June				July				August				JJA			
	pr		prc		pr		prc		pr		prc		pr		prc	
	Z	p-value	Z	p-value	Z	p-value	Z	p-value	Z	p-value	Z	p-value	Z	p-value	Z	p-value
CAP	2.89E+00	3.80E-03	2.53E+00	1.15E-02	2.21E+00	2.71E-02	8.03E-01	4.22E-01	-1.09E+00	2.74E-01	-7.50E-01	4.53E-01	2.89E+00	3.80E-03	2.53E+00	1.15E-02
USP	1.66E+00	9.65E-02	4.15E-01	6.78E-01	4.73E+00	2.19E-06	2.18E+00	2.89E-02	1.77E-01	8.59E-01	-5.31E-01	5.96E-01	1.66E+00	9.65E-02	4.15E-01	6.78E-01
SGP	3.79E-01	7.04E-01	-1.96E+00	5.04E-02	9.43E-01	3.45E-01	3.18E+00	1.46E-03	1.22E+00	2.22E-01	-1.36E-01	8.92E-01	3.79E-01	7.04E-01	-1.96E+00	5.04E-02
NWF	9.24E-01	3.55E-01	-3.46E-01	7.30E-01	1.54E+00	1.23E-01	3.16E-02	9.75E-01	1.05E+00	2.95E-01	-1.20E+00	2.30E-01	9.24E-01	3.55E-01	-3.46E-01	7.30E-01
CHP	1.76E+00	7.76E-02	4.73E+00	2.27E-06	5.03E+00	5.01E-07	7.96E+00	1.69E-15	5.66E+00	1.54E-08	5.90E-01	5.55E-01	1.76E+00	7.76E-02	4.73E+00	2.27E-06

The tables show statistically significant change similar to that shown in Sections 3.1 and 3.2. At the seasonal timescale, all three model pairings show statistically significant increases in MAM convective precipitation over CAP and USP. In contrast, only MM5-HadCM3 and MM5-CCSM are consistent in showing significant increases in MAM and JJA convective precipitation in the future over NWF. Further, only MM5-HadCM3 and MM5-CCSM agree on a statistically significant decrease in MAM total precipitation over CHP. At the monthly timescale, statistically significant changes are less consistent between the three model pairings. For total precipitation in March there is agreement over no statistically significant change; this is unsurprising considering the lack of statistically significant change in total precipitation shown in the March precipitation plots. MM5-HadCM3 and MM5-CCSM agree over a significant increase in March convective precipitation in NWF and MM5-CCSM and HRM3-HadCM3 in CAP. At the monthly scale, there is no agreement on statistically significant change between all three model pairings for any of the ecoregions.

3.4 Model Agreement

As expected from Fig. 3.1, the plots of model agreement for MAM (Fig. 3.18a) show agreement between all three model pairings on a positive change in total precipitation over much of CAP, central Saskatchewan and Alberta in NWF, southeastern and northwestern USP, and southeastern SGP. Similarly, all three pairings agreed on negative change in the southwestern part of the domain in CHP. At the monthly scale, the total precipitation plots of model agreement show a similar pattern to that of the individual model pairings. For all three pairings, the changes seen at the seasonal scale were primarily influenced by changes occurring in May. Thus, the pattern of agreement in MAM is most closely matched by the plot of model agreement for May

(Fig. 3.19c): there is agreement over positive change between all three pairings over CAP and much of USP and agreement over negative change in the southwestern part of the domain.

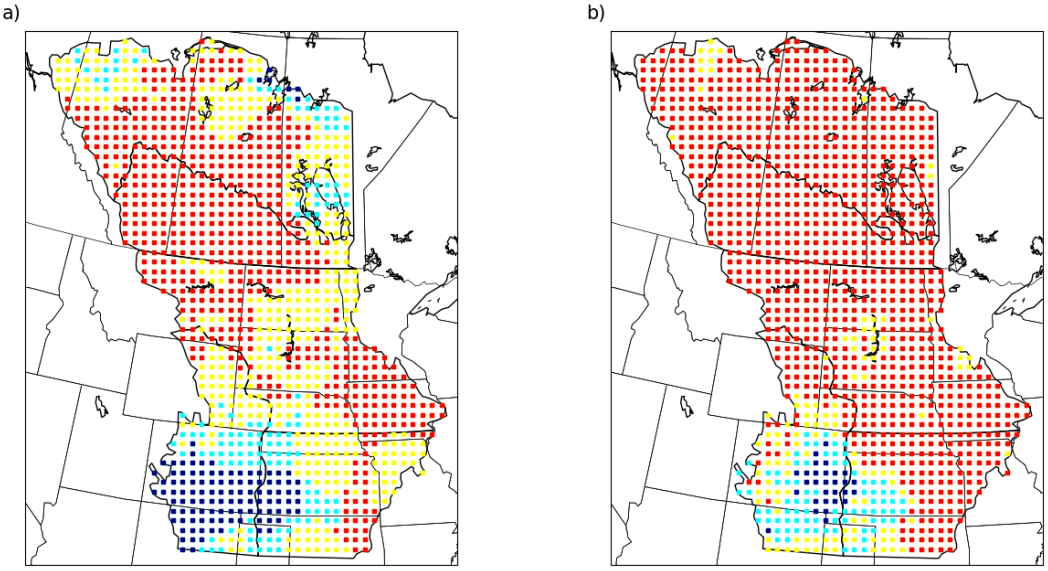

Figure 3.18 Plots of model agreement for a) total precipitation and b) convective precipitation for MAM. Red represents agreement on a positive change between three model pairings, yellow represents agreement on a positive change between two model pairings, cyan represents agreement on a negative change between two model pairings, and navy represents agreement on a negative change between three model pairings.

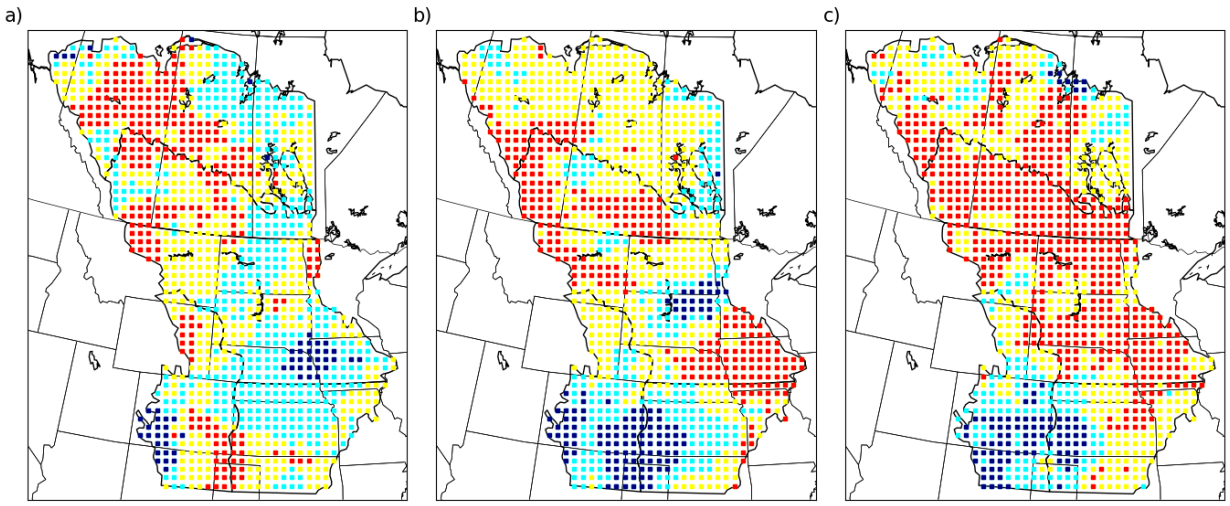

Figure 3.19 Plots of model agreement for total precipitation for a) March b) April and c) May. Legend is the same as for Fig. 3.18.

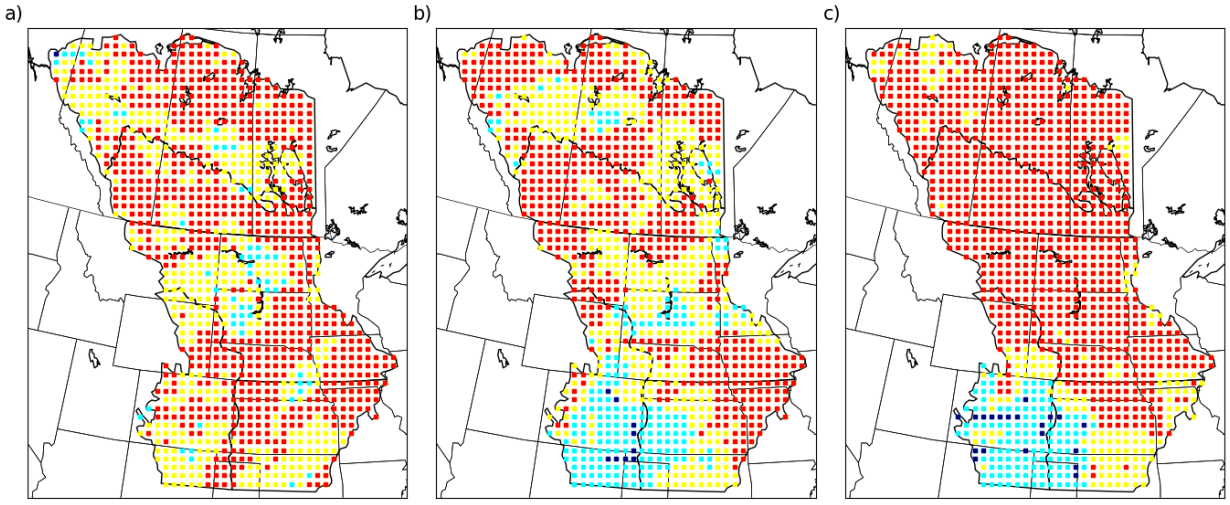

Figure 3.20 Plots of model agreement for convective precipitation for a) March b) April and c) May. Legend is the same as for Fig. 3.18.

For convective precipitation in MAM (Fig. 3.18b), there is agreement between all three pairings over almost the entire domain, excluding the southwestern part of it where there is agreement between at least two model pairings over a decrease in total precipitation. These

results are similar in pattern to that of MAM for total precipitation. Again, similar to total precipitation, the pattern of agreement in MAM is most similar to that in May (Fig. 3.20c). In April (Fig. 3.20b), the pattern of agreement is similar to that in May, except that there is agreement between at least two pairings over a larger portion of the domain than in May, both on positive and negative change. In March (Fig. 3.20a), there are small, scattered areas of agreement over negative change between two model pairings, with the rest of the domain indicating agreement over a positive change between two model pairings.

For total precipitation in JJA (Fig. 3.21a), there are only a few areas that show agreement between all three pairings about positive or negative change, with areas of positive change concentrated over NWF and a small area of negative change along the southern boundary of the domain. The rest of the domain indicates agreement between only two pairings. This is unsurprising, considering Fig. 3.9, where MM5-HadCM3 primarily indicates increases in total precipitation and HRM3-HadCM3 primarily decreases. At the monthly scale (Fig. 3.22) – similar to the monthly plots of statistically significant change – there is not much consistency between months on what has influenced the changes at the seasonal scale. In particular, over southern Alberta and Saskatchewan, there is agreement between all three model pairings over negative change in June (Fig. 3.22a) and over positive change in August (Fig. 3.22c). Neither is reflected at the seasonal scale. However, the agreement between the three pairings over positive change in Alberta in NWF reflected at the seasonal scale is also seen at the monthly scale. Further, the agreement over negative change between MM5-CCSM and HRM3-HadCM3 is reflected at the monthly and seasonal scale.

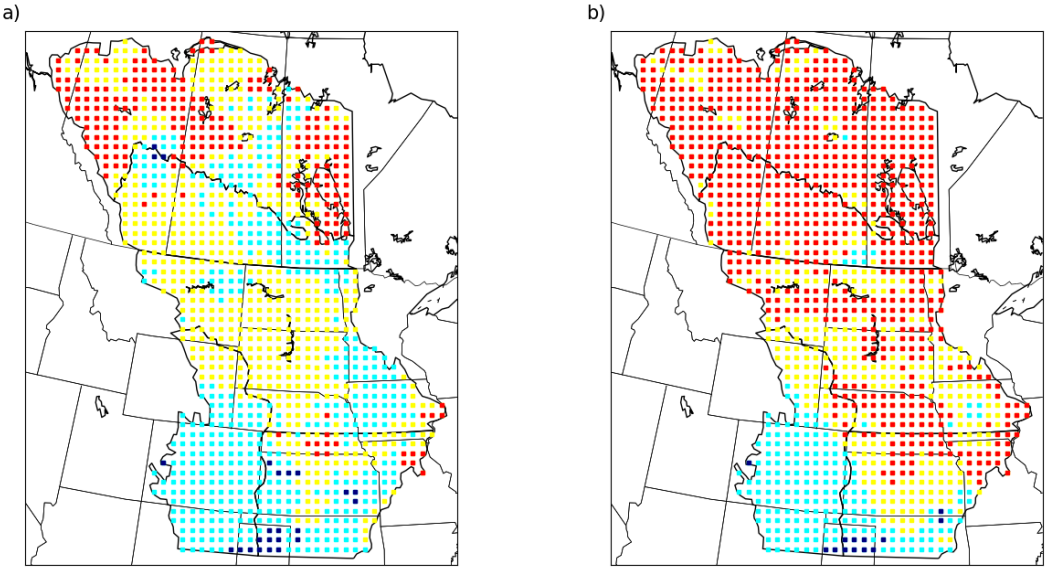

Figure 3.21 Plots of model agreement for a) total precipitation and b) convective precipitation for JJA. Legend is the same as for Fig. 3.18.

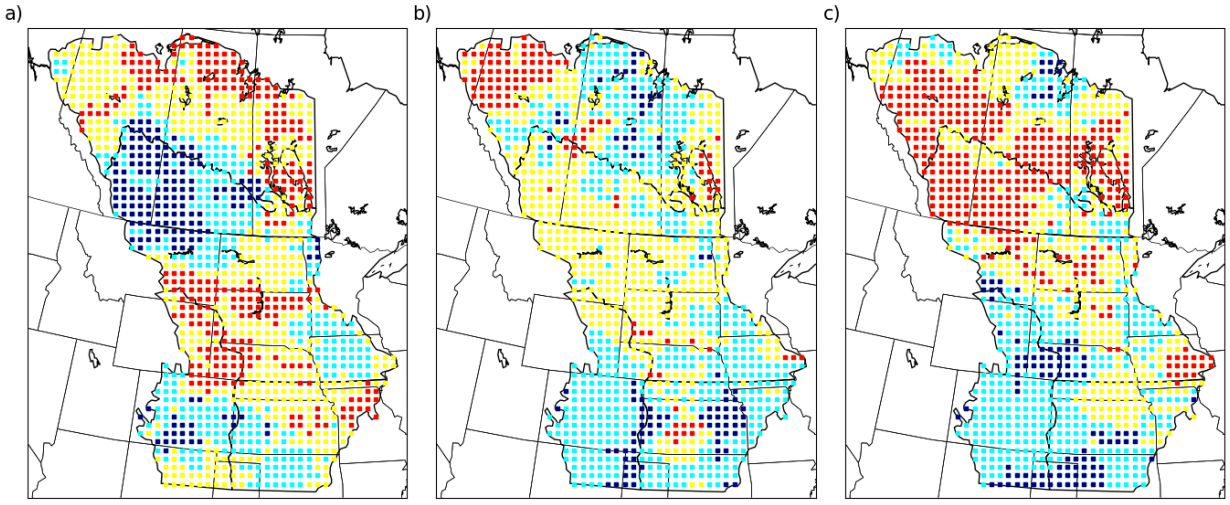

Figure 3.22 Plots of model agreement for total precipitation for a) June b) July and c) August. Legend is the same as for Fig. 3.18.

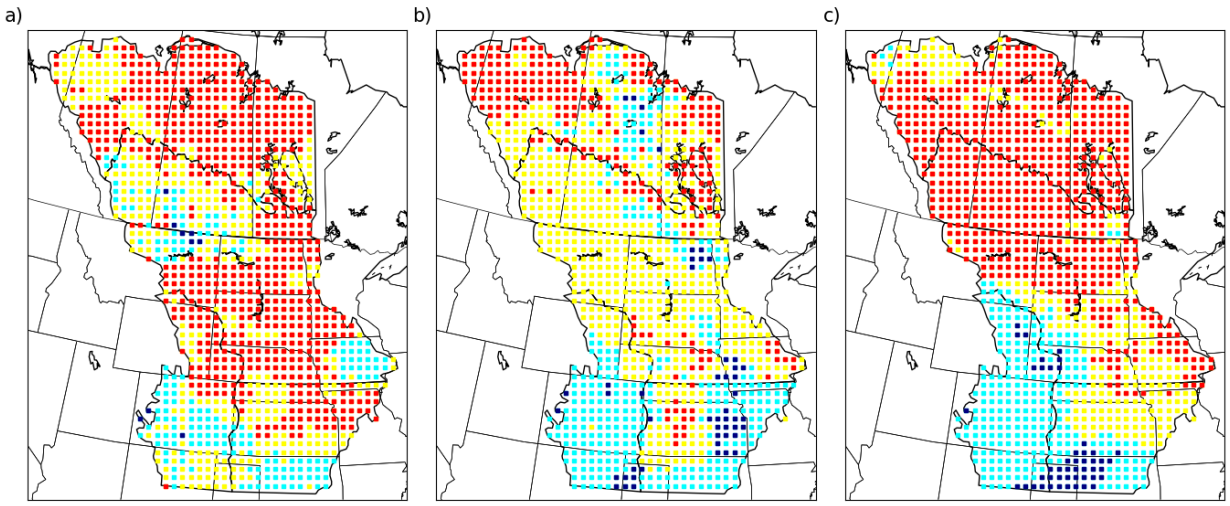

Figure 3.23 Plots of model agreement for convective precipitation for a) June b) July and c) August. Legend is the same as for Fig. 3.18.

For convective precipitation in JJA (Fig. 3.21b), there are large areas of agreement between the three model pairings over most of Alberta, Saskatchewan, and Manitoba in NWF and CAP. There are smaller areas of agreement over parts of USP and northern SGP. There is an organized region of agreement between two model pairings on negative change over CHP and part of SGP; these are MM5-CCSM and HRM3-HadCM3 since MM5-HadCM3 indicated increases over this region. The June (Fig. 3.23a) and August (Fig. 3.23c) plots show agreement over positive change between the three pairings over much of NWF and USP. In July (Fig. 3.23b), there is primarily agreement between only two model pairings over these same areas. In the southwestern part of the domain, there is a consistent region where two model pairings agree on negative change in convective precipitation, though this region is much smaller in June than in July and August. In general, the pattern of agreement seen at the seasonal scale is most closely reflected by that in August; this would suggest that the changes in August have a greater effect (i.e. change of greater magnitude) on the seasonal average than the other two months.

3.5 Discussion

The first objective of this research is to characterize the future change in convective and total precipitation over western Canada and the central U.S. Plains. The results presented in this chapter indicate either an increase in convective precipitation where there are corresponding decreases in total precipitation or concurrent increases in both convective and total precipitation. It is important to note that in each ecoregion the mechanisms through which precipitation occurs vary and thus future changes in each ecoregion have to be discussed in the context of these mechanisms. Though there are similarities, the results of the three model pairings used in this research differ spatially and in magnitude; these differences are the result of how physical processes are represented in individual models, such as the parameterization of sub-grid processes (Sobolowski & Pavelsky, 2012).

3.5.1 Colorado Rockies and High Plains

In this research, the CHP ecoregion encompasses the Colorado Rockies and the Colorado High Plains, making it a complex region in terms of precipitation, with most of the precipitation in the mountains falling in the winter as snow as opposed to the eastern plains where most of the annual precipitation falls during the summer in July and August in the form of thunderstorms (Alexander et al., 2013; Bukovsky et al., 2017). This region is also unique from the other ecoregions as it is influenced by moisture flowing from both the Gulf of Mexico and the Pacific Ocean that interacts with the Colorado Rockies (Alexander et al., 2013). There has been a projected decrease in summer precipitation over Colorado (Mahoney et al., 2013). This projected decrease is reflected by MM5-CCSM and HRM3-HadCM3 which both show primarily statistically significant decreases in total and convective precipitation over Colorado and New Mexico, though MM5-CCSM indicates increase over the northern tip of the ecoregion, in

northeast Wyoming. In contrast, MM5-HadCM3 exhibits primarily insignificant increases over Colorado and New Mexico.

3.5.2 Southern Great Plains

Bukovsky et al. (2017), who exclusively examine warm-season precipitation in SGP, characterize the region as having an annual peak in precipitation in May which results from a combination of instability from surface heating, moisture from the Gulf of Mexico, and many possible mechanisms to cause lifting, thus making thunderstorms the primary source of precipitation in this region. After May, the region is characterized by a decrease in precipitation in June, with July and August being comparably dry as summer precipitation shifts north. Bukovsky et al. (2017) further investigated the findings of Mearns et al. (2013) and Patricola and Cook (2013) using an ensemble of 17 CMIP3 simulations, 35 CMIP5 simulations, and the full NARCCAP ensemble. Mearns et al. (2013), using the ensemble mean of the 11 available NARCCAP RCM simulations, found there to be a strong signal for decreased precipitation in the future over SGP in JJA. Patricola and Cook (2013) (as cited in Bukovsky et al., 2017) found similar results using 7 NARCCAP RCMs; additionally, they found increased precipitation in April and May over the region.

Bukovsky et al. (2017) found a northward shift in convection throughout JJA with many of the simulations showing statistically significant decreases in June precipitation, indicating an earlier end to the April and May wet period that is characteristic of the region. More specifically, the pattern found was increased precipitation across the region in April, increases (decreases) in the northern (southern) half of the region in May, a similar pattern or entirely decreases in June, and decreased precipitation in July and August (Bukovsky et al., 2017). This pattern is reflected by MM5-CCSM in the results presented here; in particular, this pairing shows statistically

significant increases in convective precipitation in May and a statistically significant decrease in total and convective precipitation in August. In contrast to MM5-CCSM, the results of MM5-HadCM3 and HRM3-HadCM3 do not indicate the same pattern of change; similarly, Bukovsky et al. (2017) found that none of the HadCM3-driven RCM simulations in the NARCCAP ensemble showed a pattern of change from April through May consistent with the other RCM simulations and were considered to not be credible in their representation of future changes in precipitation over SGP. This lack of consistency is something they attribute to the upper-level jet and Great Plains low-level jet not being realistically simulated over North America by the HadCM3 and the HadCM3-driven simulations. Thus, MM5-CCSM provides the most accurate representation of future change in precipitation over SGP.

3.5.3 United States Prairies

In general, over the United States, RCM projections of future change in mean summer precipitation are questionable; this is primarily the result of differing methodologies, such as ensemble size, the domain, or the emissions scenario used (Bukovsky et al., 2017). Harding and Snyder (2014) and Harding, Snyder, and Leiss (2013) examined the central U.S. by dividing it into separate regions, including a north central region which encompasses an area similar to that of the USP ecoregion defined in this research. Their findings for this area indicate an increase in heavy rainfall events (such as thunderstorms) and a decrease in light precipitation events (Harding et al., 2013), and subsequently a decrease in the number of rainy days and an increase in the annual maximum number of consecutive days with no precipitation in the late summer months (Harding & Snyder, 2014). These latter findings agree with that of previous research and observed trends since the mid-20th century that there will be an increase in heavy rainfall events from April to July, with decreased precipitation in August and September (Harding & Snyder,

2014). Their findings are supported by prior work done by Bukovsky and Karoly (2011) over the central U.S., who found decreases in the frequency of all but heavy rainfall events, increases in the frequency and intensity of both heavy precipitation and of rain in general, and a decrease (increase) in the number of 6-hour periods with (without) rainfall. All of these findings indicate a potential future increase in both flooding and drought (Bukovsky & Karoly, 2011). In general, all three model pairings in this research do not reflect the pattern of change discussed above; they do, however, indicate increased convective precipitation as a percentage of total precipitation (Appendix A), thus agreeing with previous studies that there will be an increase in heavy rainfall events in the future. The models agree on increased convective and total precipitation in May, however, there is no consensus on a sign of change in April and June through August. The shift from increased precipitation in April through July to decreases and subsequent drying in August and September is best reflected by MM5-CCSM. It can be seen in Fig. 3.5b – c and Fig. 3.6b – c that there are increases in convective and total precipitation in April and May (excluding a region of insignificant decrease over South Dakota in April) shown in MM5-CCSM. Similarly, increases can be seen in both variables in June and July. In August, there are still increases shown over the region; however, there is an obvious shift of precipitation northward, with decreases and subsequent drying shown in the southern part of the region (Fig. 3.13c and Fig. 3.14c). The inability of MM5-HadCM3 and HRM3-HadCM3 to accurately represent this pattern of change may be the result of the same issues that yielded poor simulation of precipitation over SGP discussed by Bukovsky et al. (2017).

3.5.4 Canadian Prairies and Northwest Boreal Forest

Over western Canada, studies using RCMs to examine future changes in precipitation extremes have suggested increases in precipitation frequency and intensity. Mladjic et al. (2011)

found there to be an increase in 20-year regional return levels of 1-day (i.e. heavy rainfall events) to 7-day (i.e. longer-duration precipitation events) to increase; this increase was found more likely to be statistically significant than the increases for the 50- and 100-year return levels. Similarly, Mailhot et al. (2012) found increases in 6-hour to 5-day durations for 2- to 20-year return levels and Li et al. (2018) found increases in the amount and intensity of precipitation over western Canada. These findings would indicate an overall increase in precipitation, including short- and longer-duration precipitation events and their intensities, as opposed to findings for parts of the United States where heavy precipitation events (and their intensities) and dry days between events are projected to increase.

Over NWF, the three model pairings indicate either concurrent increases or decreases in both convective and total precipitation or increases in convective precipitation where there are decreases in total precipitation over these ecoregions. These findings agree with those discussed above that there will be an increase in both the frequency and intensity of precipitation events over western Canada. Further, all three pairings show large areas of agreement over increases in convective precipitation at the seasonal scale in JJA and in August. In June, there is a large area of agreement in NWF and in July over central Alberta. Like NWF, the results of the three model pairings over CAP are similar, showing increased convective precipitation in the future. Further, the three pairings agree over increases in convective precipitation at the seasonal scale in JJA and in August over this ecoregion.

Chapter 4 Results – Severe Weather Parameters

As stated in the Introduction, it is generally considered that there are four environmental conditions required to form a severe thunderstorm: low-level humidity, instability, strong wind shear, and a triggering mechanism to cause lifting (Stull, 2015). Dewpoint temperature is considered a good measure of humidity in the boundary layer (Stull, 2015), so we use surface dewpoint temperature and mixed-layer dewpoint temperature to represent this condition. High dewpoint temperatures are considered a good indication of a warm, moist boundary layer, which is critical for providing the necessary latent heat (i.e. thermodynamic energy) to fuel convective storms (e.g. Stull, 2015). In this research, we use surface dewpoint temperature and 50 mb mixed-layer dewpoint temperature as parameters to describe moisture in the boundary layer. Buoyant energy (i.e. instability) increases as water vapour condenses and latent heat is released (Stull, 2015); CAPE is a measure of this buoyant energy and we use three different measures of CAPE to represent instability. Similarly, we use MLCIN as a measure of the work that needs to be done by a triggering mechanism against the negative buoyancy that exists above the mixed-layer (Stull, 2015). Wind shear serves to feed warm, moist boundary-layer air into a moving thunderstorm. We use the vector wind difference between the surface and 6 km and the surface and 1 km, as it is a common surrogate measure of vector wind shear (Stull, 2015). Finally, for the purpose of this research, we use the occurrence of convective precipitation as a proxy for a triggering mechanism; this is the same method used as Trapp et al. (2007) (as cited in Tippett, Allen, Gensini, & Brooks, 2015). The other three conditions are discussed separately below, based on the conditions necessary for the formation of a severe thunderstorm.

4.1 Moisture & Thermodynamic Energy

The MM5-HadCM3 (Figs. 4.1 – 2a) plots of surface and mixed-layer dewpoint temperature show statistically significant increases across the entire domain at the seasonal and monthly timescales. The MM5-CCSM plots show similar statistically significant increases in these parameters over all of the ecoregions except CHP. At the seasonal scale (Figs. 4.1 – 2b), there are significant increases over the northern tip of the ecoregion with primarily insignificant decreases over the rest of the region. At the monthly timescale, this pattern of change is most similar to the August plots of dewpoint temperature (plots not shown).

At the seasonal scale, the HRM3-HadCM3 plots of surface dewpoint temperature (Fig. 4.1c) show statistically significant increases (though of lesser magnitude than MM5-HadCM3 and MM5-CCSM) over most of the domain except for parts of CHP. The seasonal plots of mixed-layer dewpoint temperature (Fig. 4.2c) show statistically significant increases across the entire domain. At the monthly scale (plots not shown), HRM3-HadCM3 shows significant increases in surface dewpoint and mixed-layer dewpoint temperature across the entire domain in June. The July plots of mixed-layer dewpoint temperature show significant increases across the entire domain except over central USP and western CHP. The July plots of surface dewpoint show a similar pattern of change but with small areas of significant decrease over USP and CHP. The August plots of both parameters show significant increases across the domain with significant and insignificant decreases over CHP.

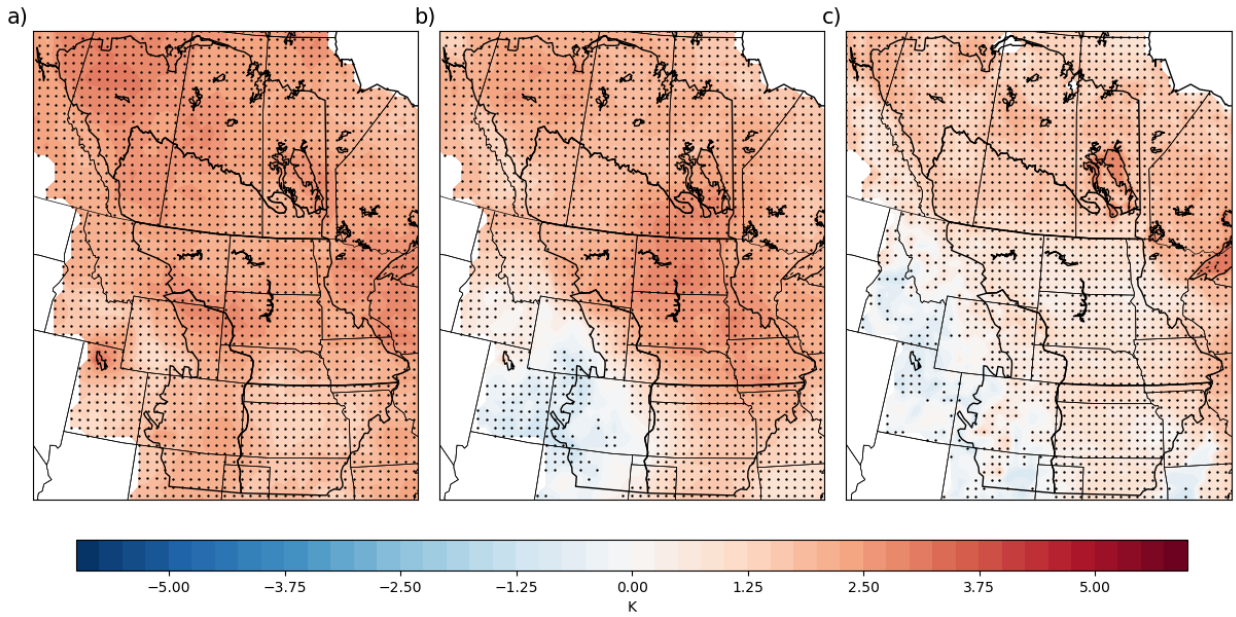

Figure 4.1 Difference (future – current) in median summer (JJA) surface dewpoint temperature for MM5-HadCM3 at 0000 UTC (b) MM5-CCSM (c) HRM3-HadCM3. Stippling indicates statistical significance at the 95% confidence level.

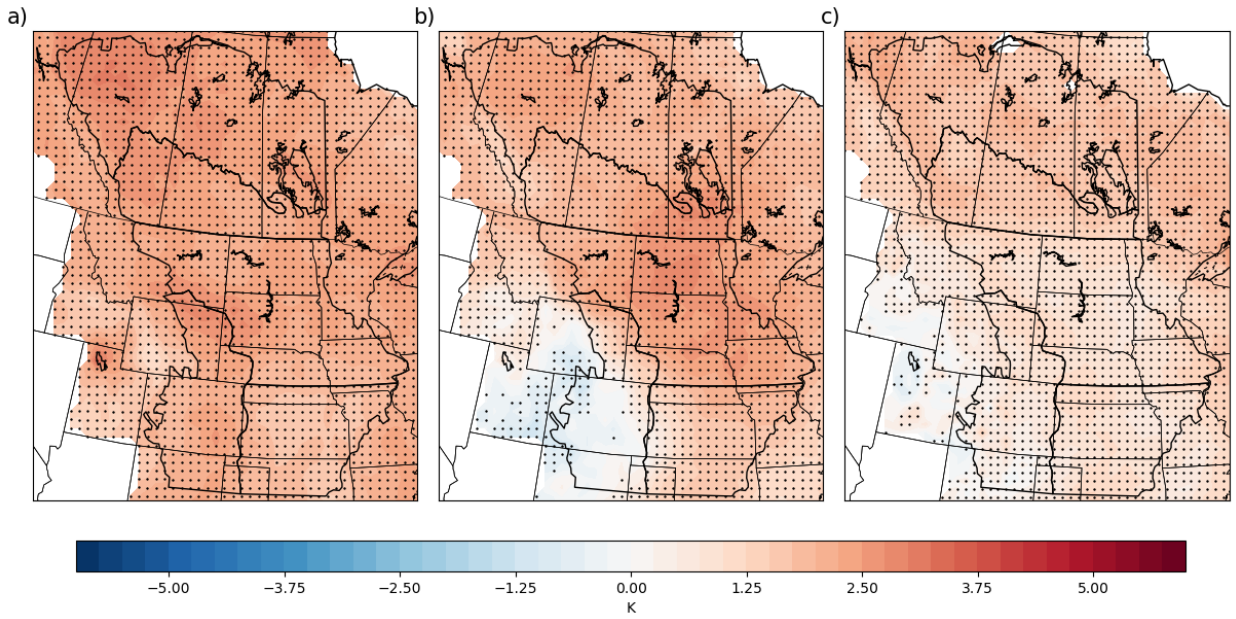

Figure 4.2 Difference (future – current) in median summer (JJA) mixed-layer dewpoint temperature for MM5-HadCM3 at 0000 UTC (b) MM5-CCSM (c) HRM3-HadCM3. Stippling indicates statistical significance at the 95% confidence level.

4.2 Instability

In general, at the seasonal scale, the MM5-HadCM3 plots of CAPE (Figs. 4.3 – 5a) show statistically significant increases that are concentrated over the northern part of the domain, including much of USP, CAP, Alberta and Saskatchewan in NWF, and the northern part of CHP. The July and August plots (Figs. 4.6 – 4.8b and Figs. 4.6 – 4.8c, respectively) of these parameters reflect this pattern of change most closely, whereas the June plots (Figs. 4.6 – 4.8a) show statistically significant increases over SGP that are not reflected at the seasonal scale. However, the plots for all three months are consistent in showing a significant increase over northern CHP.

The MM5-CCSM plots of SBCAPE and MUCAPE for JJA (Figs. 4.3 – 4b) show significant increases across USP and SGP with significant decreases over southwestern CHP and northern Saskatchewan in NWF. This is similar to the change shown in the July and August plots (Figs. 4.9 – 10b and Figs. 4.9 – 10c, respectively) for these parameters; however, the August plots do not show the significant decrease over northern Saskatchewan whereas the July plots do. In contrast, the MM5-CCSM plot of MLCAPE for JJA (Fig. 4.5b) show significant increases over most of the domain, excluding most of Saskatchewan and Manitoba in NWF where there is no significant change and a small area of significant decrease in western CHP. Again, these changes are most consistent with those in July and August (Fig. 4.11b and Fig. 4.11c, respectively).

The HRM3-HadCM3 seasonal plots of CAPE (Figs. 4.3 – 5c) show significant increases across most of the domain, excluding northwestern USP where there is no significant change and southern CHP where these are significant decreases. This is most consistent with changes in August (Figs. 4.12 – 14c), as increases in June (Figs. 4.12 – 14a) are primarily concentrated over

USP and in the southern and northwestern (over Alberta in NWF) parts of the domain. The July plots (Figs. 4.12 – 14b) for all three parameters are consistent in showing some extent of significant decrease over southern CHP. In contrast, the June plots show some extent of significant increase in this region.

At the seasonal scale, the three model pairings show organized statistically significant increases (represented as blue) in MLCIN. MM5-HadCM3 (Fig. 4.15a) shows significant increases (greater capping) over large portions of all of the ecoregions, excluding NWF where there is little statistically significant change. MM5-CCSM (Fig. 4.15b) shows increases over most of USP, SGP, and parts of CHP. HRM3-HadCM3 (Fig. 4.15c) shows statistically significant increases over almost the entire domain, except over central USP. The MM5-HadCM3 monthly plots (Fig. 4.16) show less organized regions of significant increase than at the seasonal scale, with areas of insignificant decrease interspersed between these regions. At the monthly scale, the MM5-CCSM June, July, and August plots (Fig. 4.17) are consistent with the changes seen at the seasonal scale, with significant increases in MLCIN extending across most of the southern three ecoregions and primarily insignificant change over CAP and NWF. For HRM3-HadCM3, there are organized regions of significant increase in June (Fig. 4.18a) over most of the domain, including central USP, and insignificant decreases over SGP. In July (Fig. 4.18b) there are significant increases over most of the domain, but insignificant increases and decreases across USP. In August (Fig. 4.18c), the pattern of increase is similar to that seen at the seasonal scale with a large region of statistically significant decrease over central USP in August. The changes shown by HRM3-HadCM3 in July and August appear to contribute most strongly to the changes shown at the seasonal scale.

As seen in Section 3.2, there is an overprediction of convective precipitation over Lake Winnipeg and Lake Manitoba as well as Lake Superior. Further, the model pairings occasionally show high values of CAPE and MLCIN over these lakes; for example, HRM3-HadCM3 shows high values of SBCAPE and MUCAPE at the seasonal and monthly timescales over the lakes. To the best of our knowledge, the overprediction of precipitation in these pairings over the lakes has not been discussed in prior literature. This error could be the result of how lakes are handled by the two RCMs. For example, if lakes are not represented as three-dimensional bodies of water, then their thermal stratification, heat storage capacity, and thermal inertia may be misrepresented in projections. If water bodies are projected as being warmer than in reality, this would result in increased evaporation and subsequently increased precipitation over the lakes.

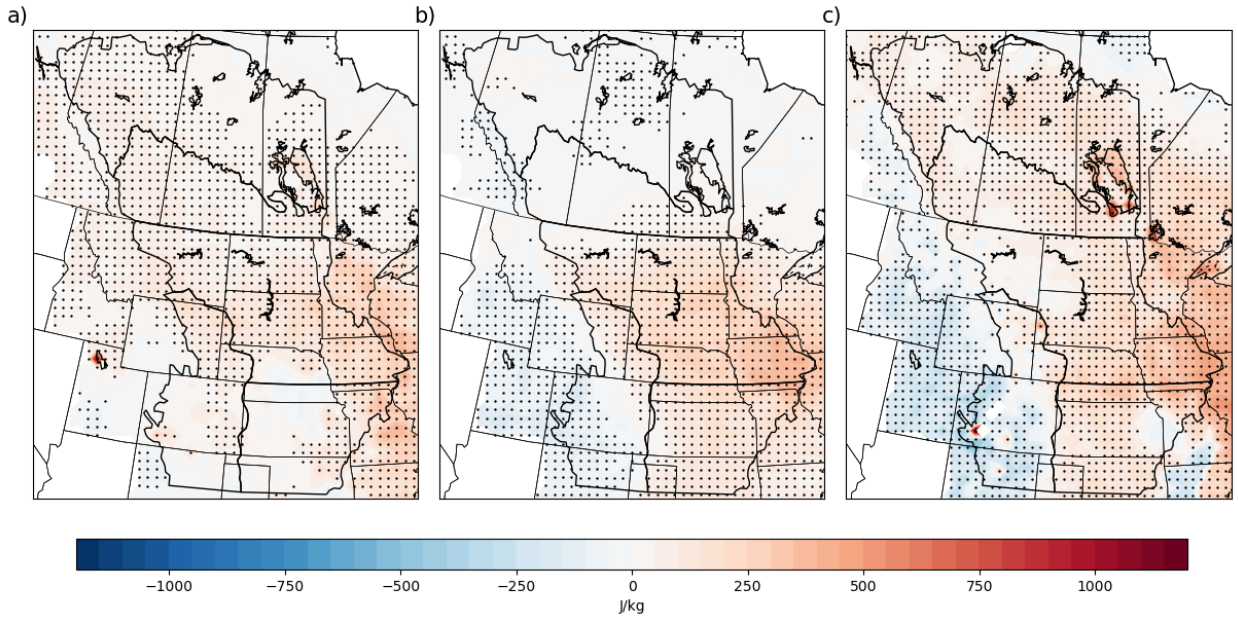

Figure 4.3 (a) Difference (future – current) in median summer (JJA) SBCAPE for MM5-HadCM3 at 0000 UTC (b) MM5-CCSM (c) HRM3-HadCM3. Stippling indicates statistical significance at the 95% confidence level.

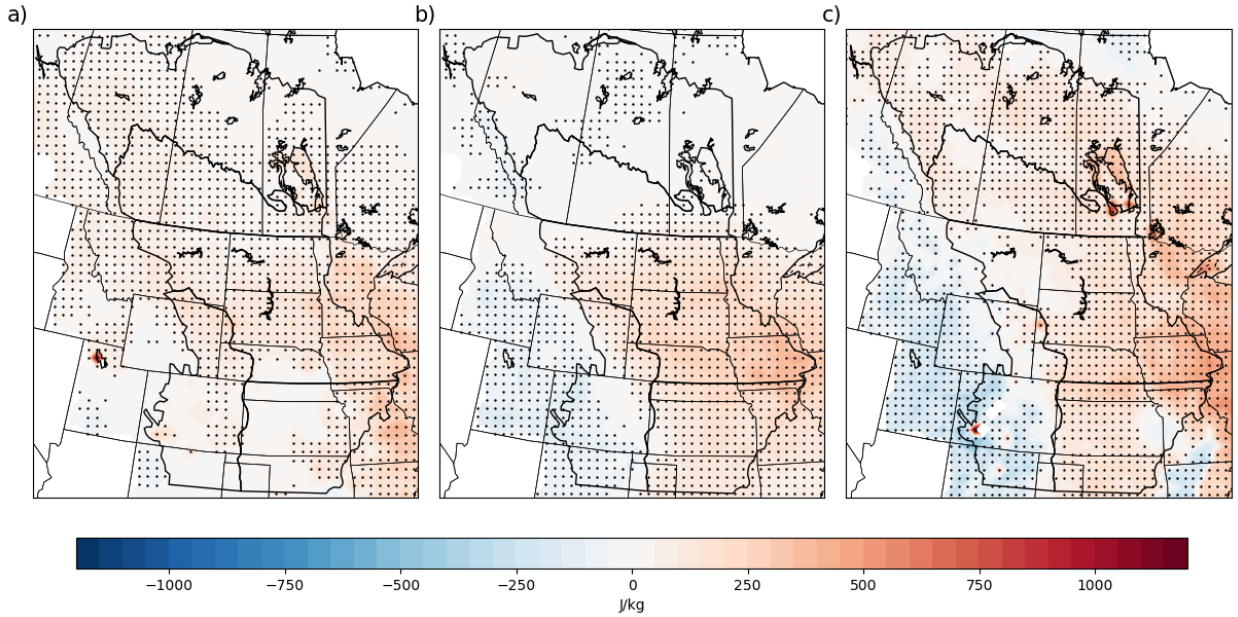

Figure 4.4 (a) Difference (future – current) in median summer (JJA) MUCAPE for MM5-HadCM3 at 0000 UTC (b) MM5-CCSM (c) HRM3-HadCM3. Stippling indicates statistical significance at the 95% confidence level.

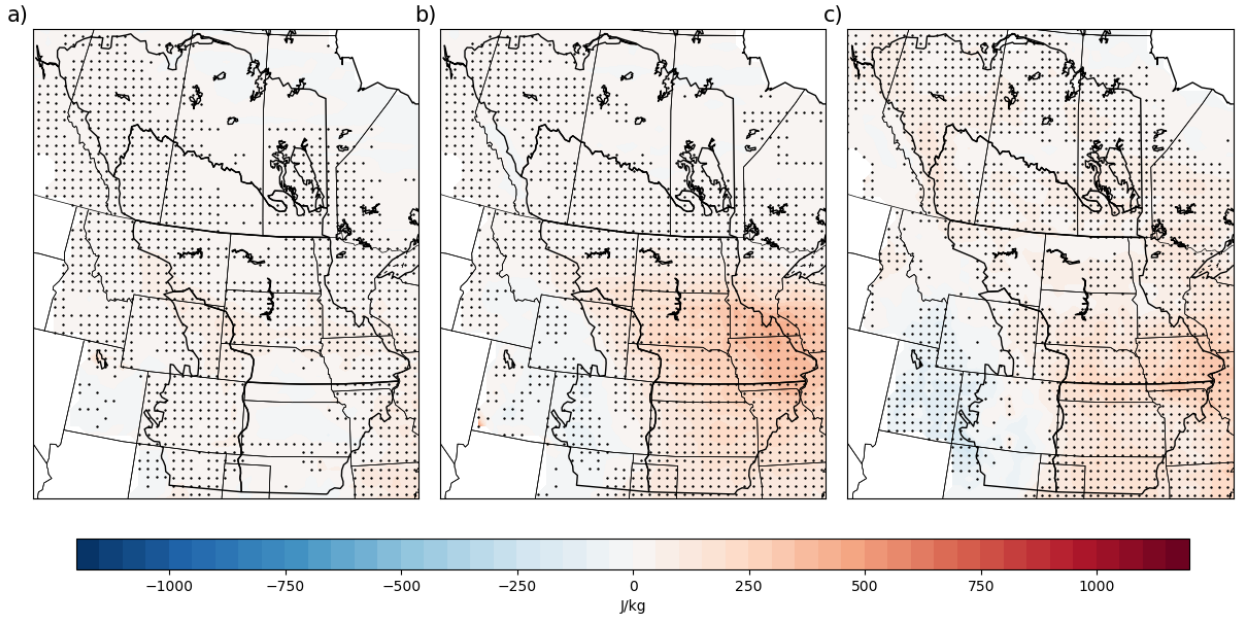

Figure 4.5 (a) Difference (future – current) in median summer (JJA) MLCAPE for MM5-HadCM3 at 0000 UTC (b) MM5-CCSM (c) HRM3-HadCM3. Stippling indicates statistical significance at the 95% confidence level.

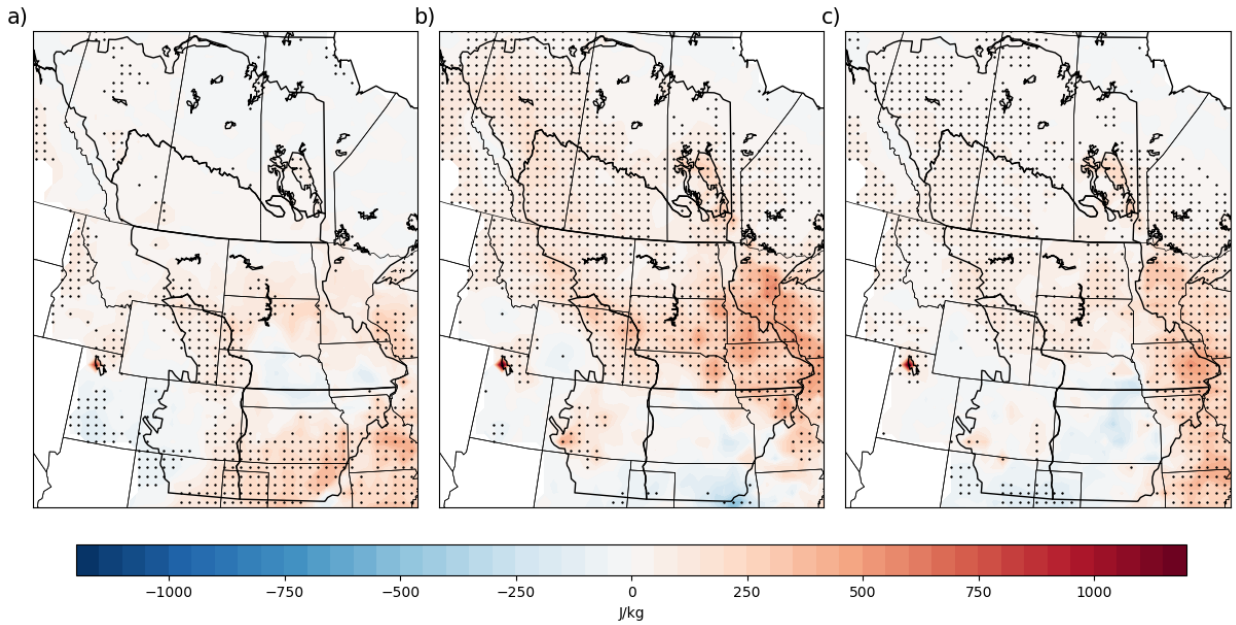

Figure 4.6 Difference (future – current) in median SBCAPE for MM5-HadCM3 for a) June b) July and c) August at 0000 UTC. Stippling indicates statistical significance at the 95% confidence level.

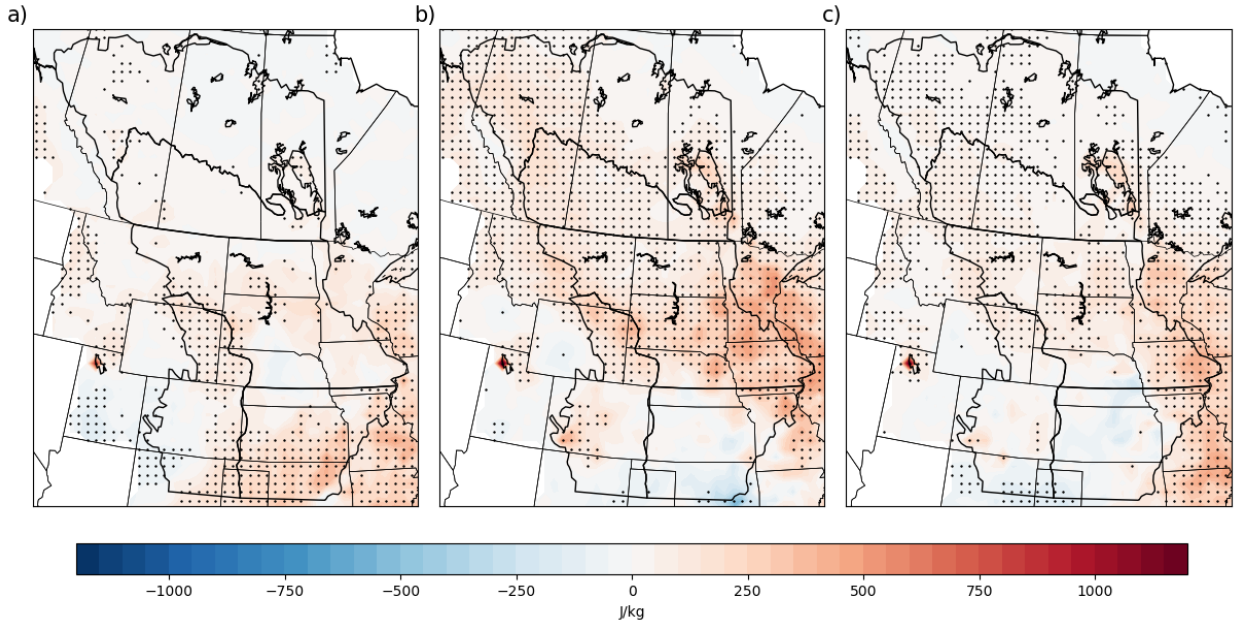

Figure 4.7 Difference (future – current) in median MUCAPE for MM5-HadCM3 for a) June b) July and c) August at 0000 UTC. Stippling indicates statistical significance at the 95% confidence level.

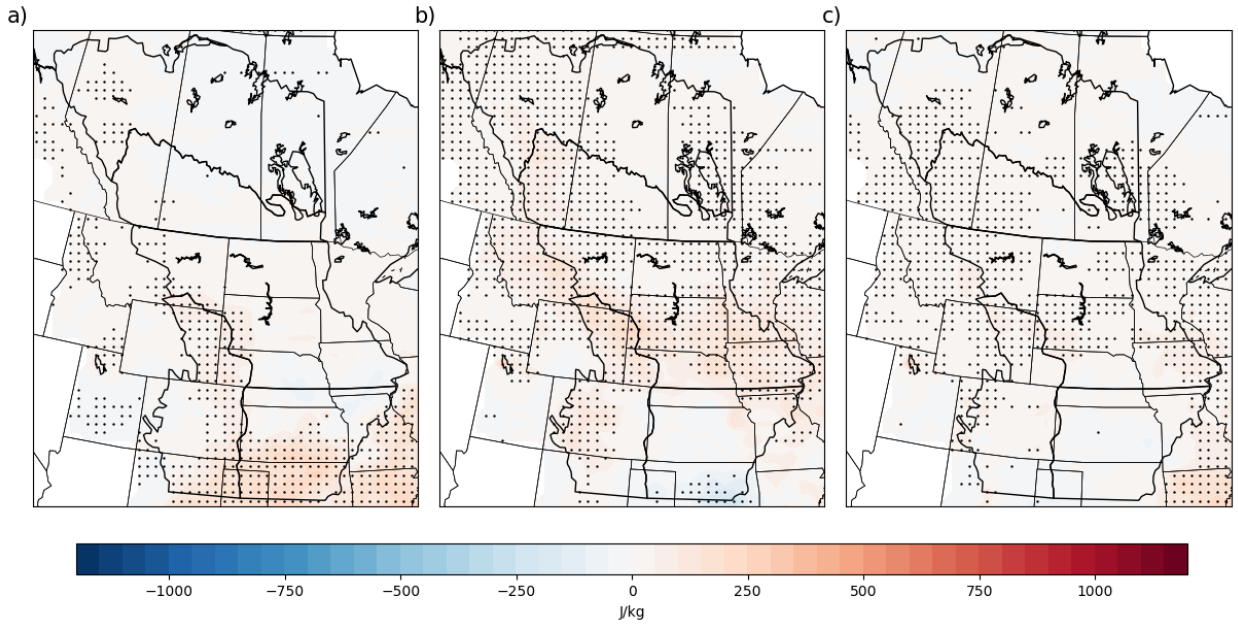

Figure 4.8 Difference (future – current) in median MLCAPE for MM5-HadCM3 for a) June b) July and c) August at 0000 UTC. Stippling indicates statistical significance at the 95% confidence level.

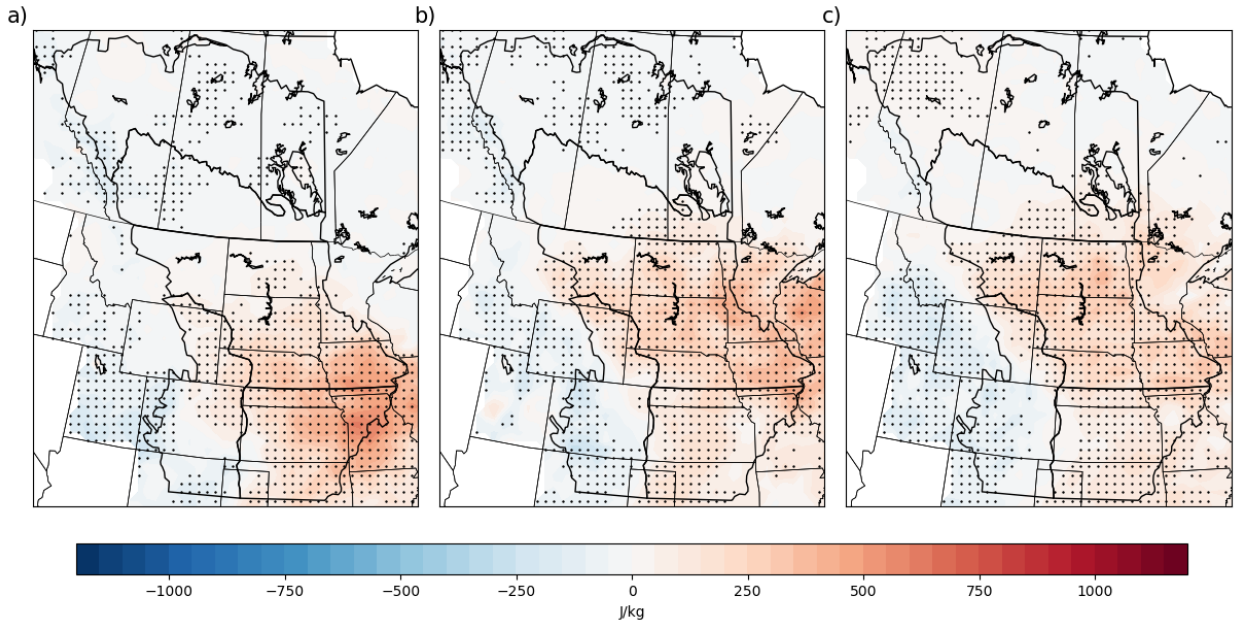

Figure 4.9 Difference (future – current) in median SBCAPE for MM5-CCSM for a) June b) July and c) August at 0000 UTC. Stippling indicates statistical significance at the 95% confidence level.

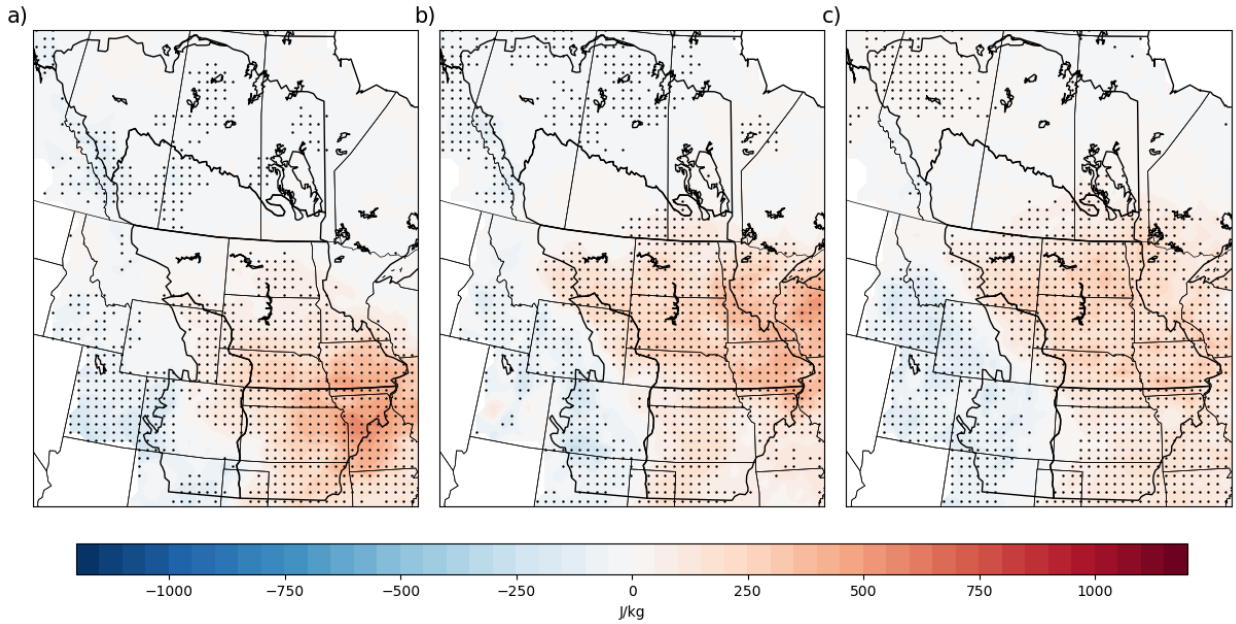

Figure 4.10 Difference (future – current) in median MUCAPE for MM5-CCSM for a) June b) July and c) August at 0000 UTC. Stippling indicates statistical significance at the 95% confidence level.

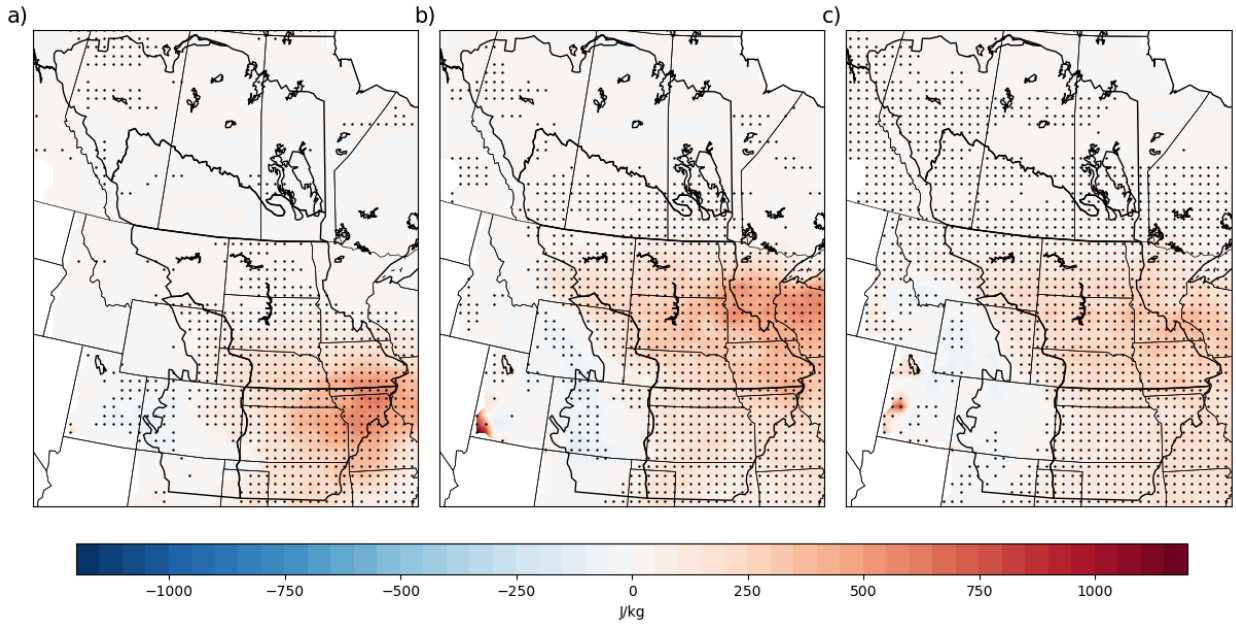

Figure 4.11 Difference (future – current) in median MLCAPE for MM5-CCSM for a) June b) July and c) August at 0000 UTC. Stippling indicates statistical significance at the 95% confidence level.

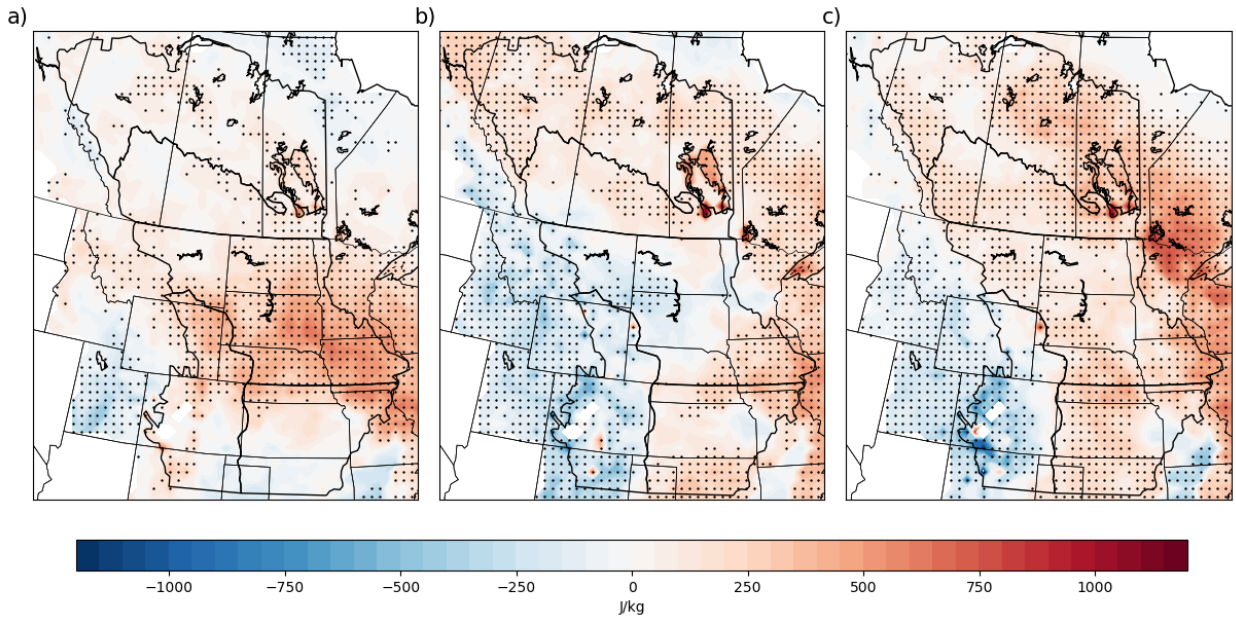

Figure 4.12 Difference (future – current) in median SBCAPE for HRM3-HadCM3 for a) June b) July and c) August at 0000 UTC. Stippling indicates statistical significance at the 95% confidence.

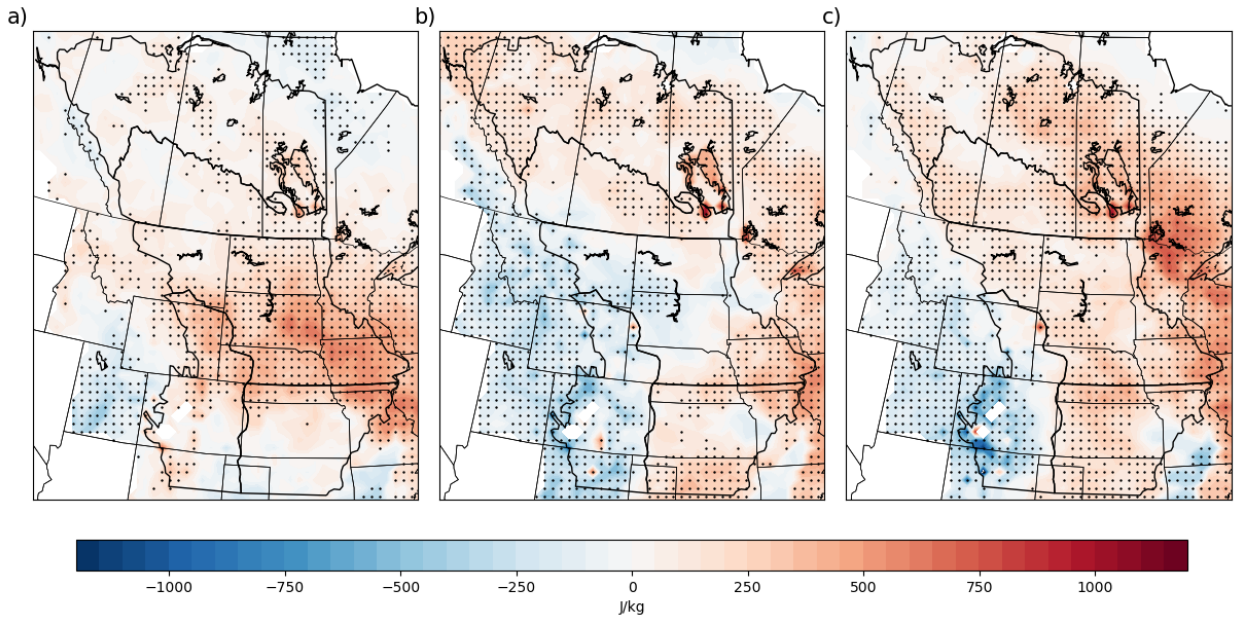

Figure 4.13 Difference (future – current) in median MUCAPE for HRM3-HadCM3 for a) June b) July and c) August at 0000 UTC. Stippling indicates statistical significance at the 95% confidence level.

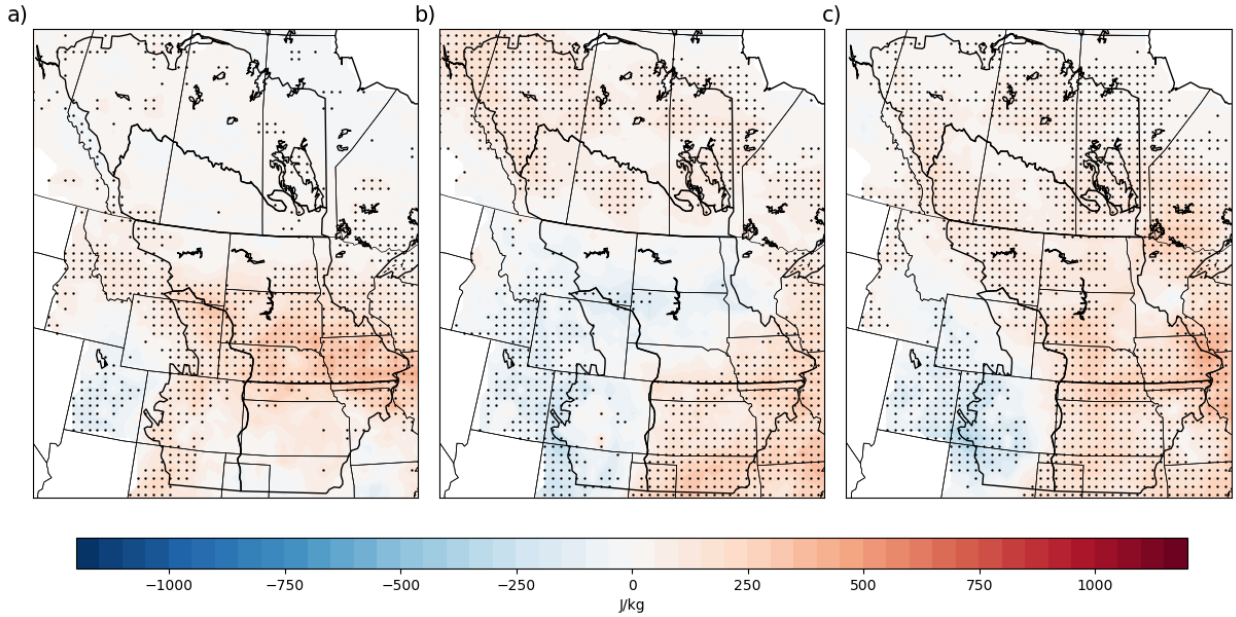

Figure 4.14 Difference (future – current) in median MLCAPE for HRM3-HadCM3 for a) June b) July and c) August at 0000 UTC. Stippling indicates statistical significance at the 95% confidence level.

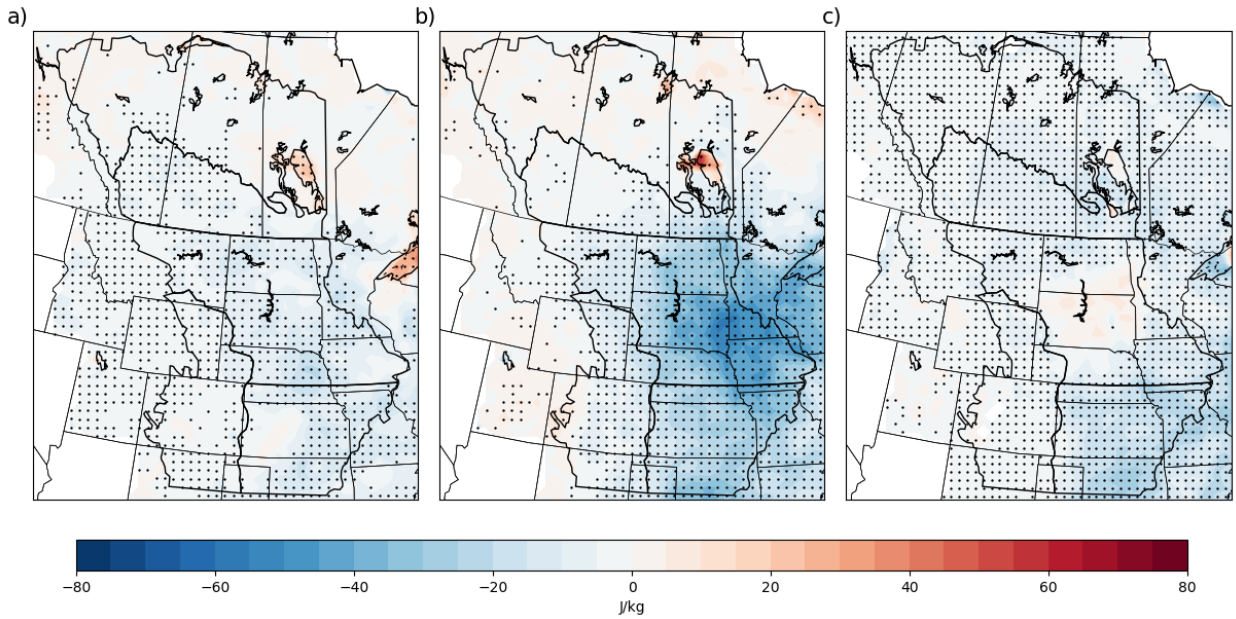

Figure 4.15 (a) Difference (future – current) in median summer (JJA) MLCIN for MM5-HadCM3 at 0000 UTC (b) MM5-CCSM (c) HRM3-HadCM3. Stippling indicates statistical significance at the 95% confidence level. Increases in convective inhibition are represented as blue and decreases in red.

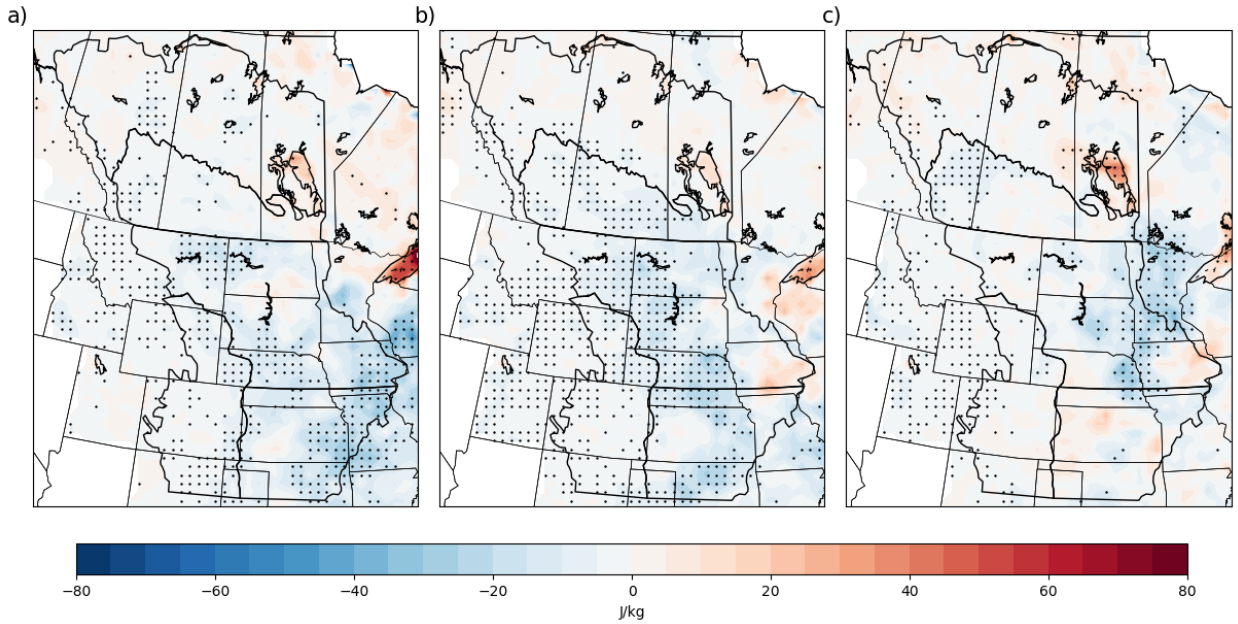

Figure 4.16 Difference (future – current) in median MLCIN for MM5-HadCM3 for a) June b) July and c) August at 0000 UTC. Stippling indicates statistical significance at the 95% confidence level.

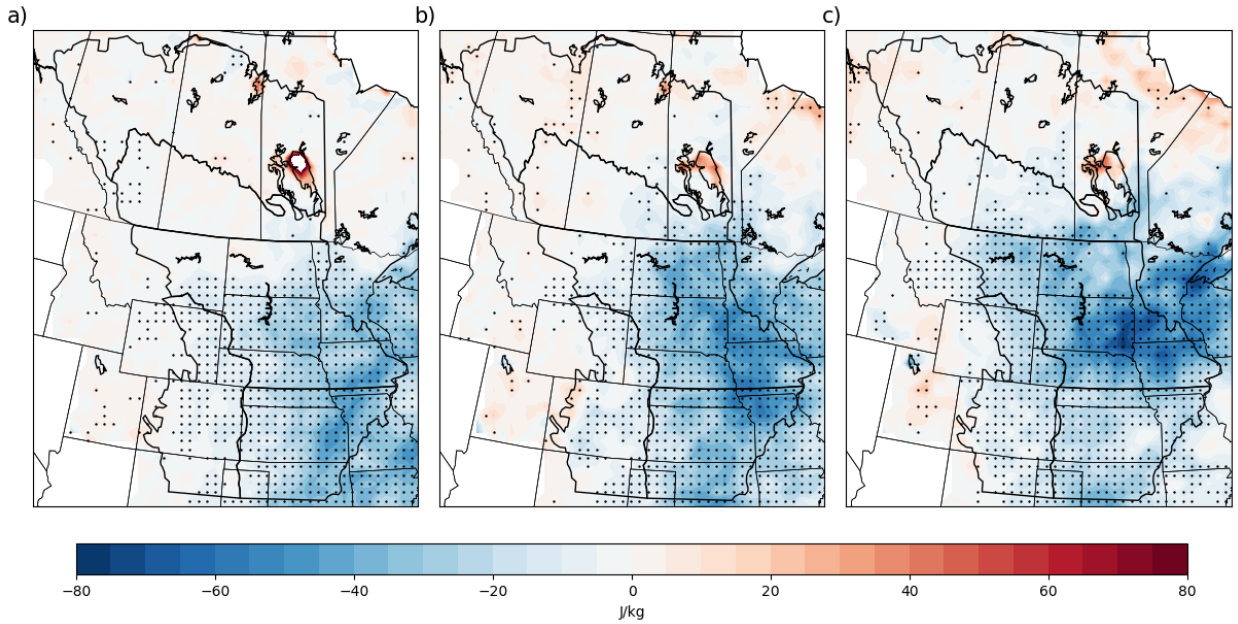

Figure 4.17 Difference (future – current) in median MLCIN for MM5-CCSM for a) June b) July and c) August at 0000 UTC. Stippling indicates statistical significance at the 95% confidence level.

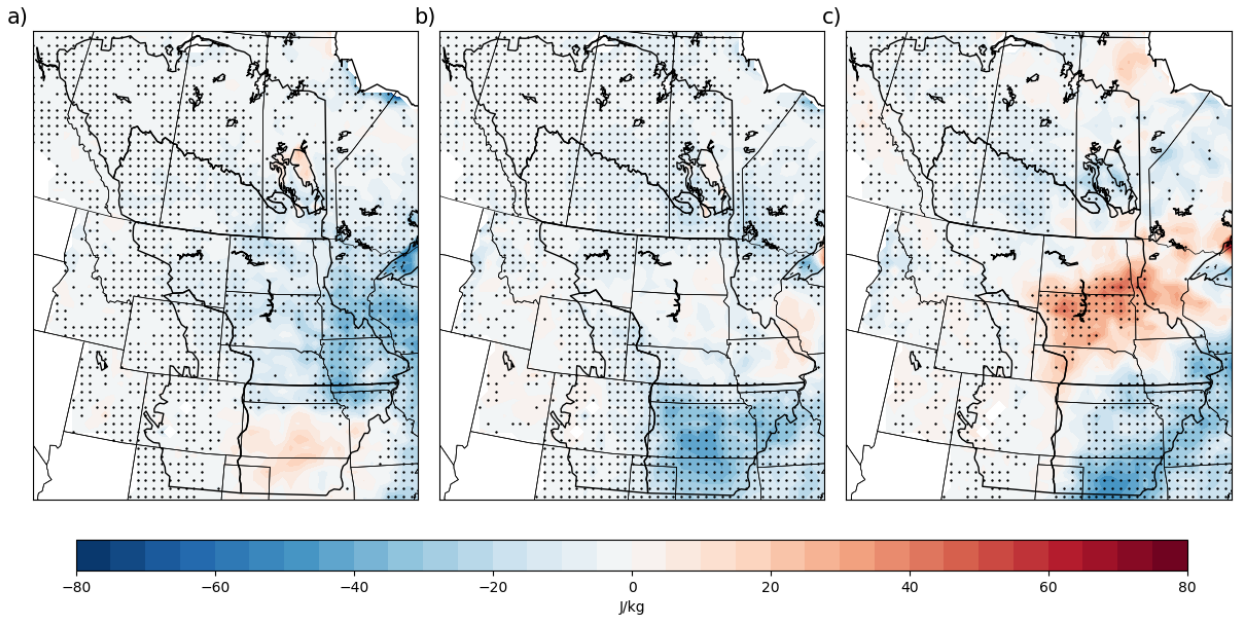

Figure 4.18 Difference (future – current) in median MLCIN for HRM3-HadCM3 for a) June b) July and c) August at 0000 UTC. Stippling indicates statistical significance at the 95% confidence level.

4.3 Vertical wind shear

At the seasonal scale, the three model pairings show primarily decreases or insignificant increases in BWD0to1km. MM5-HadCM3 and HRM3-HadCM3 (Fig. 4.19a and Fig. 4.19c, respectively) in particular show statistically significant decreases over much of the domain whereas MM5-CCSM (Fig. 4.19b) shows primarily insignificant increases across the domain. Further, at the monthly scale, MM5-CCSM (Fig. 4.23) shows very little statistically significant change in BWD0to1km, with primarily insignificant increases across the domain. In June (Fig. 4.21a), MM5-HadCM3 shows significant decreases that occur primarily over southeastern USP, northern SGP, and southeastern Saskatchewan in CAP. In July (Fig. 4.21b), the significant decreases occur on the western side of CHP, and around the boundary between SGP and USP. In August (Fig. 4.21c), the significant decreases are centred over the line between USP and SGP and follow the boundary of the Rocky Mountains. The HRM3-HadCM3 plots of BWD0to1km

for June (Fig. 4.25a) show statistically significant decreases over much of CHP, SGP, and USP as well as in central Alberta in NWF. There are also significant increases over Manitoba in NWF. The July plots (Fig. 4.25b) show a similar pattern of significant decrease over USP, SGP, and CHP to that in June. Other than a small area of significant decrease in northwestern NWF, there is little significant change over CAP and NWF. In August (Fig. 4.25c), the plots show predominately significant decreases across the domain.

The seasonal plots of BWD0to6km show mixed results. MM5-HadCM3 shows statistically significant decreases primarily over the United States in CHP, western USP, and SGP (Fig. 4.20a). Both MM5-CCSM (Fig. 4.20b) and HRM3-HadCM3 (Fig. 4.20c) show an obvious demarcation between decreases in NWF and most of CAP and increases in CHP, USP, and SGP. In particular, HRM3-HadCM3 shows significant increases concentrated over CHP and SGP. For all three model pairings, the overall pattern of change in BWD0to6km seen at the seasonal scale is most consistent with the changes seen in August. In June (Fig. 4.22a), MM5-HadCM3 shows areas of statistically significant decrease including central CHP, northwestern USP, and southern CAP. The July plots (Fig. 4.22b) show statistically significant decreases over much of the southern part of the domain, including most of CHP and SGF and western USP, as well as parts of Alberta in NWF. The August plots (Fig. 4.22c) show significant decreases over most of CHP, western and central CAP, and eastern USP and SGP, and over Manitoba and eastern Saskatchewan in eastern NWF. In June (Fig. 4.24a), MM5-CCSM shows significant increases on the eastern side of USP and north SGP, as well as over the northern tip of CHP. In July (Fig. 4.24b), there are significant increases over most of CHP, over the western side of SGP, and in central USP. In contrast to June, there are significant increases in central CAP and central NWF. The August (Fig. 4.24c) plots show significant increases over the western side of USP and

along the western edge of SGP, over much of NWF, and over Alberta in northern CAP. In June (Fig. 4.26a), HRM3-HadCM3 shows small areas of significant decrease on the western boundary of NWF and in southern SGP and CHP. In July (Fig. 4.26b), the plots show significant decrease in northwestern NWF. Further, there is a large area of significant increase in southern USP, across SGP, and much of CHP. The August plots (Fig. 4.26c) show significant increases over most of SGP and CHP but predominately significant decreases over the rest of the domain.

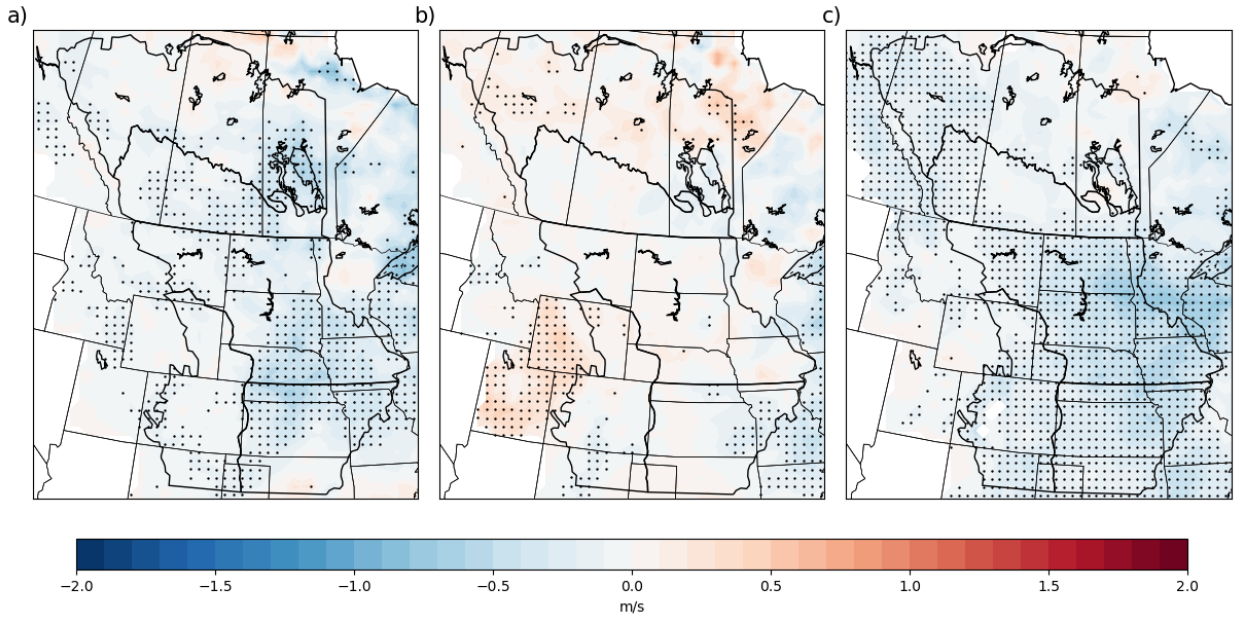

Figure 4.19 (a) Difference (future – current) in median summer (JJA) BWD0to1km for MM5-HadCM3 at 0000 UTC (b) MM5-CCSM (c) HRM3-HadCM3. Stippling indicates statistical significance at the 95% confidence level.

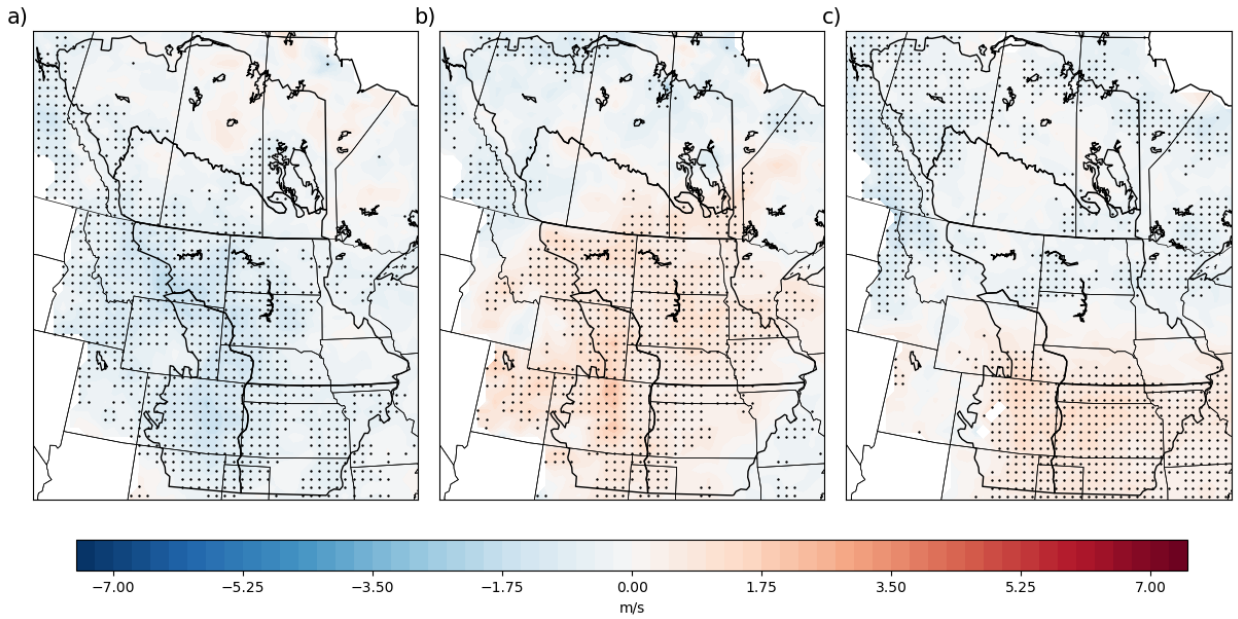

Figure 4.20 (a) Difference (future – current) in median summer (JJA) BWD0to6km for MM5-HadCM3 at 0000 UTC (b) MM5-CCSM (c) HRM3-HadCM3. Stippling indicates statistical significance at the 95% confidence level.

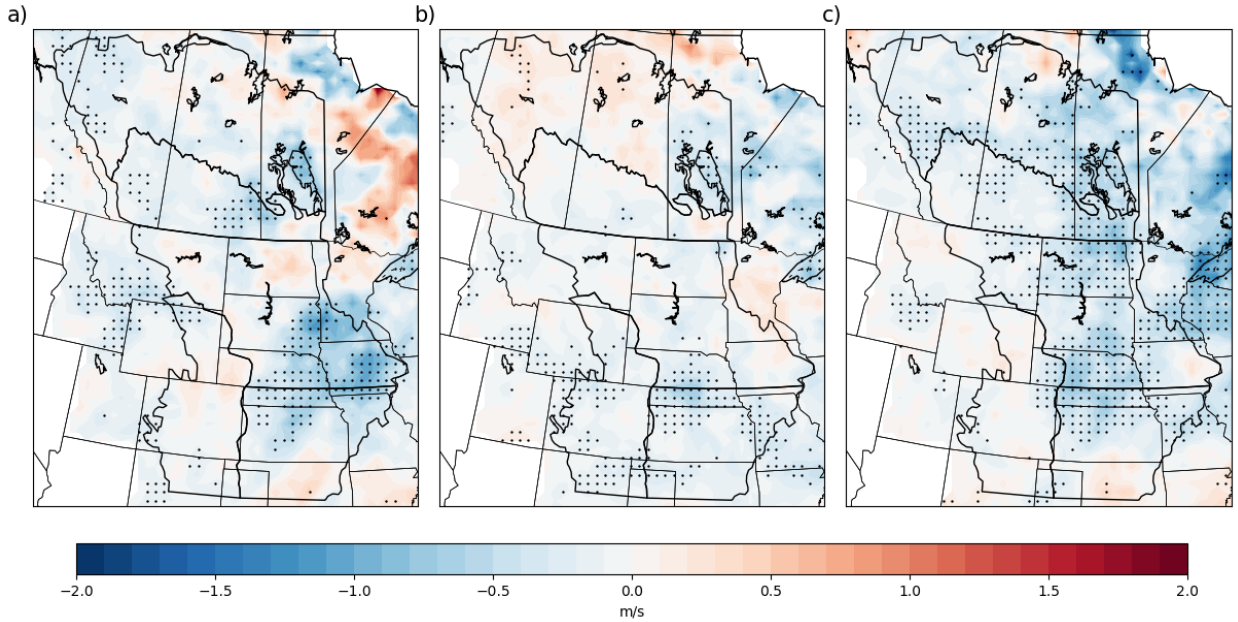

Figure 4.21 Difference (future – current) in median BWD0to1km for MM5-HadCM3 for a) June b) July and c) August at 0000 UTC. Stippling indicates statistical significance at the 95% confidence level.

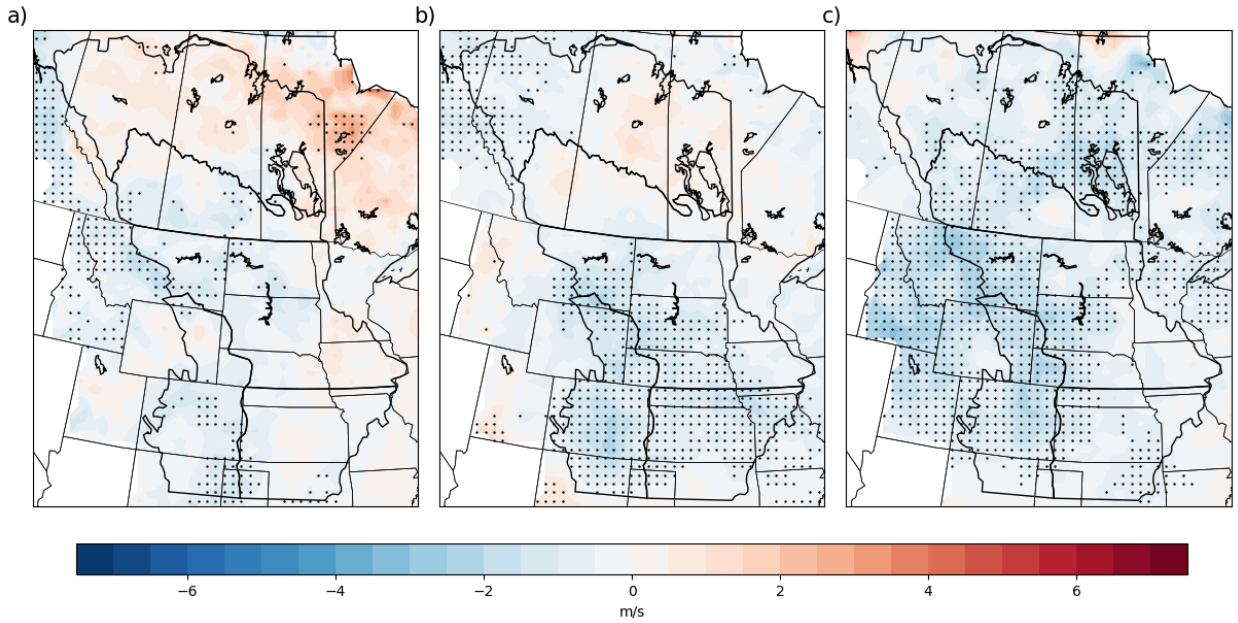

Figure 4.22 Difference (future – current) in median BWD0to6km for MM5-HadCM3 for a) June b) July and c) August at 0000 UTC. Stippling indicates statistical significance at the 95% confidence level.

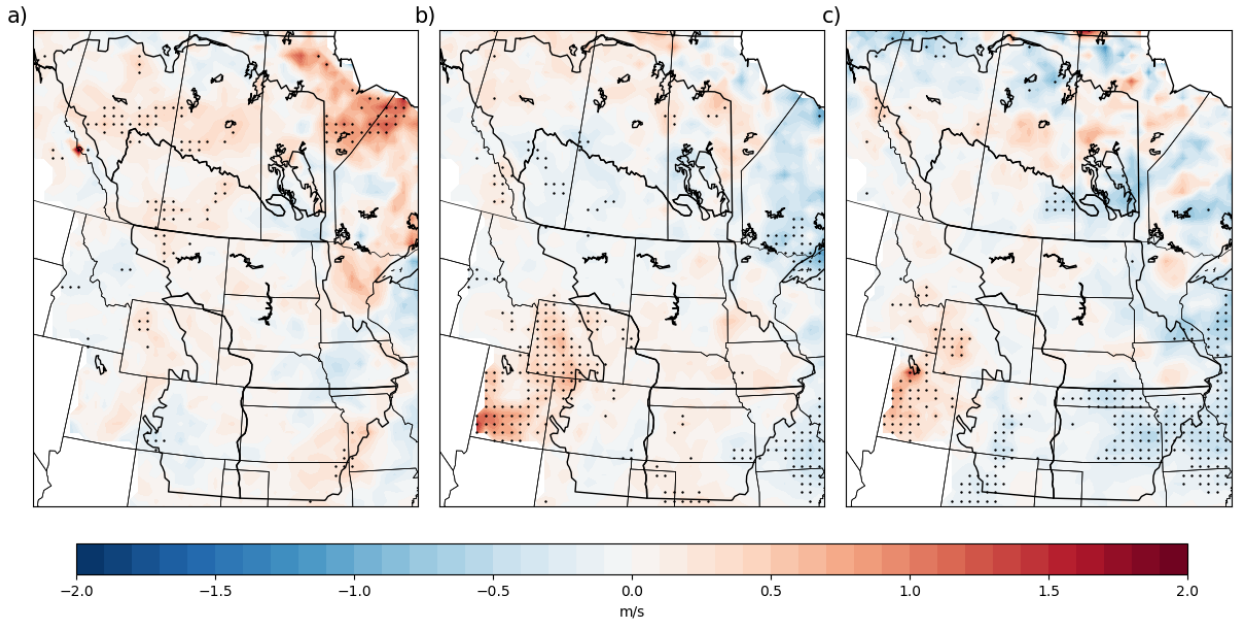

Figure 4.23 Difference (future – current) in median BWD0to1km for MM5-CCSM for a) June b) July and c) August at 0000 UTC. Stippling indicates statistical significance at the 95% confidence level.

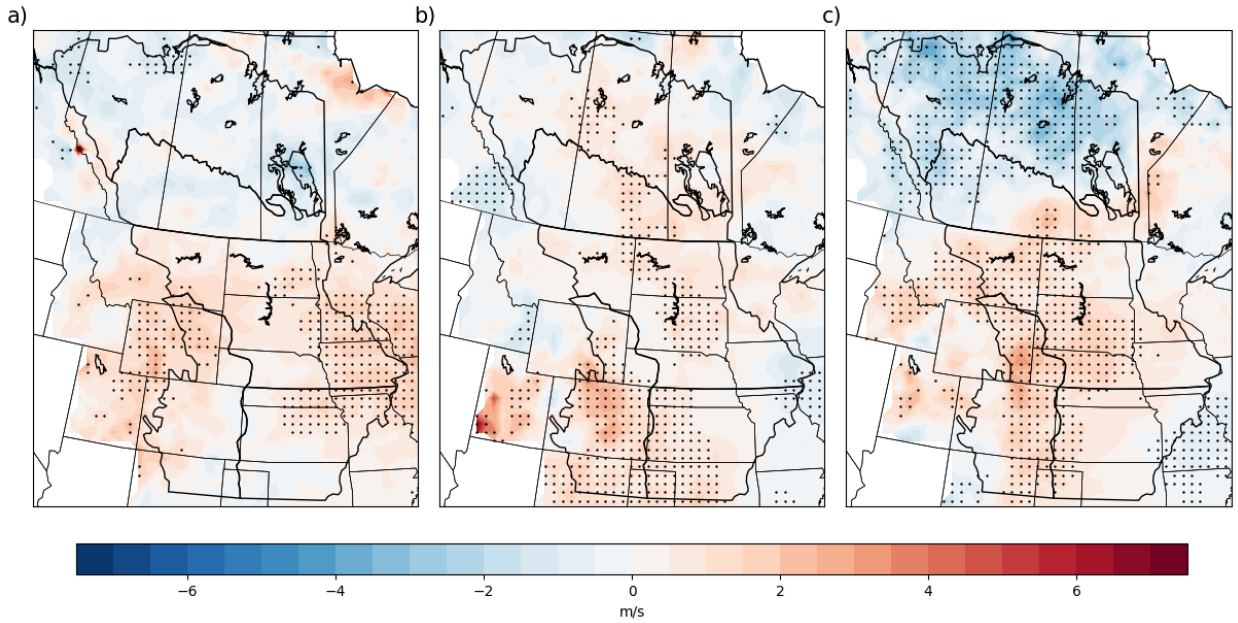

Figure 4.24 Difference (future – current) in median BWD0to6km for MM5-CCSM for a) June b) July and c) August at 0000 UTC. Stippling indicates statistical significance at the 95% confidence level.

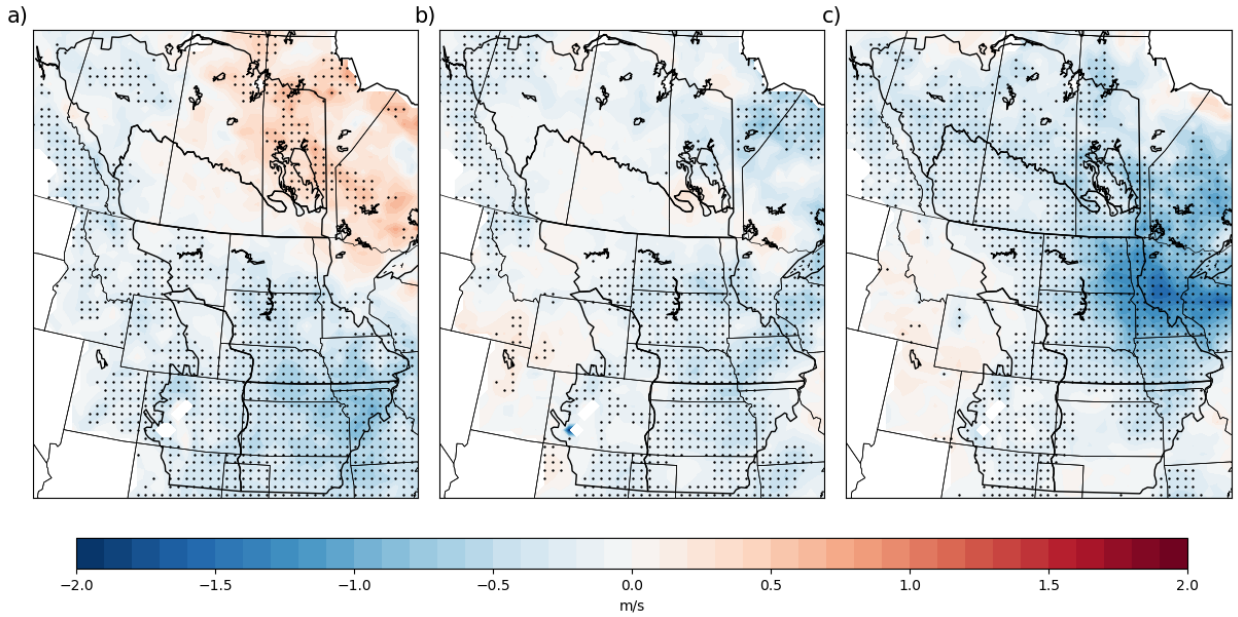

Figure 4.25 Difference (future – current) in median BWD0to1km for HRM3-HadCM3 for a) June b) July and c) August at 0000 UTC. Stippling indicates statistical significance at the 95% confidence level.

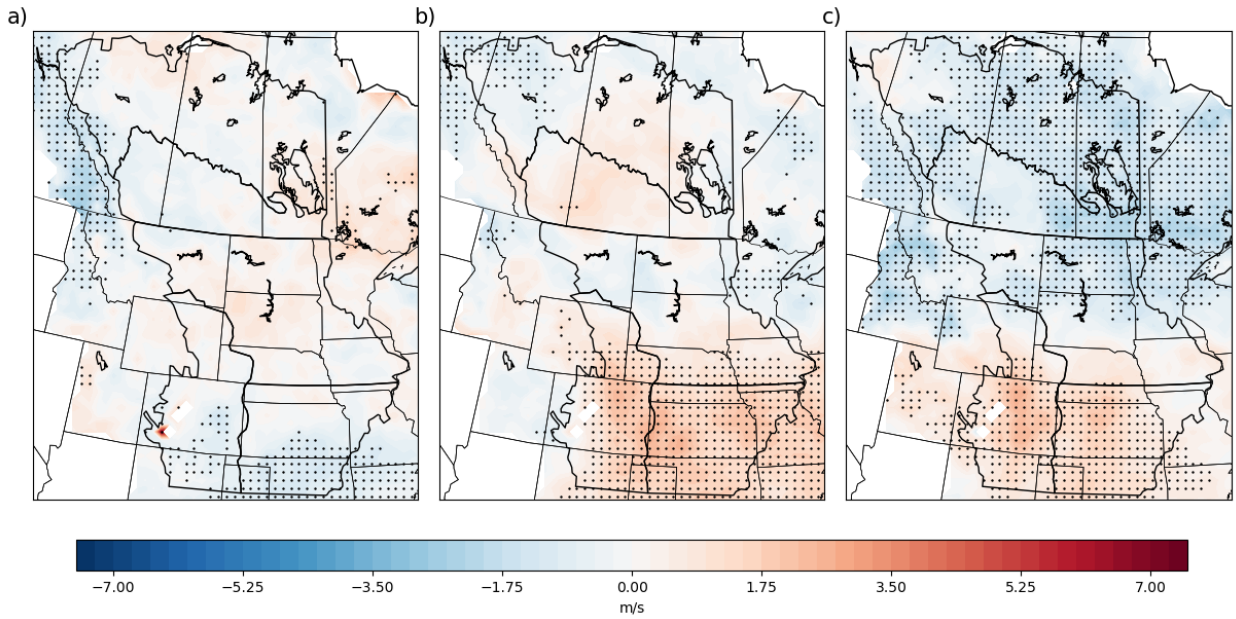

Figure 4.26 Difference (future – current) in median BWD0to6km for HRM3-HadCM3 for a) June b) July and c) August at 0000 UTC. Stippling indicates statistical significance at the 95% confidence level.

4.4 Composite parameters

The JJA plots of SCP show little agreement over change between the three model pairings. MM5-HadCM3 (Fig. 4.27a) shows few areas of statistically significant change with only consistent statistically significant decreases over southern CHP and western SGP. In contrast, MM5-CCSM (Fig. 4.27b) shows a large region of statistically significant increase that is concentrated over USP and HRM3-HadCM3 (Fig. 4.27c) shows a region of increase concentrated over eastern CHP, southwestern USP, and northwestern SGP. At the monthly timescale, MM5-HadCM3 shows the region of significant decrease over parts of CHP and SGP at the seasonal scale is present in July (Fig. 4.28b) and August (Fig. 4.28c). MM5-CCSM shows the large region of statistically significant increase at the seasonal scale shifting north from northeastern SGP in June (Fig. 4.29a) to the southern boundary of CAP in August (Fig. 4.29c). In contrast, the change at the monthly scale shown by HRM3-HadCM3 is a concentrated region

of statistically significant increase over northern CHP in June (Fig. 4.30a) and more widespread regions of increase in July (Fig. 4.30b) and August (Fig. 4.30c), covering most of SGP.

In contrast to the plots of SCP, at both the monthly and seasonal timescales, the plots of STP show primarily small, disorganized regions of statistically significant change with few organized regions of change. MM5-HadCM3 (Fig. 4.31a) shows a small region of statistically significant increase in STP over central Alberta at the seasonal scale. This region of increase is also present in July (Fig. 4.32b). MM5-CCSM (Fig. 4.31b) shows significant increases in STP over southeastern USP and northern CHP at the seasonal scale. At the monthly scale, the increase over USP is present in July (4.33b) and August (4.33c); however, there are only scattered significant increases over northern CHP at the monthly scale. HRM3-HadCM3 shows primarily small, disorganized regions of significant change at the seasonal and monthly scales.

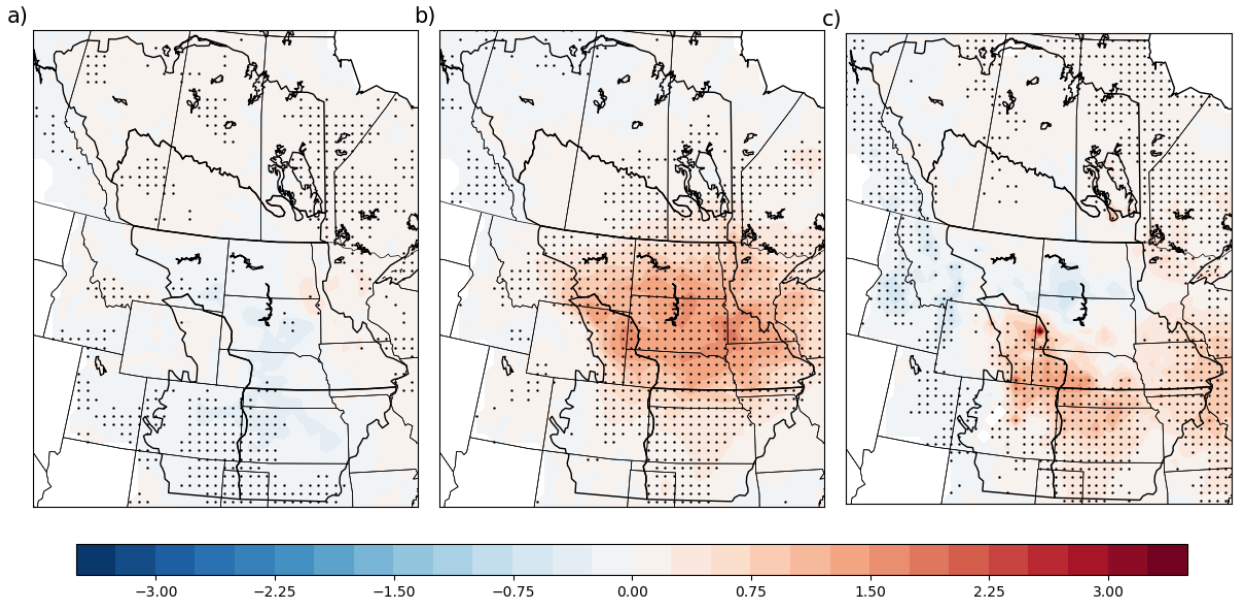

Figure 4.27 (a) Difference (future – current) in median summer (JJA) SCP for MM5-HadCM3 at 0000 UTC (b) MM5-CCSM (c) HRM3-HadCM3. Stippling indicates statistical significance at the 95% confidence level.

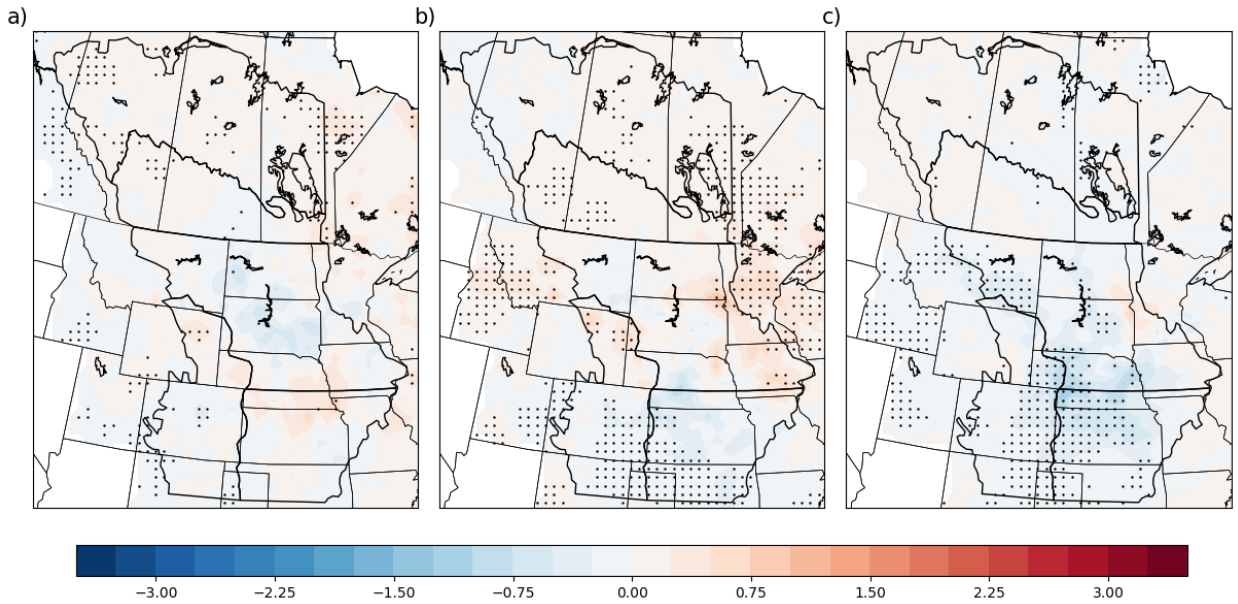

Figure 4.28 Difference (future – current) in median SCP for MM5-HadCM3 for a) June b) July and c) August at 0000 UTC. Stippling indicates statistical significance at the 95% confidence level.

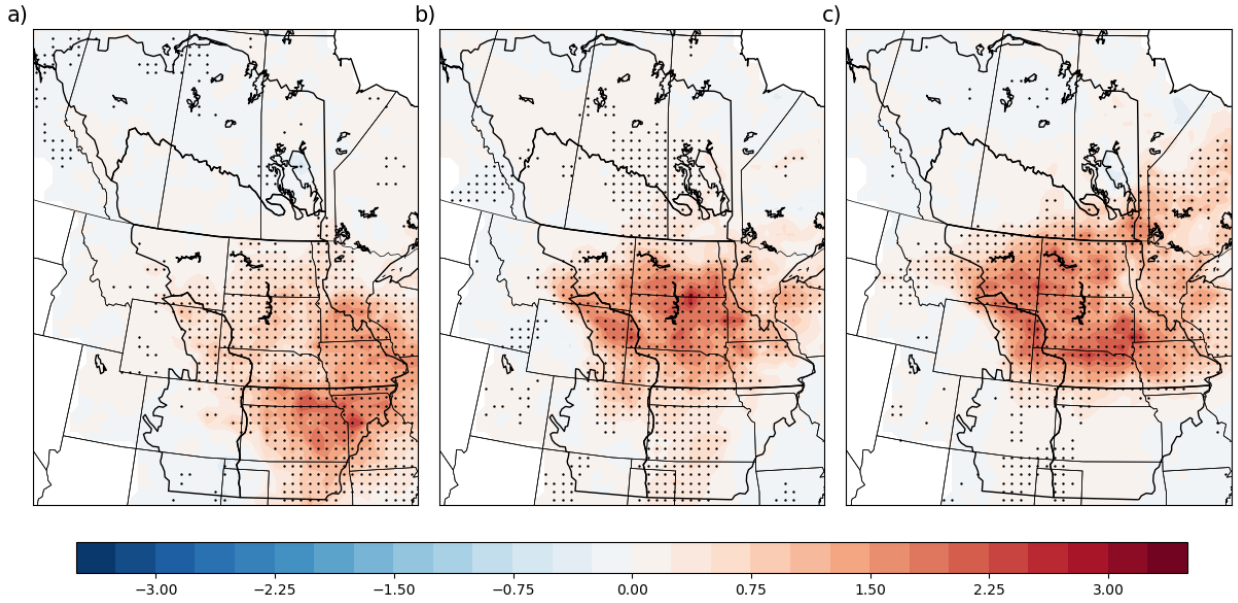

Figure 4.29 Difference (future – current) in median SCP for MM5-CCSM for a) June b) July and c) August at 0000 UTC. Stippling indicates statistical significance at the 95% confidence level.

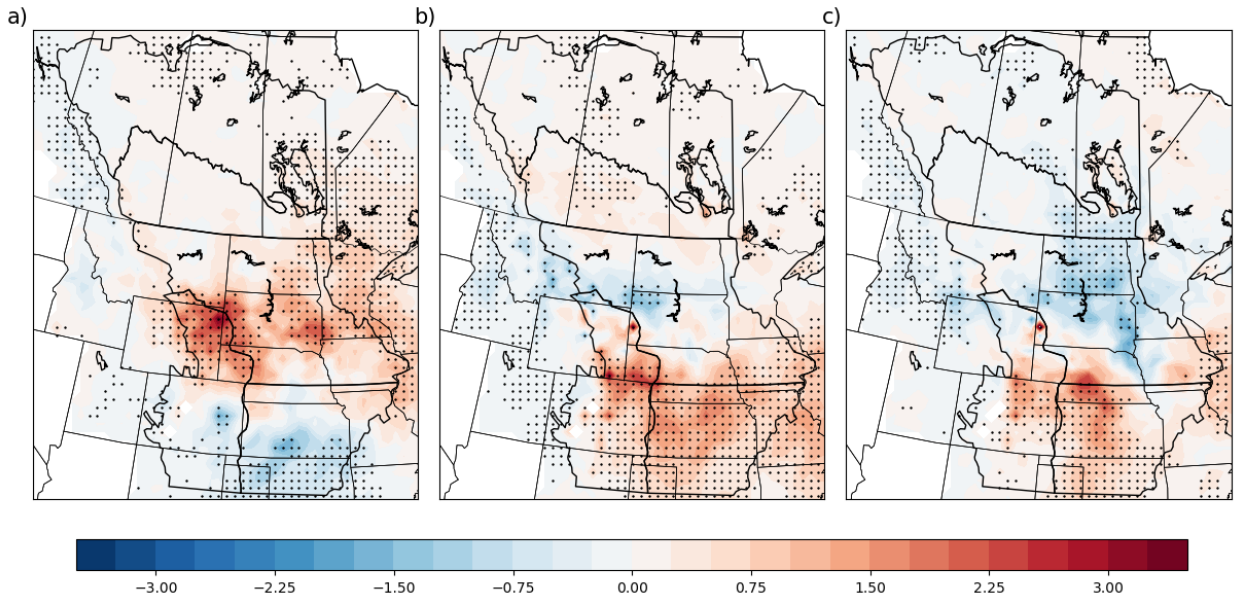

Figure 4.30 Difference (future – current) in median SCP for HRM3-HadCM3 for a) June b) July and c) August at 0000 UTC. Stippling indicates statistical significance at the 95% confidence level.

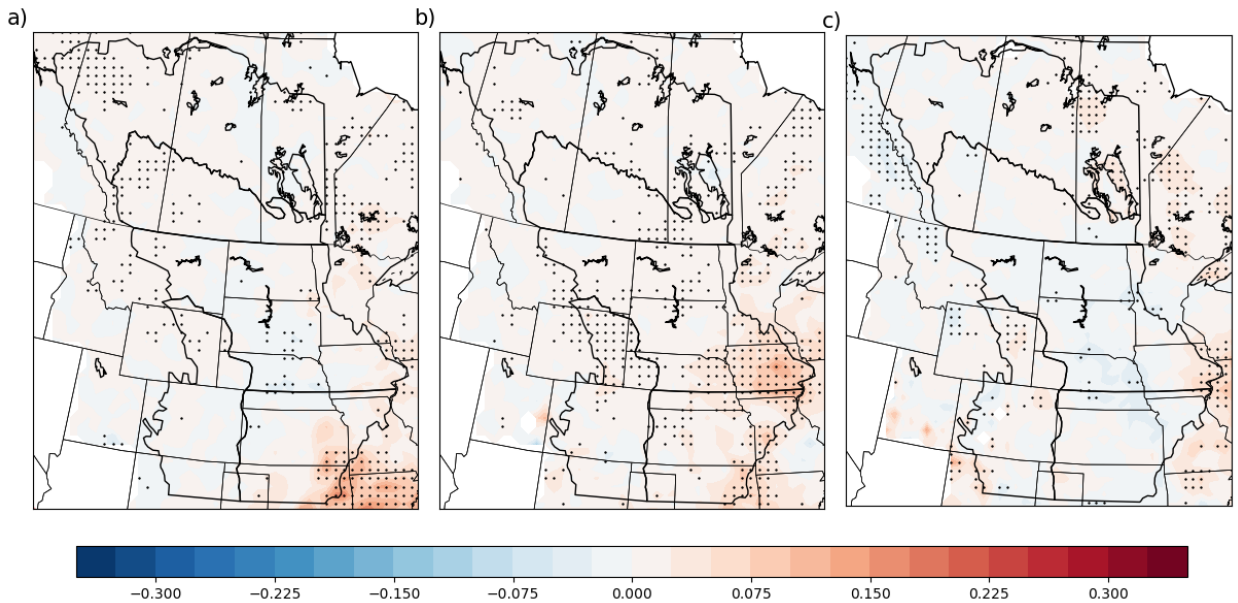

Figure 4.31 (a) Difference (future – current) in median summer (JJA) STP for MM5-HadCM3 at 0000 UTC (b) MM5-CCSM (c) HRM3-HadCM3. Stippling indicates statistical significance at the 95% confidence level.

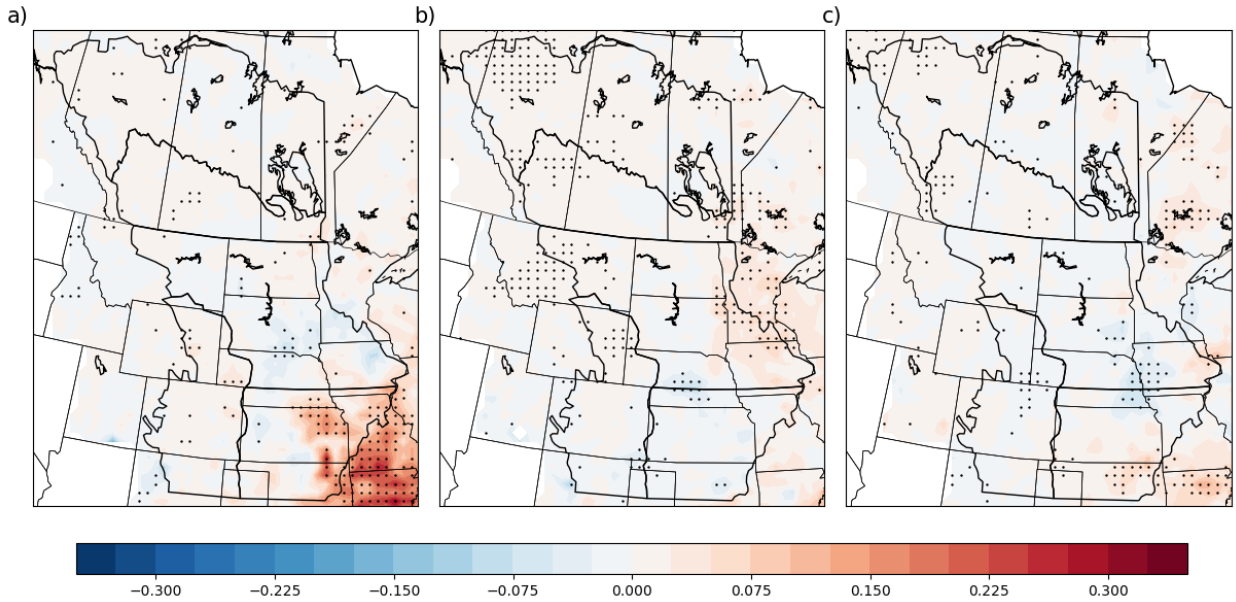

Figure 4.32 Difference (future – current) in median STP for MM5-HadCM3 for a) June b) July and c) August at 0000 UTC. Stippling indicates statistical significance at the 95% confidence level.

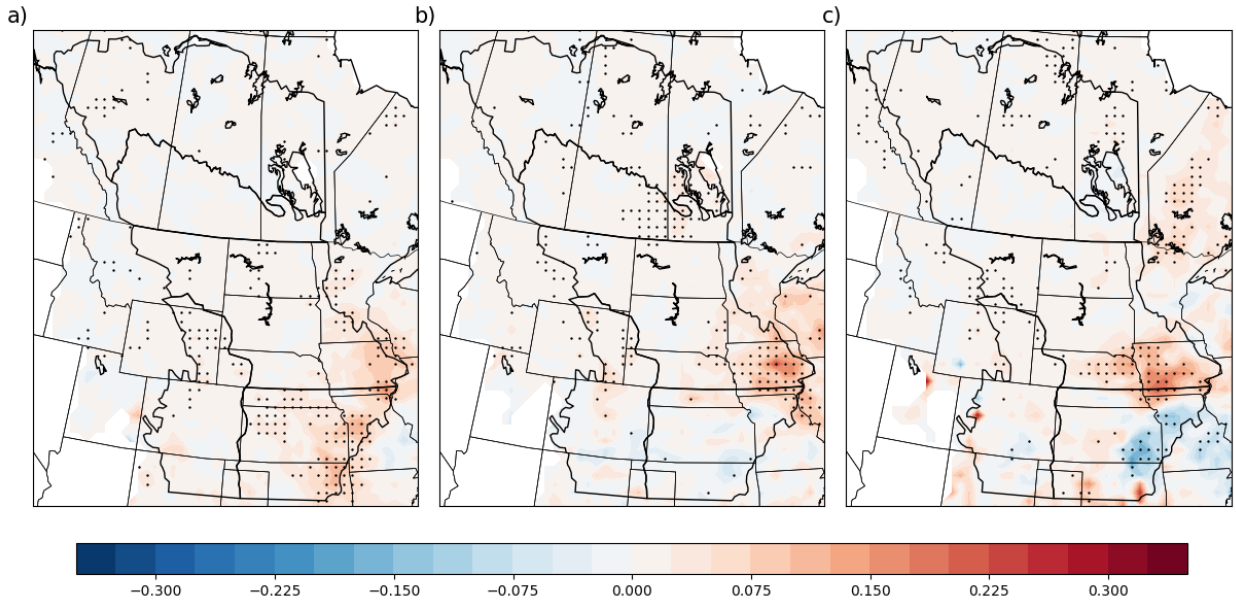

Figure 4.33 Difference (future – current) in median STP for MM5-CCSM for a) June b) July and c) August at 0000 UTC. Stippling indicates statistical significance at the 95% confidence level.

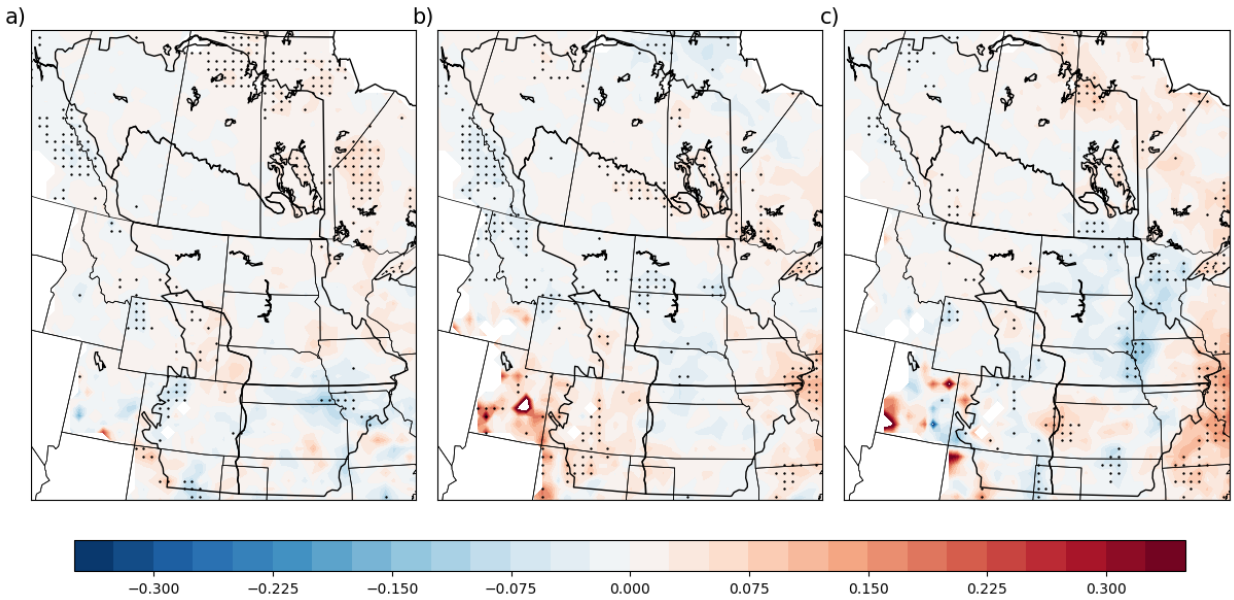

Figure 4.34 Difference (future – current) in median STP for HRM3-HadCM3 for a) June b) July and c) August at 0000 UTC. Stippling indicates statistical significance at the 95% confidence level.

4.5 Discussion

A future increase in convective precipitation implies increased potential for thunderstorms to occur and subsequently, the environment (ingredients) favourable for thunderstorm occurrence. This forms the basis for the ingredients-based methodology used in this research to examine future change in convective precipitation. Based on the results discussed in Chapter 3 it is apparent that under a scenario of increased warming, many regions within the domain will experience increased precipitation. Further, the results show simultaneous increases in convective precipitation, indicating an increase in the frequency and/or intensity of thunderstorms, despite there being increased capping (i.e. MLCIN) over many areas.

The necessary ingredients for the development of a thunderstorm are moisture, instability, and a triggering mechanism. Large wind shear is also necessary for severe thunderstorms (Stull, 2015). In particular, the daily product of CAPE and BWD0to6km – and the

number of days per year this product exceeds a certain threshold – has been shown to be effective at discriminating between environments conducive to severe thunderstorms and those that are not (Diffenbaugh, Sherer, & Trapp, 2013; Gensini et al., 2014; Hoogewind, Baldwin, & Trapp, 2017; Trapp et al., 2007; Trapp et al., 2009). These two parameters play a role in the occurrence of thunderstorms – and subsequently the occurrence of convective precipitation – as CAPE represents "the energy that is available to feed the vertical movement of the air (updraft) to produce precipitation and to generate a downdraft associated with the evaporation of the falling precipitation" (Paquin, de Elia, & Frigon, 2014, p. 176). Brooks et al. (2003) describe CAPE as "a combination of steep lapse rates in the mid-troposphere and abundant boundary-layer moisture" (p. 82). Further, wind shear "prolongs and intensifies storms by physically displacing deep-convective updrafts from rain shafts and promoting storm-scale rotation" (Seeley & Romps, 2015, p. 2443 – 2444). As such, BWD0to6km impacts thunderstorms through enhanced organization, intensity, and longevity, commonly referred to as convective mode (Trapp et al., 2009). It is thought that in a warmer and moister climate, CAPE will increase (Mahoney et al., 2013) whereas increased temperature would result in a reduced latitudinal temperature gradient and thus a reduction in the vertical wind shear (Trapp et al., 2009).

Studies examining future change in CAPE and wind shear have found increases in CAPE along with decreases in wind shear in the contiguous U.S. (Trapp et al., 2007; Van Klooster & Roebber, 2009; Del Genio, Yao, & Jonas, 2007). These results suggest that instability rather than shear will be the dominant influence in future convective environments, resulting in an overall increase in the potential for thunderstorms to occur (Van Klooster & Roebber, 2009) and environments that are more conducive to the formation of severe thunderstorms than in the current period (Bukovsky et al., 2017).

The results presented here are similar to those found in previous research, with all three model pairings showing primarily statistically significant increases in the three CAPE parameters and decreases in BWD0to1km, although the BWD0to6km results are more mixed. Though previous research has found increased CAPE and decreased shear and suggested that this will result in an overall increase in thunderstorm potential, the environments most conducive to the formation of severe thunderstorms are those with both large CAPE and shear. Since this research examines 30-year mean and median changes, we do not attempt an examination of the daily product of CAPE and shear. Instead, this discussion will focus on the regions of the domain where there is statistically significant simultaneous change in both MLCAPE and BWD0to6km (Fig. 4.35, Fig. 4.36, and Fig. 4.37); changes in SCP, STP, and MLCIN and how they relate to changes in convective precipitation will also be addressed.

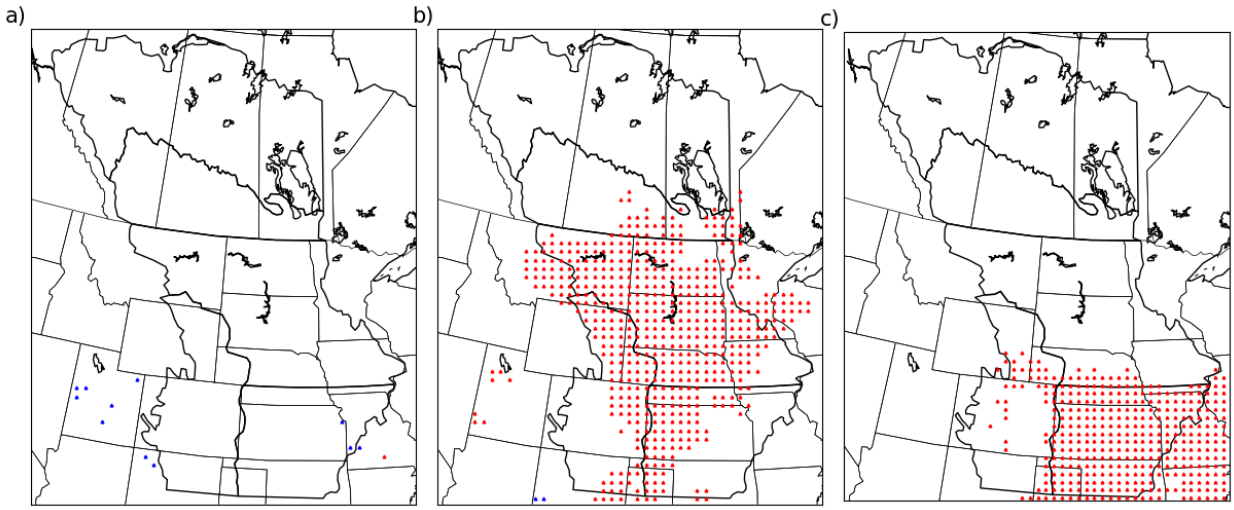

Figure 4.35 Statistical significance at the 95% confidence level in both MLCAPE and BWD0to6km for JJA. Red stippling represents statistically significant increases and blue represents statistically significant decreases. (a) MM5-HadCM3 (b) MM5-CCSM (c) HRM3-HadCM3.

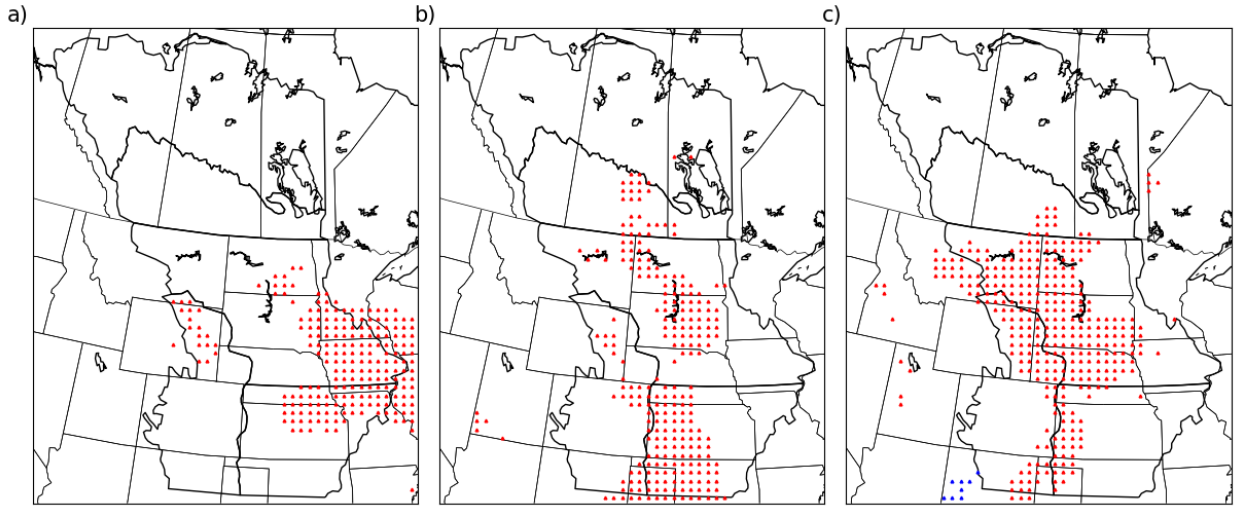

Figure 4.36 Statistically significant change at the 95% confidence level in both MLCAPE and BWD0to6km for MM5-CCSM. (a) June (b) July and (c) August.

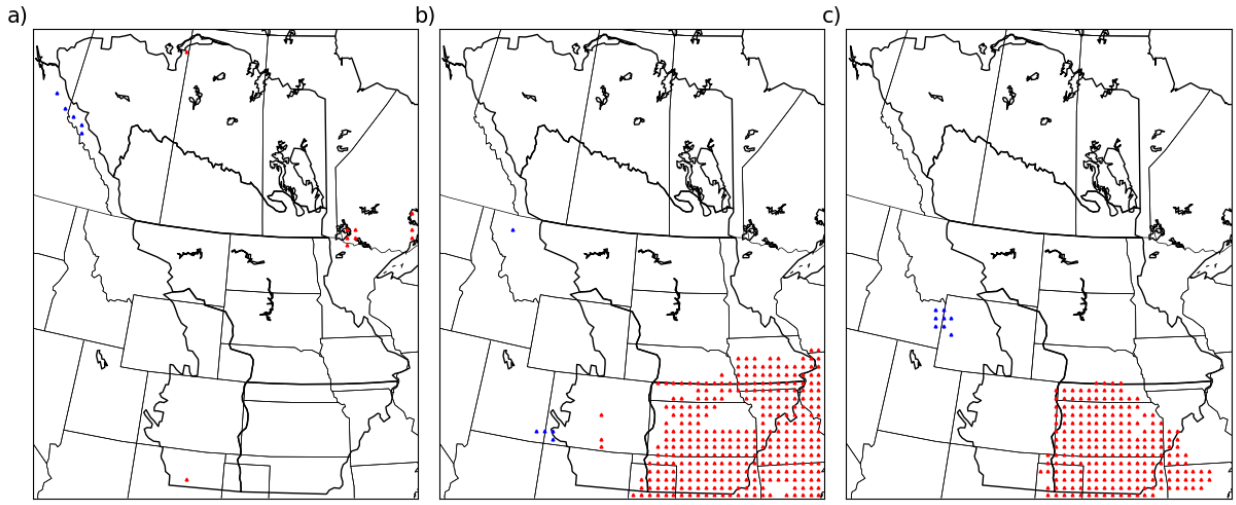

Figure 4.37 Statistically significant change at the 95% confidence level in both MLCAPE and BWD0to6km for HRM3-HadCM3. (a) June (b) July and (c) August.

4.5.1 MM5-HadCM3

The MM5-HadCM3 results are the most mixed of the three model pairings. There are few gridpoints showing statistically significant increases in both MLCAPE and BWD0to6km, at both the seasonal (Fig. 4.35a) and monthly scale (plots not shown). Despite this, MM5-HadCM3 shows primarily increases – both statistically significant and insignificant – in convective

precipitation over the domain. These increases correspond to increased seasonal and monthly MLCAPE; further, the progression of MLCAPE from June through August reflects the climatological shift of thunderstorms from SGP to CAP from June through August. Wind shear and MLCIN do not appear to have a strong influence on changes in convective precipitation as convective precipitation consistently increases over northern CHP and western USP and over central Manitoba in NWF, despite primarily decreasing BWD0to6km and increasing MLCIN over these regions. The result of increased convective precipitation and MLCAPE over Alberta in NWF and CAP, northern CHP, and central Manitoba in NWF could suggest changes in thunderstorm activity. Over CAP and NWF in Alberta and over central Manitoba in NWF, increases in convective precipitation and MLCAPE suggest greater likelihood of storm initiation (triggering) in the future (Trapp et al., 2007) and greater potential for intense thunderstorms to occur, respectively. However, over northern CHP, decreases in BWD0to6km suggest a potential decrease in the organization and longevity of storms in the future. This suggests increased potential for disorganized, short-lived thunderstorms for this region.

4.5.2 MM5-CCSM

In contrast to MM5-HadCM3, MM5-CCSM and HRM3-HadCM3 show large, organized regions where there are statistically significant increases in both MLCAPE and BWD0to6km, at both the seasonal and monthly timescales. For MM5-CCSM at the seasonal timescale (Fig. 4.35b), the increases in these two parameters and SCP correspond to statistically significant increases in convective precipitation over USP but not over western SGP and eastern CHP where there are insignificant changes or significant decreases in convective precipitation. Similarly, at the monthly scale, MLCAPE and BWD0to6km (Fig. 4.36) and SCP are shown to increase over northeast SGP, southeast USP, and northern CHP in June (Fig. 4.36a), central USP and western

SGP in July (Fig. 4.36b), and over western USP, the boundary between SGP and CHP, and northern CHP in August (Fig. 4.36c). These regions correspond to areas where there are either statistically insignificant changes or insignificant decreases in convective precipitation. Further, large regions of increase in SCP exist over USP in June, July, and August where there are corresponding insignificant increases in convective precipitation. This discrepancy between changes in convective precipitation and MLCAPE, BWD0to6km, and SCP is likely the result of increases in MLCIN which are extensive across the southern three ecoregions. These results suggest that while there may be decreased frequency of storms over these areas, the storms that do occur have the potential to be more severe.

In contrast, statistically significant increases in convective precipitation occurring over northern CHP in June and across the boundary between USP and CAP in July and August correspond to statistically significant increases in MLCAPE and BWD0to6km. Further, increases in convective precipitation are juxtaposed with increases in SCP, indicating that stronger BRN shear and SRH0to3km may contribute to stronger supercell thunderstorms in the future over these areas. Further, statistically significant increases in STP coincide with the significant increases in SCP, MLCAPE, and BWD0to6km over southeast Saskatchewan and southwest Manitoba in CAP. This suggests that the environment in this region may be more conducive in the future to tornadic severe thunderstorms when they do occur.

In addition to the statically significant increase in convective precipitation in northern USP, MM5-CCSM shows significant increases over CAP and NWF, particularly in August. Excluding the areas of southern CAP mentioned above, these changes in precipitation do not correspond to increases in BWD0to6km and MLCAPE juxtaposed or SCP. Further, there are only scattered statistically significant changes in MLCIN over this region. Though lesser than the

statistically significant increases over the southern three ecoregions, it appears that statistically significant increases in MLCAPE are influencing these increases in convective precipitation, particularly over central Alberta in June and August and the southern Prairies in July and August. Increases in convective precipitation and MLCAPE suggest increases in the frequency and intensity of storms over these areas.

4.5.3 HRM3-HadCM3

The HRM3-HadCM3 plots bear some similarities to those for MM5-CCSM. June shows no meaningful increases in MLCAPE and BWD0to6km but large increases across SGP in July and August (Fig. 4.37b and Fig. 4.37c, respectively). However, the July and August plots of convective precipitation show mostly statistically insignificant changes over this region. It is notable as well that the statistically significant increases in SCP for July and August do not correspond to those in convective precipitation. Further, there are statistically significant increases in MLCIN over SGP in July and August, which likely plays a role in the lack of significant increases seen in convective precipitation over this region. These convective precipitation results for SGP, along with statistically significant increases in MLCAPE, BWD0to6km, MLCIN, and SCP, suggest that though the triggering/frequency of storms may not increase in the future, storms that do occur will have greater potential to be severe.

Over Canada in NWF and CAP, the HRM3-HadCM3 results for convective precipitation and MLCAPE are similar to those for MM5-HadCM3 and MM5-CCSM. In June and July there are primarily insignificant changes or significant decreases in BWD0to6km across CAP and NWF in August. Further, there are large areas of statistically significant increase in MLCIN and SCP shows only small regions of statistically significant change over the two ecoregions. Despite these results, HRM3-HadCM3 shows statistically significant increases in convective

precipitation (with no significant decreases) over NWF and CAP. In particular, these changes are occurring over central Manitoba in June, central Alberta in July, and along the Rocky Mountains in central and southern Alberta in August. Like MM5-HadCM3 and MM5-CCSM, the pattern of increases – significant and insignificant – seen in convective precipitation over NWF and CAP corresponds closely to statistically significant increases in MLCAPE. Like the other two model pairings, these findings indicate the influence of instability on thunderstorms in the future.

4.5.4 Lapse Rates

CAPE can be thought of as a combination of steep lapse rates in the mid-troposphere and large amounts of low-level moisture (Brooks et al., 2003) and increases in these two parameters are considered to be good indicators of increased convective potential (Brooks et al., 2007). This research defines the mid-tropospheric lapse rate as that between 700 and 500 mb, though steep lapse rates may exist outside of this layer (Brooks et al., 2007). However, even with shallower lapse rates over western Canada (Fig. 4.38), increased low-level moisture appears to be sufficient for increased CAPE values. Shallower lapse rate values indicate smaller changes in temperature with height, weaker positive buoyancy, and a shift toward a taller, thinner CAPE profile. All three of the model pairings indicate this shift over western Canada. In contrast, MM5-CCSM and HRM3-HadCM3 (Fig. 4.38b and Fig. 4.38c, respectively) suggest steeper lapse rates over southern parts of the domain. This suggests larger temperature changes with height, greater buoyancy, and a shift toward a wider, shorter CAPE profile. However, these changes in the lapse rate profiles do not always correspond to increases in CAPE. For example, over CHP, MM5-CCSM and HRM3-HadCM3 show either significant decreases in CAPE or insignificant changes over this region. This may be the result of changes in low-level moisture, as these two pairings indicate significant decreases, insignificant changes, or significant increases of a lesser

magnitude in dewpoint temperature than MM5-HadCM3 (which showed significant increases in dewpoint temperature across the entire domain) over this region. As stated by Paquin et al. (2014), these findings highlight the role of increased low-level moisture as a source of instability and driver of thunderstorms under the influence of a changing climate.

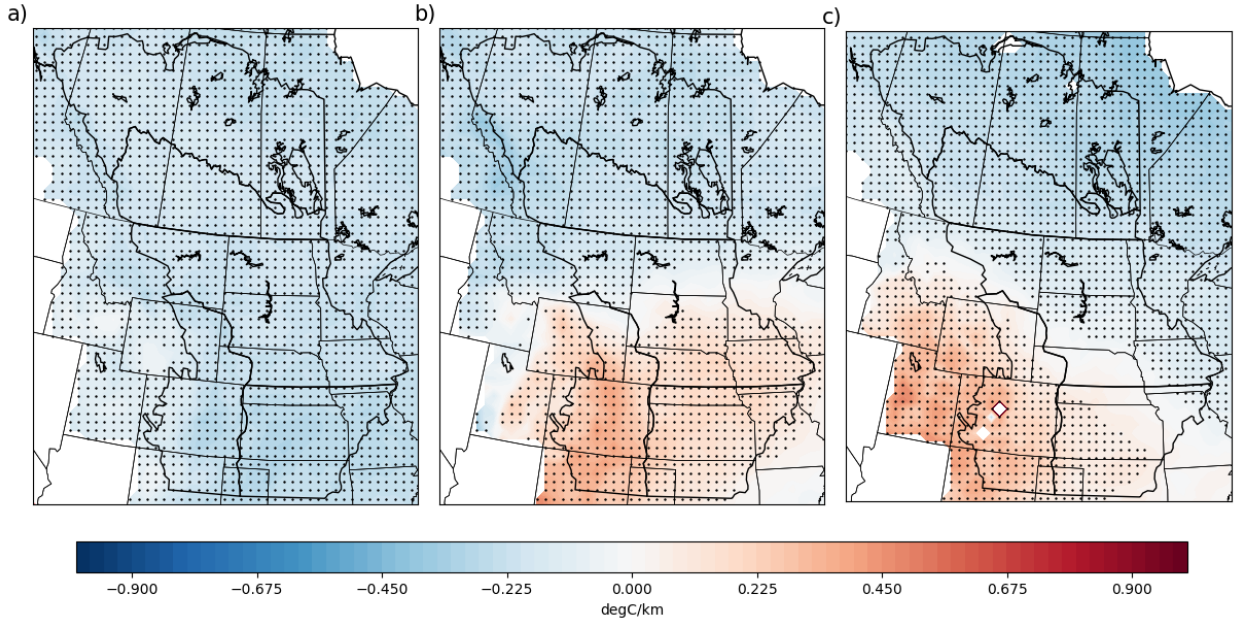

Figure 4.38 (a) Difference (future – current) in median summer (JJA) mid-level lapse rate (700 – 500 mb) for MM5-HadCM3 at 0000 UTC (b) MM5-CCSM (c) HRM3-HadCM3. Stippling indicates statistical significance at the 95% confidence level.

4.5.5 Summary

The three model pairings used in this research indicate a number of regions that may see increased frequency and/or intensity of thunderstorms throughout the warm season (JJA). MM5-HadCM3 (Fig. 4.39) indicates that over Alberta in CAP and NWF and central Manitoba in NWF there may be increases in the frequency and/or intensity of convective precipitation. Further, this pairing indicates a potential increase in weaker thunderstorms over northern CHP. MM5-CCSM (Fig. 4.40) indicates that central Alberta in NWF may see increases in the frequency and/or intensity of convective precipitation. Over central USP and across the boundary between USP

and CAP, MM5-CCSM suggests these regions may see more severe storms. Finally, over northern CHP and western SGP, this pairing suggests these areas may see fewer but stronger storms. HRM3-HadCM3 (Fig. 4.41) shows central Manitoba in NWF may see increases in the frequency and/or intensity of convective precipitation. This pairings suggests SGP may see less frequent but stronger storms. Finally, HRM3-HadCM3 indicates a region over the boundary between SGP and USP that may see more severe storms.

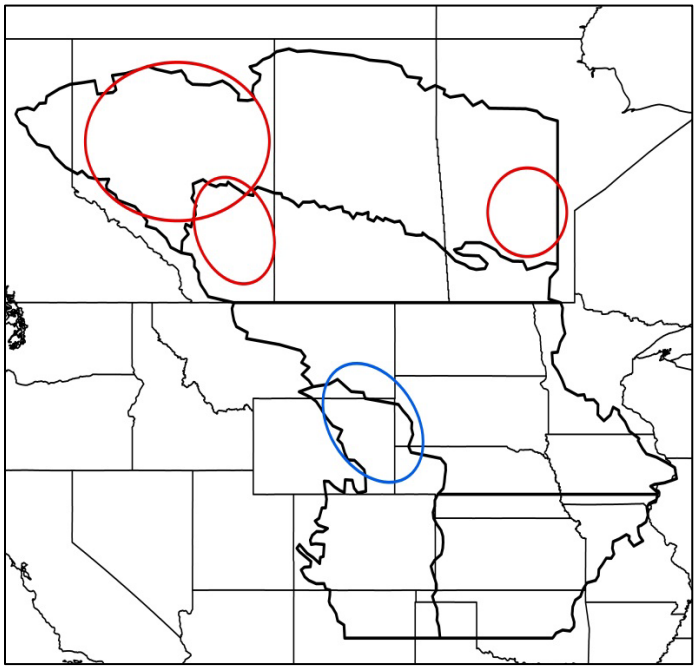

Figure 4.39 Summary of findings for MM5-HadCM3. Red indicates areas that may see increases in the frequency and/or intensity of convective precipitation. Blue indicates areas likely to see weaker thunderstorms.

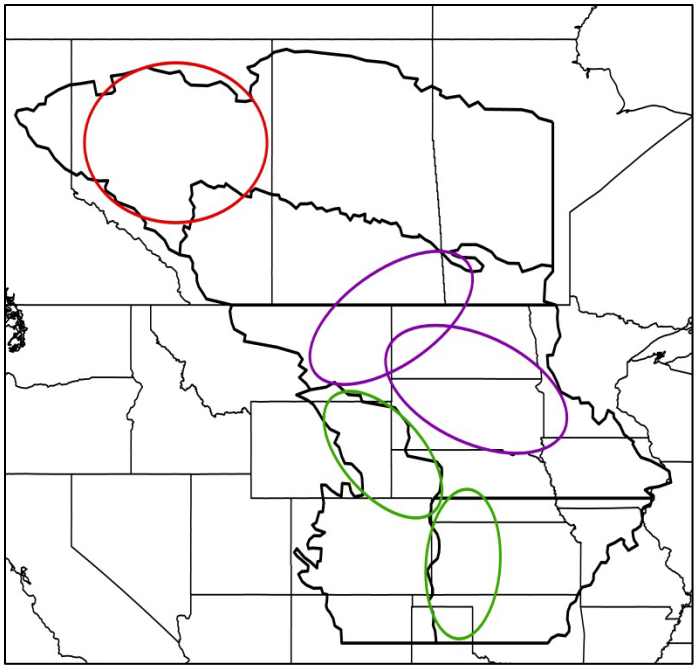

Figure 4.40 Summary of findings for MM5-CCSM. Red indicates areas that may see increases in the frequency and/or intensity of convective precipitation. Purple indicates areas that may see more severe thunderstorms. Green indicates areas that may see fewer but stronger thunderstorms.

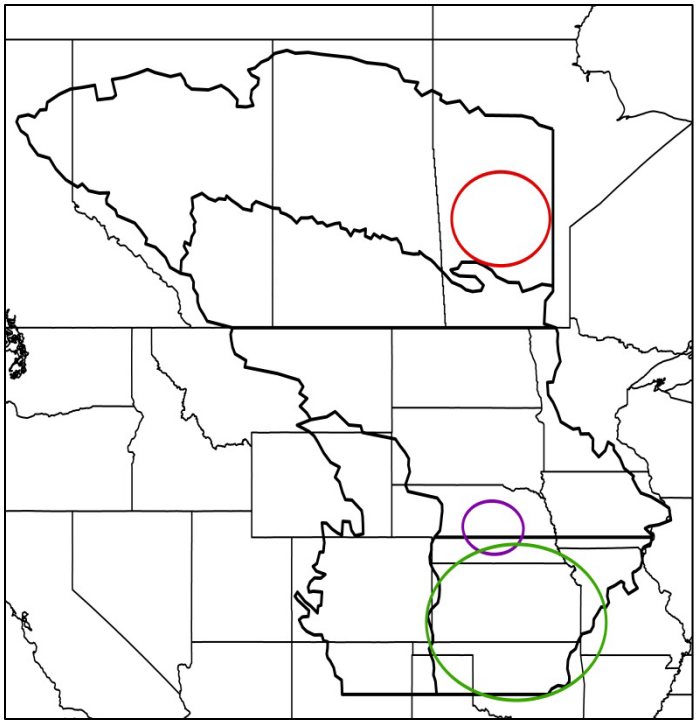

Figure 4.41 Summary of findings for HRM3-HadCM3. Red indicates areas that may see increases in the frequency and/or intensity of convective precipitation. Purple indicates areas that may see more severe thunderstorms. Green indicates areas that may see fewer but stronger thunderstorms.

Chapter 5 Conclusion

5.1 Summary and Conclusions

Increased global mean surface temperature has resulted from an increase in greenhouse gas concentrations in the atmosphere. These increases may result in increased moisture and instability and subsequently increases in the number and/or intensity of thunderstorms in the future (Lee, 2012). Thunderstorms are a common atmospheric phenomenon in North America and may yield extreme weather like heavy rainfall, lightning, high winds, tornadoes, and hail. As such, they pose significant threats societally and economically. Considering the potential damage thunderstorms can cause, it is important to examine the relationship between global climate change and thunderstorms. Examining this relationship has posed challenges to researchers, primarily due to the small spatial and temporal scales of thunderstorms and their subsequent inability to be resolved by GCMs and systems of meteorological observing stations. With their smaller spatial resolution, RCMs have been found to better represent mesoscale atmospheric processes, such as thunderstorms and environments conducive to thunderstorm development (Curry et al., 2016; Paeth & Mannig, 2013; Wang et al., 2015). This research seeks to address these challenges and examine the relationship between global climate change and thunderstorms. Three RCM-GCM pairings from NARCCAP – selected due to their ability to reproduce spatial patterns of precipitation and hail climatology – are used to examine future changes in thunderstorm environments over western Canada and the central and northern U.S. Plains. Broken down into the two main objectives of this thesis, the findings of this research can be summarized as follows:

1) **Characterize the future change in convective and total precipitation over western Canada and the central U.S. Plains**

In general, the precipitation results show coincident increases in convective and total precipitation or increases in convective precipitation where there are decreases or lesser increases in total precipitation. This suggests an increase in the frequency and/or intensity of thunderstorms in the future. More specifically, however, the results of the model pairings differ spatially; these results can be summarized as follows:

- Over CHP, MM5-CCSM and HRM3-HadCM3 show statistically significant decreases in convective and total precipitation, which agrees with the findings of other research (e.g. Mahoney et al., 2013); in contrast, MM5-HadCM3 shows primarily statistically insignificant increases over this region.
- In agreement with the climatology of SGP and predicted changes from other studies (e.g. Bukovsky et al., 2017), MM5-CCSM shows increases in convective and total precipitation in April and May and decreases in June through August; in contrast, MM5-HadCM3 and HRM3-HadCM3 do not reflect these projected changes over the region.
- In agreement with previous findings (e.g. Harding et al., 2013; Harding & Snyder, 2014) of future increases (decreases) in heavy (light) precipitation events, all three model pairings show increased convective precipitation as a percentage of total precipitation over USP; however, only MM5-CCSM agrees with these findings that there will be increased precipitation from April through July and decreases in August.
- Over western Canada, in NWF and CAP, previous research (e.g. Mladjic et al., 2011) has indicated there will be increases in both heavy and light precipitation events; the three model pairings show increased convective precipitation as a percentage of total precipitation for these regions, indicating a possible future increase in heavy convective rainfall events.

2) Characterize the future change in severe weather environment over western Canada and the central U.S. Plains

In this research, a number of severe weather parameters were examined that represent the ingredients necessary for severe thunderstorm formation which are low-level moisture, instability, a proxy for a convective trigger (occurrence of convective precipitation), and vertical wind shear. Two composite parameters, the SCP (Supercell Composite Parameter) and STP (Significant Tornado Parameter), were also calculated using information from the U.S. Storm Prediction Center (SPC). Surface and mixed-layer dewpoint temperatures were used to represent moisture, SBCAPE, MUCAPE, MLCAPE, and MLCIN to represent changes in instability, and BWD0to6km and BWD0to1km to represent changes in vertical wind shear. In addition to plots of each of these parameters, plots of concurrently statistically significant changes in MLCAPE and BWD0to6km were created, as environments with both CAPE and wind shear have been found to be the most conducive to organized thunderstorms. The results of the severe weather parameter analysis for the warm season (JJA) are summarized below:

- Over northern CHP, MM5-CCSM shows statistically significant increases in BWD0to6km, MLCAPE, SCP, and convective precipitation and MM5-HadCM3 shows statistically significant increases in convective precipitation and CAPE over this region; MM5-CCSM indicates an increase in severe thunderstorms whereas MM5-HadCM3 suggests an increase in non-severe thunderstorms.
- Over SGP, HRM3-HadCM3 and MM5-CCSM shows statistically significant increases in MLCAPE, BWD0to6km, SCP, and MLCIN but correspondingly insignificant increases in convective precipitation; these model pairings suggest increased potential for severe

thunderstorms in the future that may not be realized because of increased convective inhibition.

- Over USP, MM5-CCSM shows statistically significant increases in MLCAPE, BWD0to6km, SCP, MLCIN, and convective precipitation whereas MM5-HadCM3 shows significant increases in only CAPE and convective precipitation; MM5-CCSM indicates increases in severe thunderstorms in the future despite increased capping and MM5-HadCM3 indicates a future increase in non-severe thunderstorms.
- MM5-HadCM3, MM5-CCSM, and HRM3-HadCM3 all show increased convective precipitation and CAPE over much of NWF and CAP indicating the influence of CAPE in the future; this may result in increased frequency and/or intensity of thunderstorms.

5.2 Societal and Economic Impacts

Future changes in convective and total precipitation over the domain will have societal and economic impacts that vary between ecoregions. As previously stated, thunderstorms can produce extreme weather like heavy rainfall, hail, and lightning. These hazards pose significant societal and economic threats. In this section, the results of this research are discussed in the context of some of these hazards.

Though increases in global average surface temperature may result in increased instability and subsequently increases in the number and/or intensity of thunderstorms, it may also lead to increased evaporation rates, and potentially more arid environments (Burn & Hesch, 2007). In an examination of April – October evaporation over the Canadian Prairie Provinces, Burn and Hesch (2007) found that, in general, increasing trends in evaporation occurred over the northern part of the domain and decreasing trends over the southern part of the domain. In CAP and NWF, there has been increased water demand from the agricultural and industrial sectors

(Khaliq et al., 2015). This demand will only be exacerbated by increased evaporation rates. In addition to increased demand for water, drier conditions in the future would also affect wetlands in the boreal forest region of Canada, as they form closed drainage basins under dry conditions, not discharging to a natural drainage system (Khaliq et al., 2015); this would impact water availability from the rivers and lakes that make up these drainage systems.

Increased convective precipitation over NWF is significant as fire plays an important role in the life cycle of Canadian boreal forest; in particular, it has been found that approximately 80% of fires in this region are caused by lightning strikes (Wotton, Nock, & Flannigan, 2010). As lightning is a common hazard of thunderstorms, increases in convective precipitation would result in increased lightning strikes and potentially an increase in the number of forest fires in the summer period, though increased precipitation would result in increased surface moisture which decreases the potential for ignition when lightning strikes (Wotton et al., 2010). If there are future increases in both heavy precipitation events and the number of dry days, there could be both increases in precipitation and increased potential for ignition.

Similar to CAP, USP contains agriculturally important areas, and in the past, drought and heavy precipitation events have resulted in significant economic losses over the Midwest and Great Plains (Harding et al., 2013). The projected changes found in this research, and in prior research for USP (Harding et al., 2013; Harding & Snyder, 2014), suggest there will be an increase in heavy precipitation events and the number of dry days between events, suggesting a greater potential for drought. Similarly changes could occur over the Front Range in CHP where decreased precipitation has been found (Mahoney et al., 2013).

As mentioned in Chapter 1, thunderstorms produce extreme weather like hail; hail is a weather phenomenon of particular concern because it can cause significant damage to property

and agriculture (Mahoney et al., 2012). The three model pairings from NARCCAP used in this research were initially selected by Brimelow et al. (2017) and used to examine changes in hail frequency and intensity between the current and future time periods. Modeling hail is difficult due to the small-scale processes involved in hail formation, an issue Brimelow et al. (2017) address by using the data from the NARCCAP models as input for the one-dimensional cloud model HAILCAST. It is anticipated that a warmer, moister climate will result in stronger thunderstorms, stronger updrafts, and increased production of hail; however, a warmer climate will also result in a higher melting level height and thus increased melting of small hailstones before they reach the surface (Mahoney et al., 2012). The results of Brimelow et al. (2017) agree with these anticipated future changes. They used mean multi-model accumulated kinetic energy as a measure of hail occurrence and hail size, finding primarily increases in this parameter as well as increases in the number of days where hail aloft melted before reaching the surface. These results imply stronger updrafts, which is in agreement with the results presented here of increased CAPE for which there are primarily increases over the domain.

5.3 Future Research

Despite the added value of RCMs beyond their global counterparts in modeling thunderstorms, there are errors inherent in the use of RCMs and in climate modeling in general. In the dynamical downscaling of GCMs to regional spatial scales, RCMs inherit not only the large-scale biases of their driving GCMs but also generate additional biases as they directly simulate regional climate dynamics that depend on different representations of physical processes (Fan, Bradley, & Rawlins, 2015). This is referred to as “model uncertainty” and can be summarized as “imperfect representations of key processes and feedback in the climate system by various climate models” (Fan et al., 2015, p. 10569). In addition to model uncertainty, both

Fan et al. (2015) and Sobolowski and Pavelsky (2012) discuss two other forms of uncertainty associated with the use of RCMs: “natural variability uncertainty”, which refers to “internal climate variability on interannual and decadal timescales, which may strengthen or offset future climate response to anthropogenic forcing” (Fan et al., 2015, p. 10569), and “scenario uncertainty”, which refers to uncertainty “due to estimated trajectories of global development and future emissions” (Sobolowski & Pavelsky, 2012, para. 4). This final form of uncertainty is best addressed by selecting a scenario that is as realistic as possible in terms of future climate change.

Various methods have been suggested and evaluated to address model uncertainty and natural variability uncertainty. Model uncertainty results from the need for RCMs to parameterize physical processes that occur at a sub-grid scale, such as convection and boundary layer mixing (Mahoney et al., 2013). To address this issue, a number of studies have used high-resolution dynamical downscaling, referred to as convection-permitting models (CPMs) (spatial resolution < 4 km) to examine localized precipitation events like thunderstorms (Alexander et al., 2013). For example, Trapp et al. (2010) (as cited in Mahoney et al., 2013) used a model with 4.25 km spatial resolution to explicitly resolve convection and found it captured the diurnal cycle and geographic distribution of convective weather and Liu et al. (2017) found the 4 km resolution WRF model performed well in modeling the spatial and temporal patterns of seasonal and annual precipitation over the United States. Prein et al. (2015) examined numerous studies using CPMs and summarized their added value, including the representation of extreme precipitation at finer temporal resolutions, improved representation of the diurnal cycle and of deep convection, and the largest added value to be in regions with complex topography (e.g. mountainous regions) and in extreme events. However, despite the added value of CPMs, they

have issues primarily associated with computational constraints. Because of these constraints, CPMs typically have to be run over shorter time periods, smaller domains, and a fewer number of realizations can be run (Prein et al., 2015).

To address natural variability uncertainty, it has been proposed that a large number of realizations need to be run versus only one realization as was done in the case of NARCCAP. Further, to address both forms of uncertainty, it has been suggested that a multi-model ensemble approach be used. It is intended that the combination of results from multiple models can lead to "more consistent and reliable forecasts by reducing the characteristic biases and uncertainties of any individual model" (Mailhot et al., 2012, p. 1152). All of these approaches to reducing climate model uncertainty require extensive computational resources and are limited by computation constraints; thus, studies employing these methods will advance as technology advances (Prein et al., 2015).

The Coordinated Regional Climate Downscaling Experiment (CORDEX) is a framework initiated by the World Climate Research Programme (WCRP). CORDEX allows for a model evaluation framework by examining how well models perform in reproducing observed climate conditions as well as a climate projection framework by evaluating the maximum contribution of difference sources of uncertainty (Giorgi, Jones, & Asrar, 2009). The domains of CORDEX cover most land areas of the world, including North America. The North American CORDEX Program (2014) uses different climate change scenarios, multiple realizations of different GCMs as driving models, and a matrix of six GCMs driving five different RCMs at different spatial resolutions to address scenario, natural variability, and model uncertainty, respectively. North American CORDEX is intended to build on the knowledge and experience gained from NARCCAP (North American CORDEX Program, 2014).

In addition to the use of CPMs, multi-model ensembles, and a larger number of realizations, another approach in using climate models to examine changes in convective and total precipitation is to examine storm properties. This research uses 30-year monthly and seasonal averages of convective and total precipitation, making it difficult to determine if increases in convective precipitation are the result of changes in the frequency or intensity of thunderstorms. Yu, Jiang, Gautum, Zhang, and Acharya (2015) used the NARCCAP ensemble to examine three storm properties: storm duration, inter-storm period, and storm intensity by identifying independent storm events. This type of analysis is important as future changes in these parameters will affect decisions around adaptation and mitigation. For example, increased storm intensity would result in increased potential for flooding; this means that the construction of urban drainage systems would have to be adapted (Yu et al., 2015). Thus, future research in future changes in convective and total precipitation over western Canada and the central U.S. Plains should involve an examination of these storm properties versus exclusively long-term averages.

References

Alexander, M. A., Scott, J. D., Mahoney, K., & Barsugli, J. (2013). Greenhouse-gas induced changes in summer precipitation over Colorado in NARCCAP regional climate models. *Journal of Climate, 26*(21), 8690-8697. doi: 10.1175/JCLI-D-13-00088.1

Brimelow, J. C., Reuter, G. W., & Poolman, E. R. (2002). Modeling Maximum Hail Size in Alberta Thunderstorms. *Weather and Forecasting, 17*(5), 1048-1062. doi: http://dx.doi.org/10.1175/1520-0434(2002)017<1048:MMHSIA>2.0.CO;2

Brimelow, J. C., Burrows, W. R., Hanesiak, J. M. (2017). The changing hail threat over North America in response to anthropogenic climate change. *Nature Climate Change, 7*, 516-522. doi: 10.1038/nclimate3321

Brooks, H. E., Lee, J. W., & Craven, J. P. (2003). The spatial distribution of severe thunderstorm and tornado environments from global reanalysis data. *Atmospheric Research, 67-68*, 73-94. doi:10.1016/S0169-8095(03)00045-0

Brooks, H. E., Anderson, A. R., Riemann, K., Ebbers, I., & Flachs, H. (2007). Climatological aspects of convective parameters from the NCAR/NCEP reanalysis. *Atmospheric Research, 83*(2), 294-305. doi: 10.1016/j.atmosres.2005.08.005

Brooks, H. E. (2013). Severe thunderstorms and climate change. *Atmospheric Research, 123*, 129-138. doi: 10.1016/j.atmosres.2012.04.002

Bukovsky, M. S. & Karoly, D. J. (2011). A regional modeling study of climate change impacts on warm-season precipitation in the central United States. *Journal of Climate, 24*, 1985-2002. doi: 10.1175/2010JCLI3447.1

Bukovsky, M. S., McCrary, R. R., Seth, A., & Mearns, L. O. (2017). A mechanistically credible, poleward shift in warm-season precipitation projected for the U.S. southern Great Plains? *Journal of Climate, 30*(20), 8275-8298. doi: 10.1175/JCLI-D-16-0316.1

Burn, D. H., & Hesch, N. M. (2007). Trends in evaporation for the Canadian Prairies. *Journal of Hydrology, 336*(1-2), 61-73. doi: 10.1016/j.jhydrol.2006.12.011

Chapman McGrew Jr., J. & Monroe, C. B. (2009). *An Introduction to Statistical Problem Solving in Geography* (2nd ed.). Long Grove, IL: Waveland Press, Inc.

Committee on Extreme Weather Events and Climate Change Attribution (CEWECCA). (2016). *Attribution of Extreme Weather Events in the Context of Climate Change*. Washington, DC: The National Academies Press.

Convection. (n.d.). In *Glossary of Meteorology*. Retrieved from http://glossary.ametsoc.org/wiki/Convection

Curry, C. L., Tencer, B., Whan, K., Weaver, A. J., Giguère, M., & Wiebe, E. (2016). Searching for added-value in simulating climate change extremes with a high-resolution regional climate model over western Canada. *Atmosphere-Ocean, 54*(4), 364-384. doi: 10.1080/07055900.2016.1158146

Del Genio, A. D., Yao, M.-S., Jonas, J. (2007). Will moist convection be stronger in a warmer climate? *Geophysical Research Letters, 34*(16). doi: 10.1029/2007GL030525

Diffenbaugh, N. S., Sherer, M., Trapp, R. J. (2013). Robust increases in severe thunderstorm environments in response to greenhouse forcing. *Proceedings of the National Academy of Sciences, 110*(41), 16361-16366. doi: 10.1073/pnas.1307758110

Fan, F., Bradley, R. S., & Rawlins, M. A. (2015). Climate change in the Northeast United States: An analysis of the NARCCAP multi-model simulations. *Journal of Geophysical Research: Atmospheres, 120*(20), 569-592. doi: 10.1002/2015JD023073

Gensini, V. A., Ramseyer, C., & Mote, T. L. (2014). Future convective environments using NARCCAP. *International Journal of Climatology, 34*(5), 1699-1705. doi: 10.1002/joc.3769

Giorgi, F., Jones, C., Asrar, G. R. (2009). Addressing climate information needs at the regional level: the CORDEX framework. *WMO Bulletin, 58*(3), 175-183. Retrieved from https://public.wmo.int/en/bulletin/addressing-climate-information-needs-regional-level-cordex-framework

Harding, K. J., Snyder, P. K., & Liess, S. (2013). Use of dynamical downscaling to improve the simulation of Central U.S. warm season precipitation in CMIP5 models. *Journal of Geophysical Research: Atmospheres, 118*(22), 12522-12536. doi: 10.1002/2013JD019994

Harding, K. J. & Snyder, P. K. (2014). Examining future changes in the character of Central U.S. warm-season precipitation using dynamical downscaling. *Journal of Geophysical Research: Atmospheres, 119*(23), 13116-13136. doi: 10.1002/2014JD022575

Hoogewind, K. A., Baldwin, M. E., & Trapp, R. J. (2017). The impact of climate change on hazardous convective weather in the United States: Insight from high-resolution dynamical downscaling. *Journal of Climate, 30*, 10081-10100. doi: 10.1175/JCLI-D-16-0885.1

Intergovernmental Panel on Climate Change (IPCC). (2000). *IPCC Special Report: Emissions Scenarios.* N. Nakicenovic and R. Swart (Eds.). Cambridge University Press, Cambridge, UK.

Intergovernmental Panel on Climate Change (IPCC). (2013). *Climate Change 2013: The Physical Science Basis. Contribution of Working Group I to the Fifth Assessment Report of the Intergovernmental Panel on Climate Change*. Stocker, T.F., D. Qin, G. -K. Plattner, M. Tignor, S.K. Allen, J. Boschung, A. Nauels, Y. Xia, V. Bex and P.M. Midgley (Eds.). Cambridge University Press, Cambridge, United Kingdom and New York, NY, USA.

Kapsch, M.-L., Kunz, M., Vitolo, R., & Economou, T. (2012). Long-term trends of hail-related weather types in an ensemble of regional climate models using a Bayesian approach. *Journal of Geophysical Research, 117*(D15). doi: 10.1029/2011JD017185

Khaliq, M. N., Sushama, L., Monette, A., & Wheater, H. (2015). Seasonal and extreme precipitation characteristics for the watersheds of the Canadian Prairie Provinces as simulated by the NARCCAP multi-RCM ensemble. *Climate Dynamics, 44*(1-2), 255-277. doi: 10.1007/s00382-014-2235-0

Lee, C. C. (2012). Utilizing synoptic climatological methods to assess the impacts of climate change on future tornado-favourable environments. *Natural Hazards, 62*(2), 325-343. doi: 10.1007/s11069-011-9998-y

Li, G., Zhang, X, Cannon, A. J., Murdock, T. Sobie, S., Zwiers, F., … Qian, B. (2018). Indices of Canada's future climate for general and agricultural adaptation applications. *Climatic Change, 148*(1-2), 249-263. doi: 10.1007/s10584-018-2199-x

Liu, C., Ikeda, K., Rasmussen, R., Barlage, M., Newman, A. J., Prein, A. F., … Yates, D. (2017). Continental-scale convection-permitting modeling of the current and future climate of North American. *Climate Dynamics, 49*(1-2), 71-95. doi: 10.1007/s00382-016-3327-9

Lucas-Picher, P., Wulff-Nielsen, M., Christenson, J. H., Aðalgeirsdóttir, G., Mottram, R., & Simonsen, S. B. (2012). Very high resolution regional climate model simulations over Greenland: Identifying added value. *Journal of Geophysical Research: Atmospheres, 117*(D2). doi: 10.1029/2011JD016267

Mahoney, K., Alexander, M. A., Thompson, G., Barsugli, J. J., & Scott, J. D. (2012). Changes in hail and flood risk in high-resolution simulations over Colorado's mountains. *Nature Climate Change, 2*(2), 125-131. doi: 10.1038/nclimate1344

Mahoney, K., Alexander, M., Scott, J. D., Barsugli, J. (2013). High-resolution downscaled simulations of warm-season extreme precipitation events in the Colorado Front Range under past and future climates. *Journal of Climate, 26*, 8671-8689. doi: 10.1175/JCLI-D-12-00744.1

Mailhot, A., Beauregard, I. Talbot, G., Caya, D. & Biner, S. (2012). Future changes in intense precipitation over Canada assessed from multi-model NARCCAP ensemble simulations. *International Journal of Climatology, 32*(8), 1151-1163. doi: 10.1002/joc.2343

Mearns, L. O., McGinnis, S., Arritt, R., Biner, S., Duffy, P., Gutowski, W., …, Zoellick, C. (2007). *The North American Regional Climate Change Assessment Program* [Dataset]. Retrieved from https://www.earthsystemgrid.org/project/NARCCAP.html

Mearns, L. O., Gutowski, W., Jones, R., Leung, R., McGinnis, S., Nunes, A. & Qian, Y. (2009). A Regional Climate Change Assessment Program for North America, *Eos Transactions American Geophysical Union, 90*(36), 311–311, doi: 10.1029/2009EO360002

Mearns, L. O., Sain, S., Leung, L. R., Bukovsky, M. S., McGinnis, S., Biner, S., …, Sloan, L. (2013). Climate change projections of the North American Regional Climate Change Assessment Program (NARCCAP). *Climatic Change, 120*(4), 965-975. doi: 10.1007/s10584-013-0831-3

Mladjic, B., Sushama, L., Khaliq, M. N., Laprise, R., Caya, D., & Roy, R. (2011). Canadian RCM projected changes to extreme precipitation characteristics over Canada. *Journal of Climate, 24*(10), 2565-2584. doi: 10.1175/2010JCLI3937.1

North American CORDEX Program (NA-CORDEX). (2014). *Briefing Document*. Retrieved from https://na-cordex.org/briefing-document

Paeth, H. & Mannig, B. (2013). On the added value of regional climate modeling in climate change assessment. *Climate Dynamics, 41*(3-4), 1057-1066. doi: 10.1007/s00382-012-1517-7

Paquin, D., de Elia, R., Frigon, A. (2014). Change in North American atmospheric conditions associated with deep convective and severe weather using CRCM4 climate projections. *Atmosphere-Ocean, 52*(3), 175-190. doi: 10.1080/07055900.2013.877868

Prein, A. F., Langhans, W., Fosser, G., Ferrone, A., Ban, N., Goergen, K., … Leung, R. (2015). A review on regional convection-permitting climate modeling: Demonstrations, prospects, and challenges. *Reviews of Geophysics, 53*(2), 323-361. doi: 10.1002/2014RG000475

Sanderson, M. G., Hand, W. H., Groenemeijer, P., Boorman, P. M., Webb, J. D. C.,& McColl, L. J. (2014). Projected changes in hailstorms during the 21st century over the UK. *International Journal of Climatology, 35*(1), 15-24. doi: 10.1002/joc.3958

Seeley, J. T. & Romps, D. M. (2015). The effect of global warming on severe thunderstorms in the United States. *Journal of Climate, 28*, 2443-2458. doi: 10.1175/JCLI-D-14-00382.1

Sobolowski, S. & Pavelsky, T. (2012). Evaluation of present and future North American Regional Climate Change Assessment Program (NARCCAP) regional climate simulations over the southeast United States. *Journal of Geophysical Research, 117*(D1). doi: 10.1029/2011JD016430

Stull, R. B. (2015). *Practical Meteorology: An algebra-based survey of atmospheric science.* Vancouver, BC: University of British Columbia.

Thompson, R. L., Edwards, R., Hart, J. A. (2002, August). *Evaluation and Interpretation of the Supercell Composite and Significant Tornado Parameters at the Storm Prediction Center.* Paper presented at the 21st Conference on Severe Local Storms, San Antonio, Texas. Retrieved from https://www.spc.noaa.gov/publications/thompson/sigtor.pdf

Thompson, R. L, Edwards, R., Hart, J. A., Elmore, K. L, & Markowski, R. (2003). Close Proximity Soundings within Supercell Environments Obtained from the Rapid Update Cycle. *Weather and Forecasting, 18*, 1243-1261. doi: 10.1175/1520-0434(2003)018<1243:CPSWSE>2.0.CO;2

Tippett, M. K., Allen, J. T., Gensini, V. A., & Brooks, H. E. (2015). Climate and hazardous convective weather. *Current Climate Change Reports, 1*(2), 60-73. doi: 10.1007/s40641-015-0006-6

Torma, C., Giorgi, F., & Coppola, E. (2015). Added value of regional climate modeling over areas characterized by complex terrain – Precipitation over the Alps. *Journal of Geophysical Research: Atmospheres, 120*(9), 3957-3972. doi: 10.1002/2014JD022781

Trapp, R. J., Diffenbaugh, N. S., Brooks, H. E., Baldwin, M. E., Robinson, E. D., & Pal, J. S. (2007). Changes in severe thunderstorm environment frequency during the 21st century caused by anthropogenically enhanced global radiative forcing. *Proceedings of the National Academy of Sciences, 104*(50), 19719-19723. doi: 10.1073/pnas.0705494104

Trapp, R. J., Diffenbaugh, N. S., & Gluhovsky, A. (2009). Transient response of severe thunderstorm forcing to elevated greenhouse gas concentrations. *Geophysical Research Letters, 36*(1). doi: 10.1029/2008GL036203

Van Klooster, S. L., & Roebber, P. J. (2009). Surface-based convective potential in the contiguous United States in a business-as-usual future climate. *Journal of Climate, 22*(12), 3317-3330. doi: http://dx.doi.org/10.1175/2009JCLI2697.1

Walawender, E., Kielar, R., & Ustrnul, Z. (2015). Use of RegCM gridded dataset for thunderstorm favorable conditions analysis over Poland – climatological approach. *Theoretical and Applied Climatology*, *127*(1-2), 229-240. doi: 10.1007/s00704-015-1620-x

Wang, J., Swati, F. N. U., Stein, M. L., & Kotamarthi, V. R. (2015). Model performance in spatiotemporal patterns of precipitation: New methods for identifying value added by a regional climate model. *Journal of Geophysical Research: Atmospheres, 120*(4), 1239-1259. doi: 10.1002/2014JD022434

Wehner, M. F. (2013). Very extreme seasonal precipitation in the NARCCAP ensemble: model performance and projections. *Climate Dynamics, 40*(1-2), 59-80. doi: 10.1007/s00382-012-1393-1

World Meteorological Organization. (2018). *Guide to Climatological Practices (WMO-No. 100)* (3rd ed.). Retrieved from https://library.wmo.int/doc_num.php?explnum_id=5541

Wotton, B. M., Nock, C. A., & Flannigan, M. D. (2010). Forest fire occurrence and climate change in Canada. *International Journal of Wildland Fires, 19*(3), 253-271. doi: 10.1071/WF09002

Yu, Z., Jiang, P., Gautam, M. R., Zhang, Y., Acharya, K. (2015). Changes of seasonal storm properties in California and Nevada from an ensemble of climate projections. *Journal of Geophysical Research, 120*(7), 2676-2688. doi: 10.1002/2014JD022414

Appendix A: Precipitation Percentages

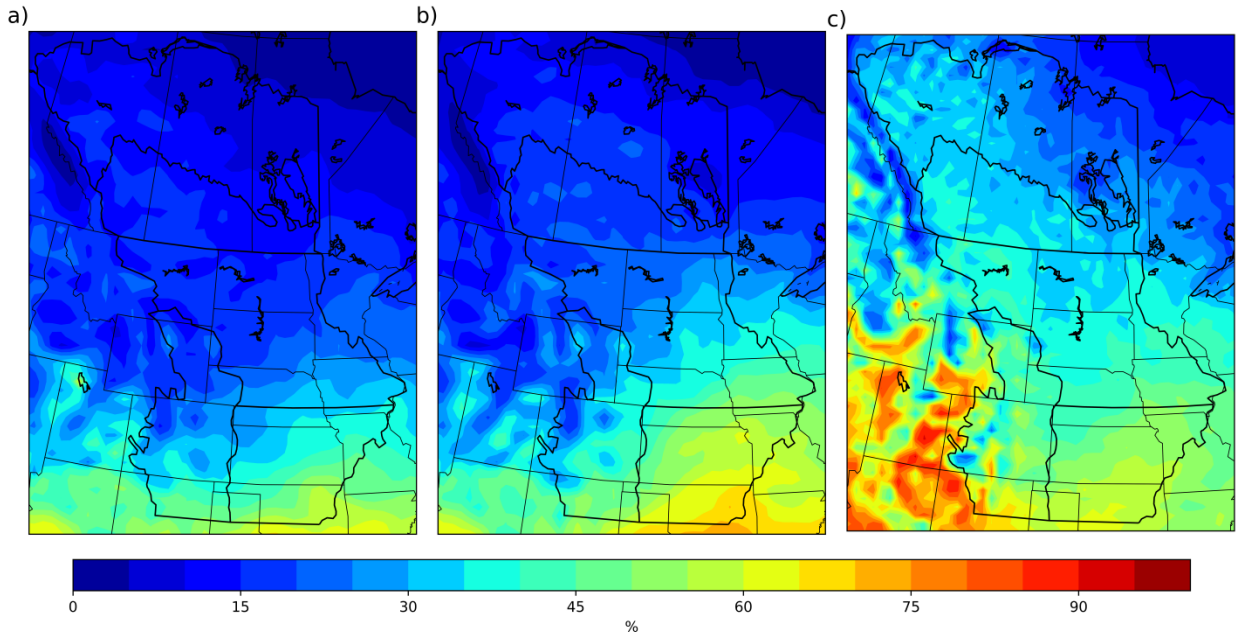

Figure A.1 Convective precipitation as a percentage of total precipitation for the current period in spring (MAM) for a) MM5-HadCM3 b) MM5-CCSM and c) HRM3-HadCM3.

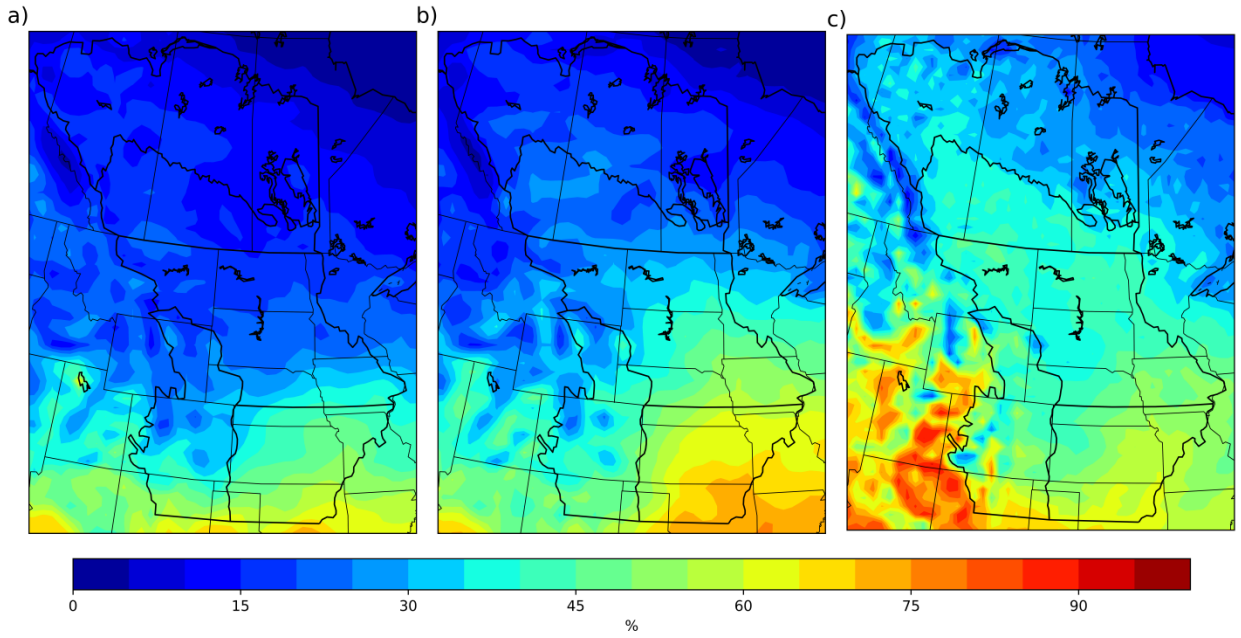

Figure A.2 Convective precipitation as a percentage of total precipitation for the future period in spring (MAM) for a) MM5-HadCM3 b) MM5-CCSM and c) HRM3-HadCM3.

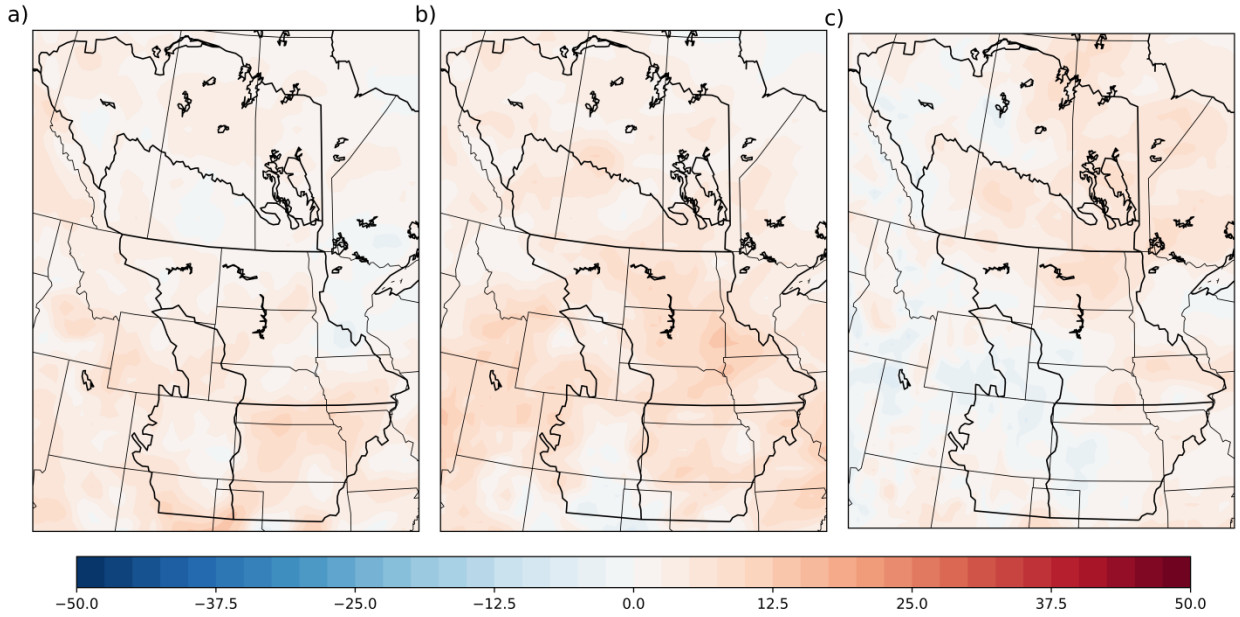

Figure A.3 Difference (future – current) in convective precipitation as a percentage of total precipitation in spring (MAM) for a) MM5-HadCM3 b) MM5-CCSM and c) HRM3-HadCM3.

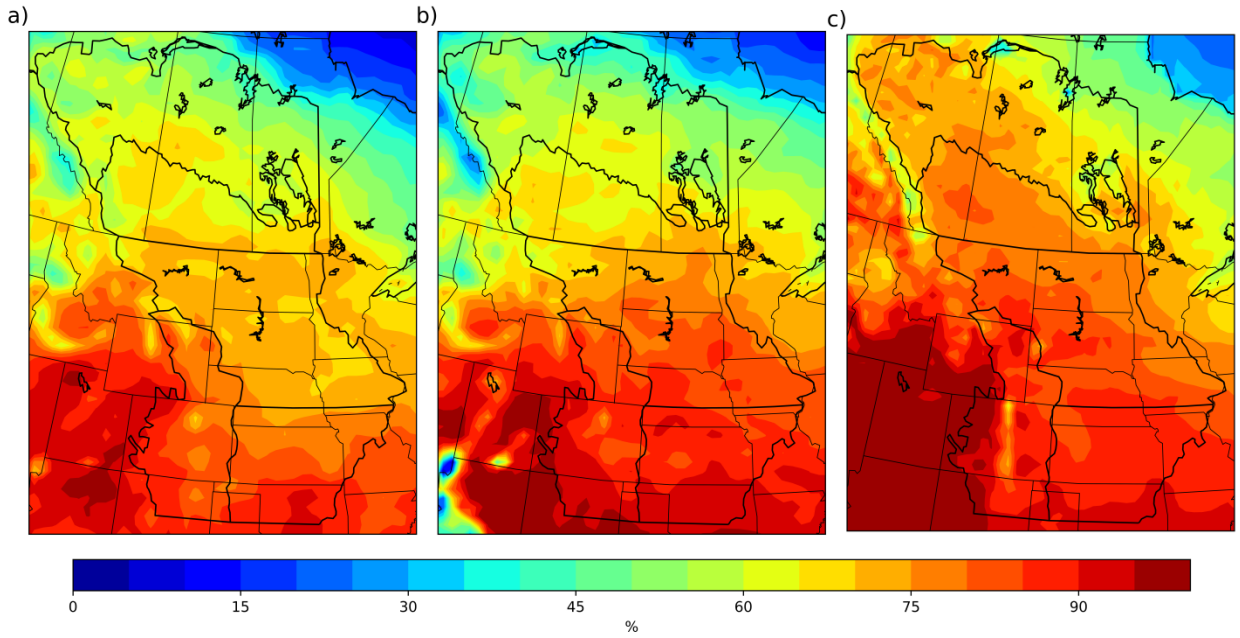

Figure A.4 Convective precipitation as a percentage of total precipitation for the current period in summer (JJA) for a) MM5-HadCM3 b) MM5-CCSM and c) HRM3-HadCM3.

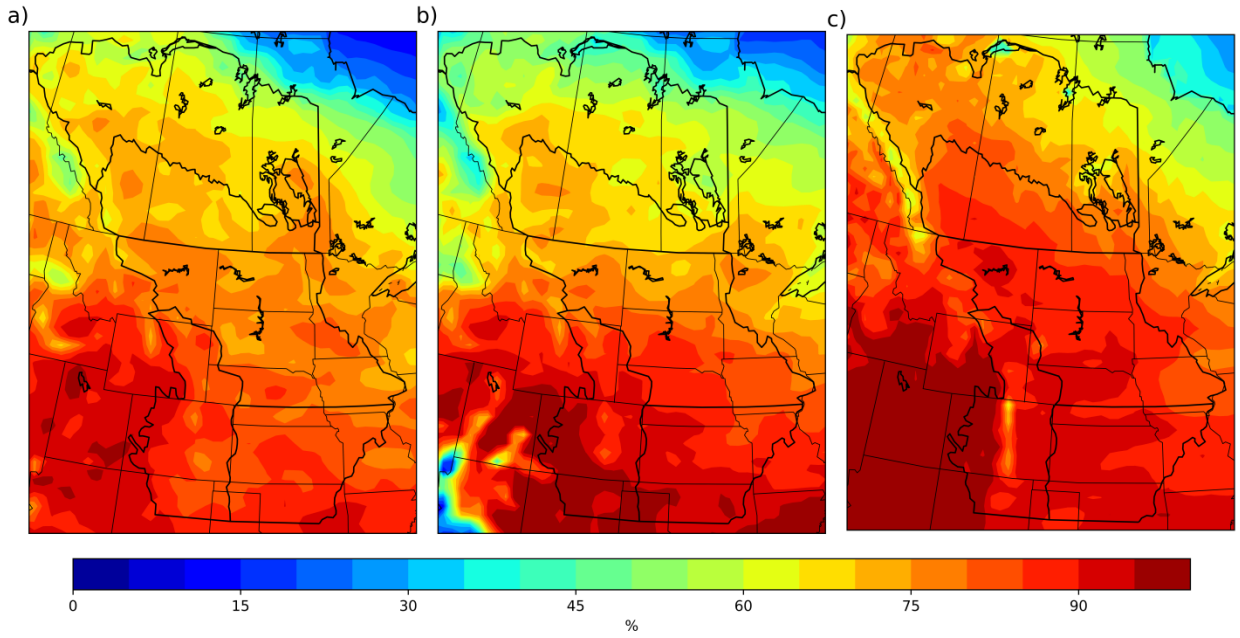

Figure A.5 Convective precipitation as a percentage of total precipitation for the future period in summer (JJA) for a) MM5-HadCM3 b) MM5-CCSM and c) HRM3-HadCM3.

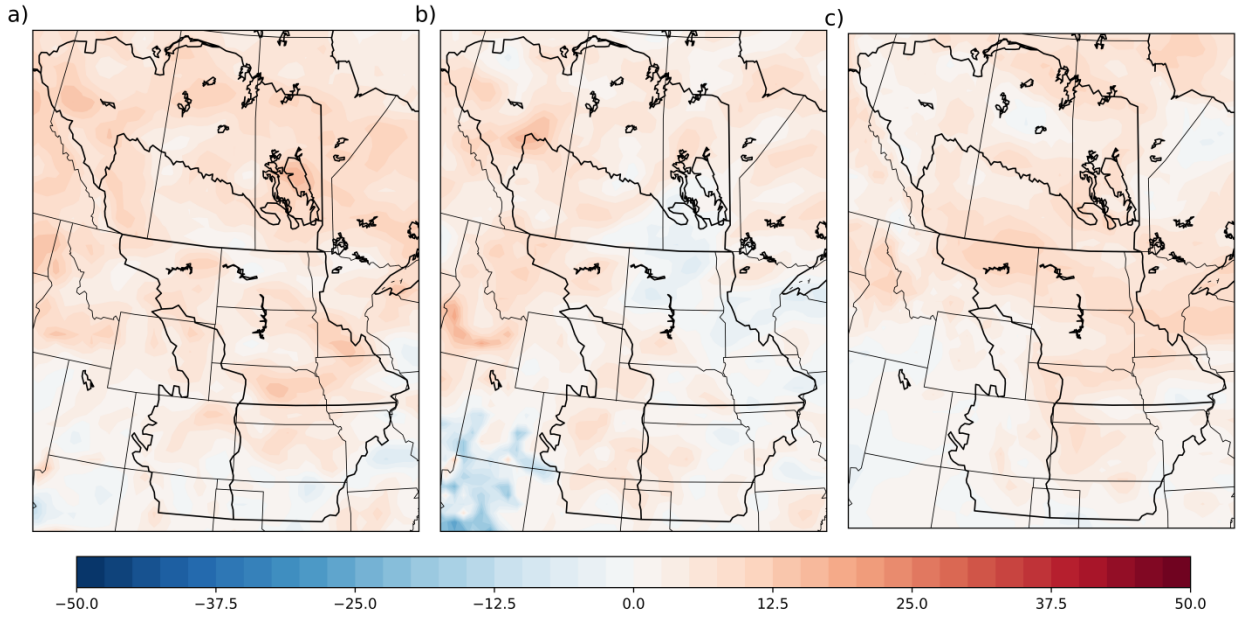

Figure A.6 Difference (future – current) in convective precipitation as a percentage of total precipitation in summer (JJA) for a) MM5-HadCM3 b) MM5-CCSM and c) HRM3-HadCM3.

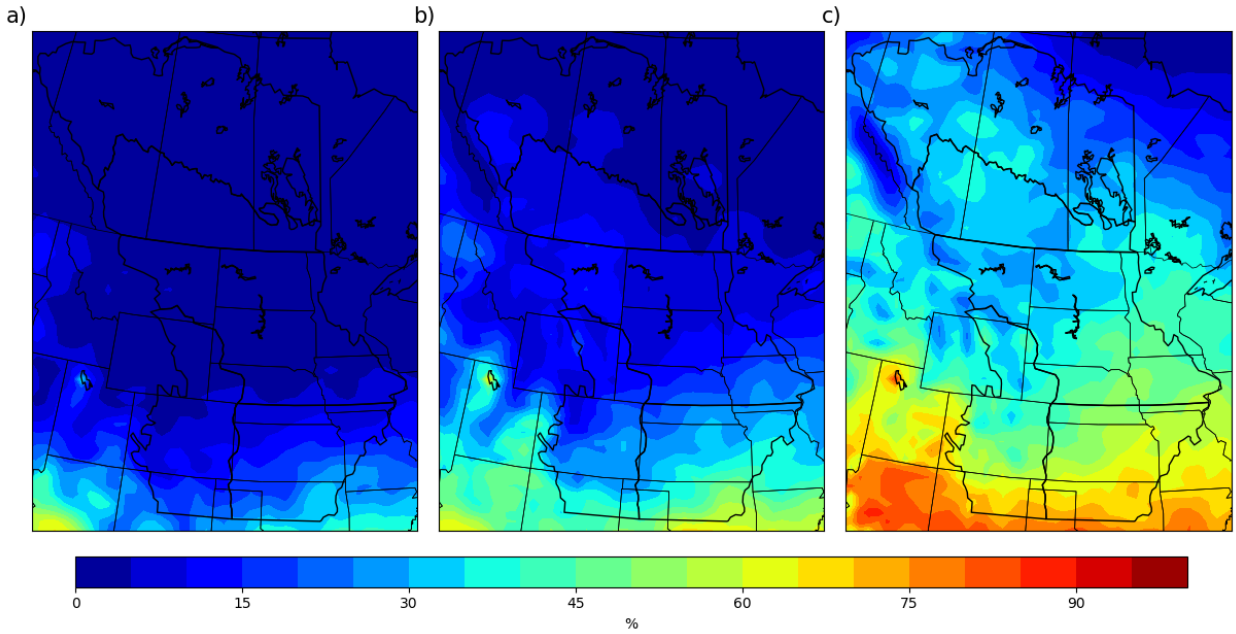

Figure A.7 Convective precipitation as a percentage of total precipitation for the current period in spring (MAM) for MM5-HadCM3 for a) March b) April and c) May.

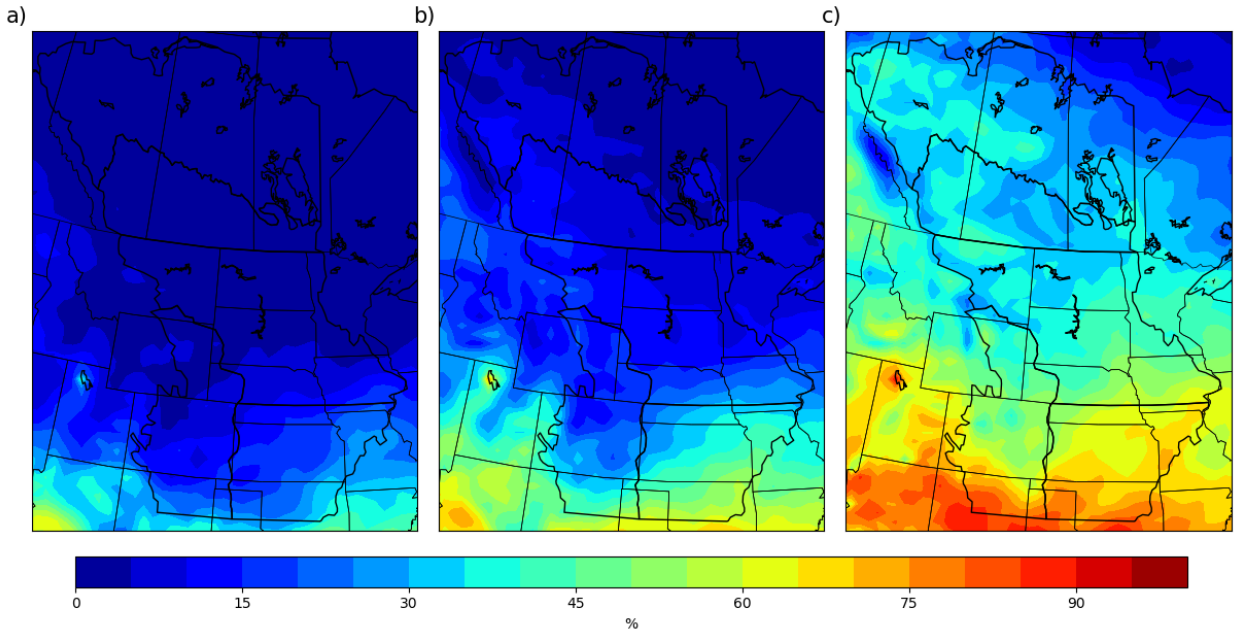

Figure A.8 Convective precipitation as a percentage of total precipitation for the future period in spring (MAM) for MM5-HadCM3 for a) March b) April and c) May.

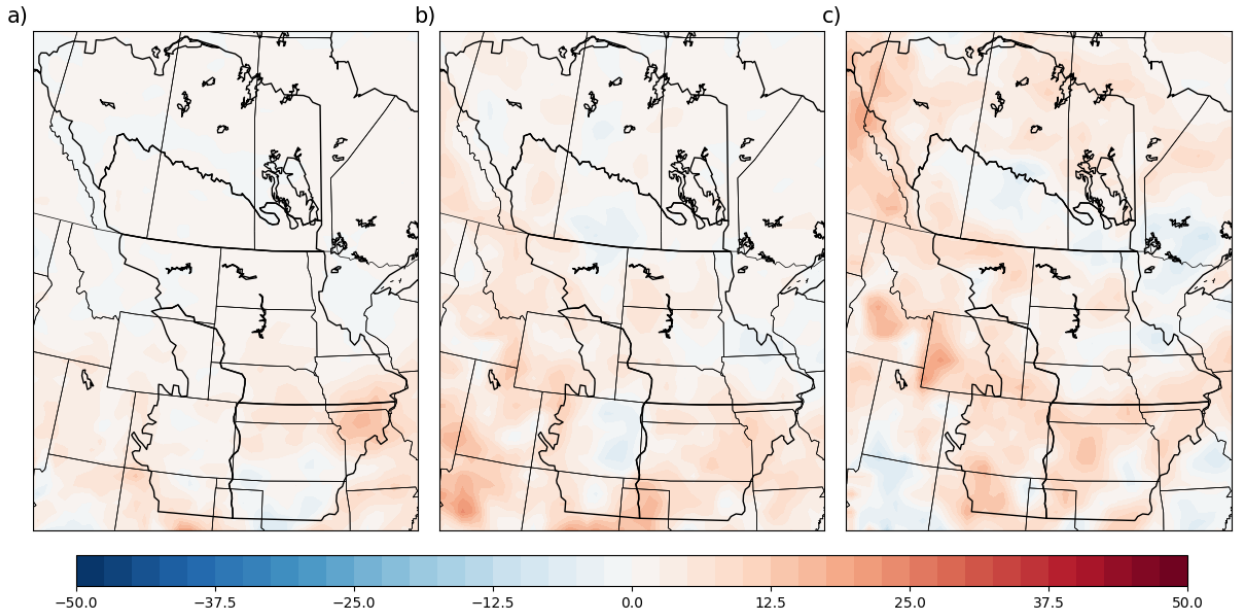

Figure A.9 Difference (future – current) in convective precipitation as a percentage of total precipitation in spring (MAM) for MM5-HadCM3 for a) March b) April and c) May.

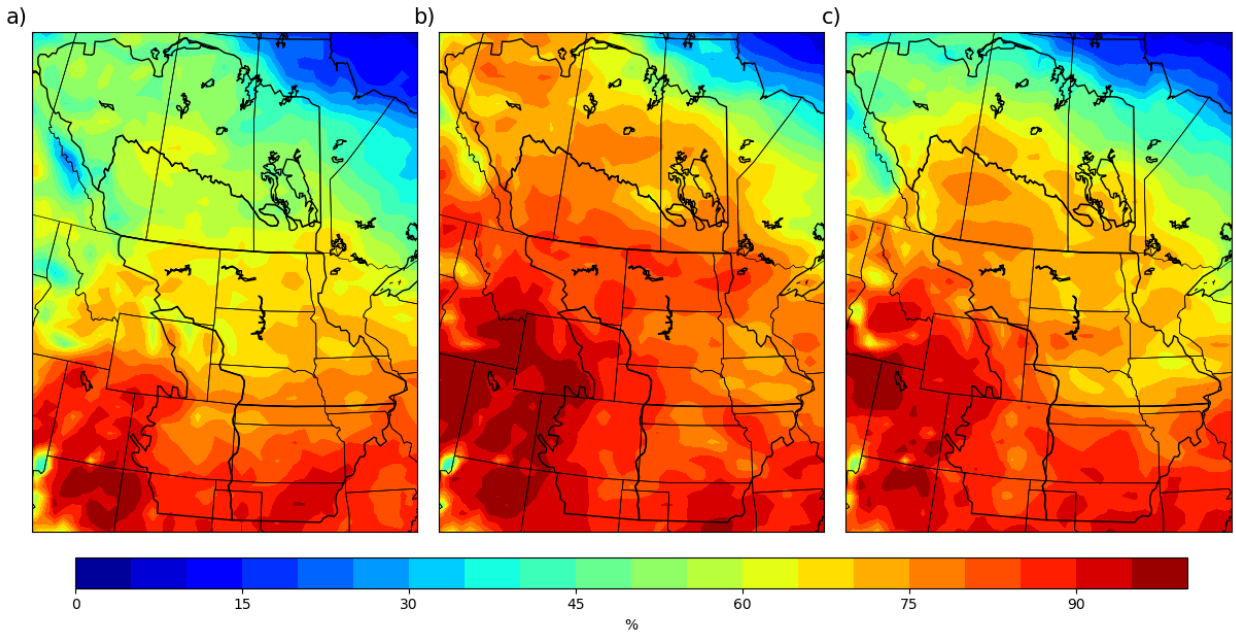

Figure A.10 Convective precipitation as a percentage of total precipitation for the current period in summer (JJA) for MM5-HadCM3 for a) June b) July and c) August.

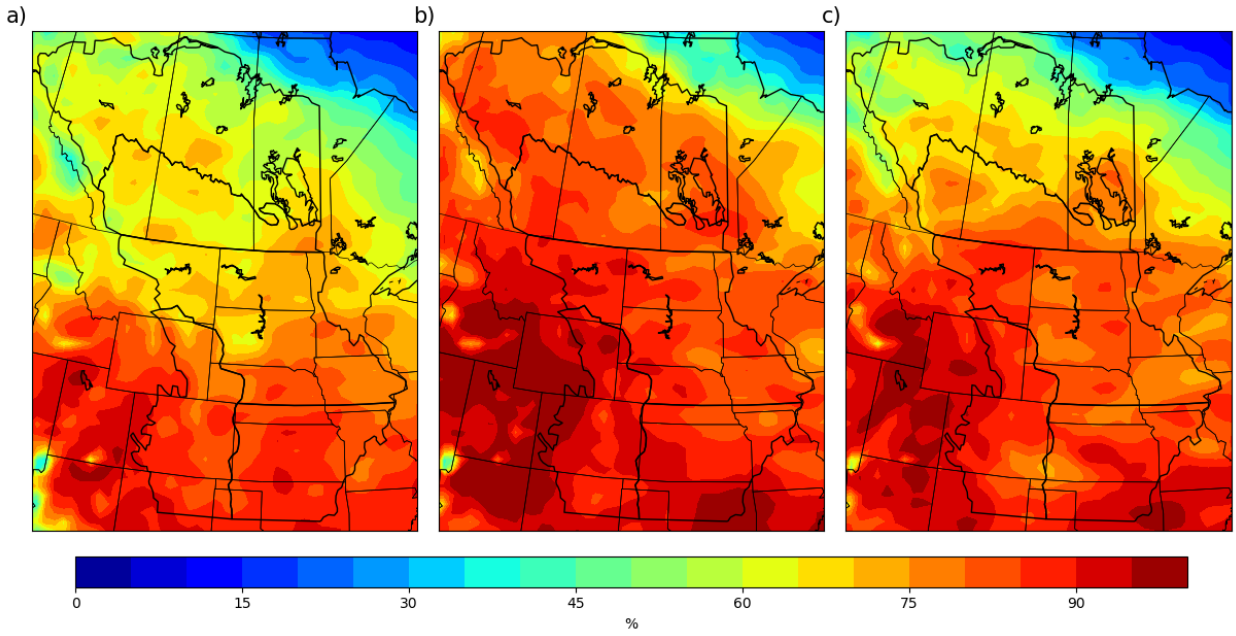

Figure A.11 Convective precipitation as a percentage of total precipitation for the future period in summer (JJA) for MM5-HadCM3 for a) June b) July and c) August.

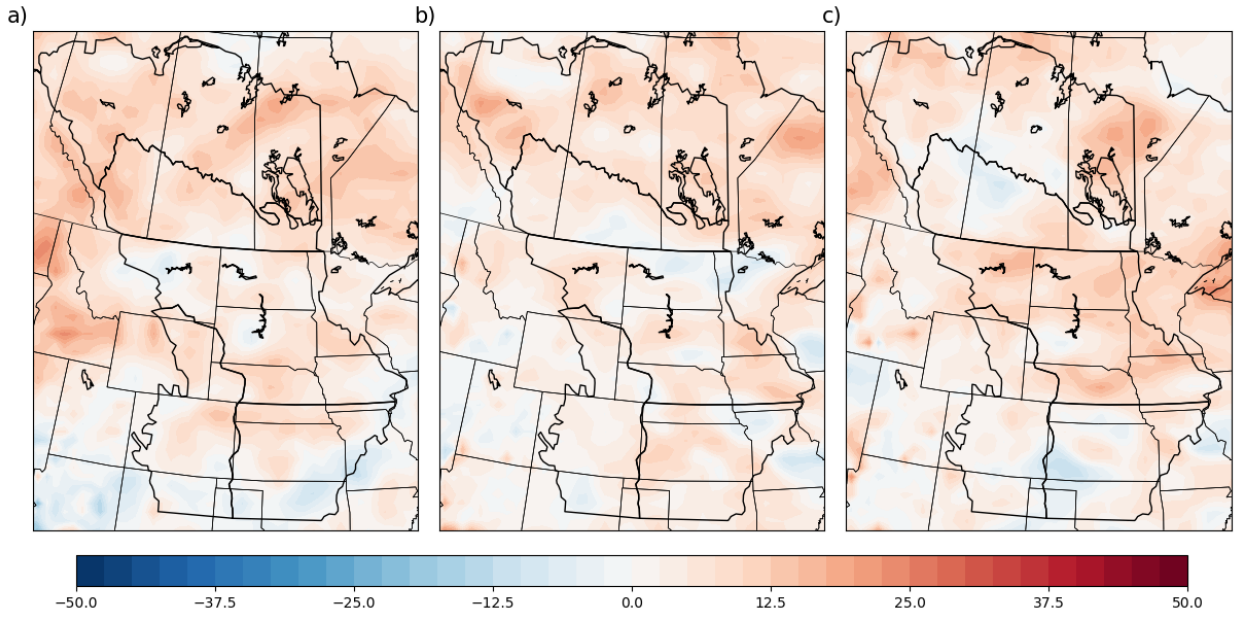

Figure A.12 Difference (future – current) in convective precipitation as a percentage of total precipitation in summer (JJA) for MM5-HadCM3 for a) June b) July and c) August.

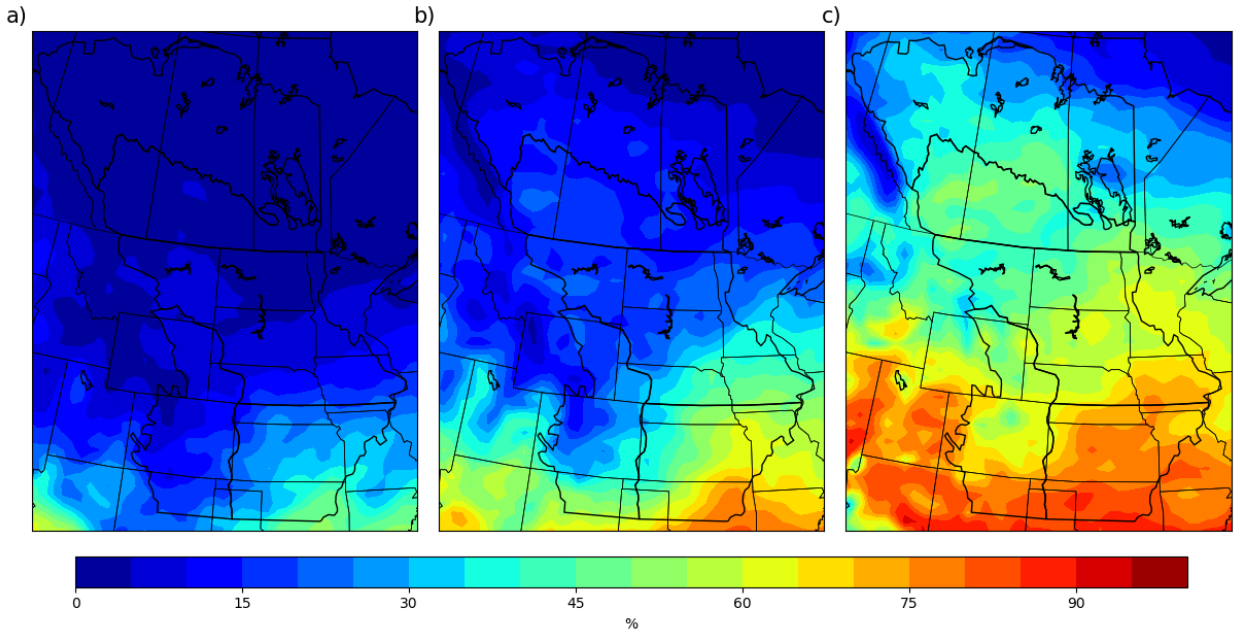

Figure A.13 Convective precipitation as a percentage of total precipitation for the current period in spring (MAM) for MM5-CCSM for a) March b) April and c) May.

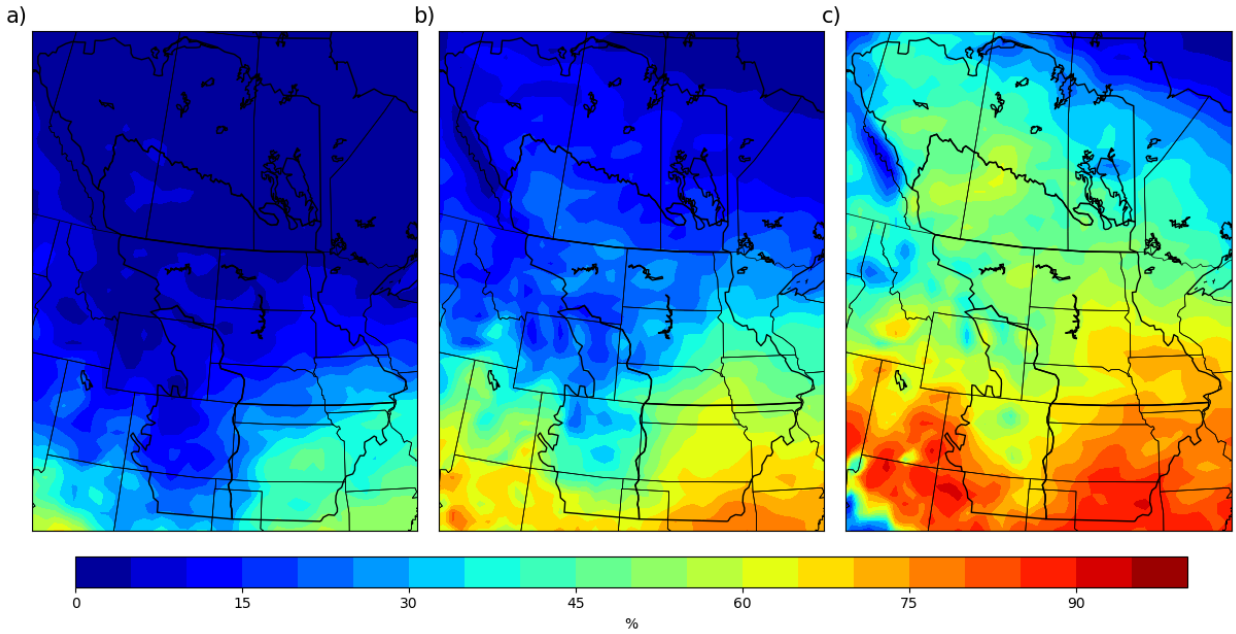

Figure A.14 Convective precipitation as a percentage of total precipitation for the future period in spring (MAM) for MM5-CCSM for a) March b) April and c) May.

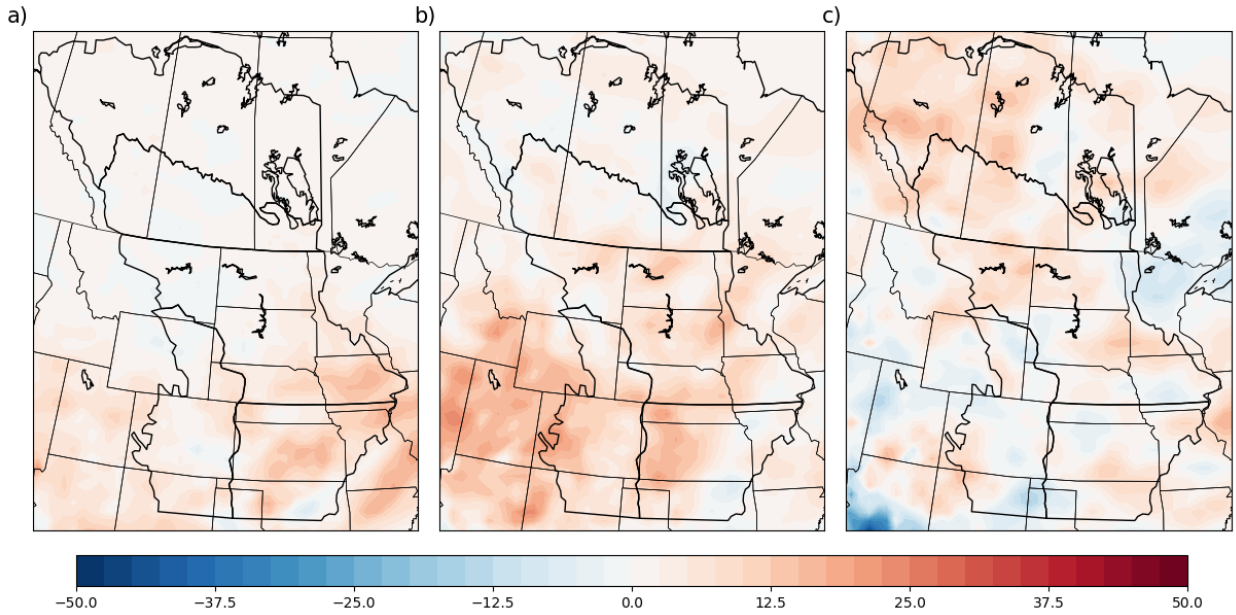

Figure A.15 Difference (future – current) in convective precipitation as a percentage of total precipitation in spring (MAM) for MM5-CCSM for a) March b) April and c) May.

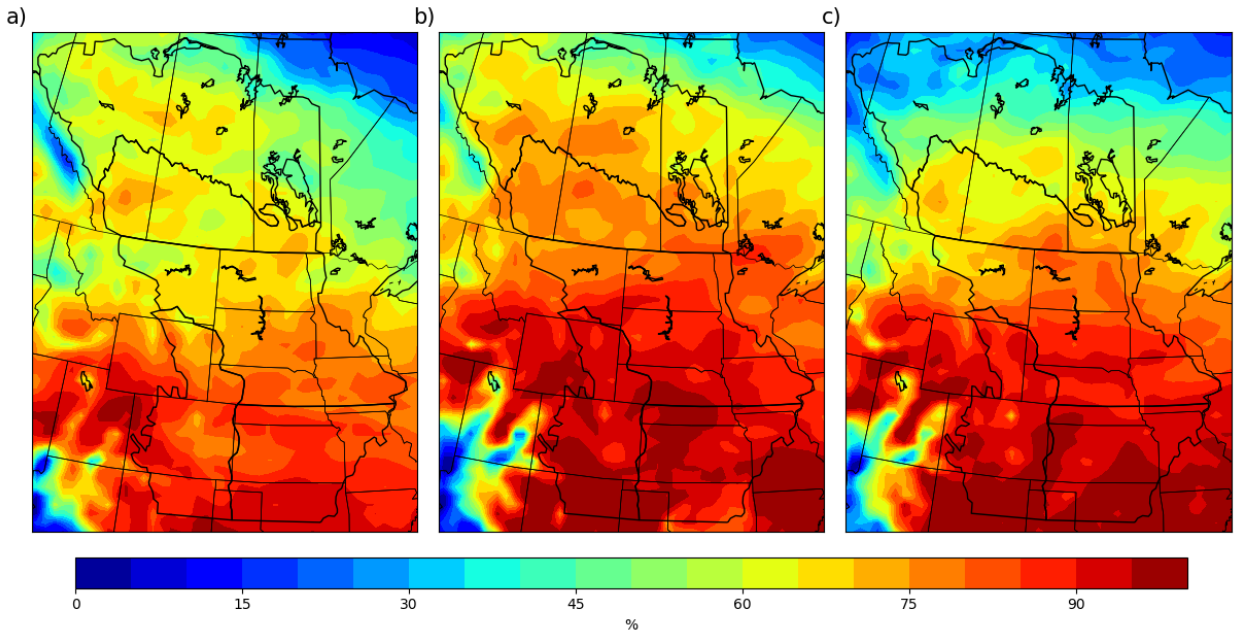

Figure A.16 Convective precipitation as a percentage of total precipitation for the future period in summer (JJA) for MM5-CCSM for a) June b) July and c) August.

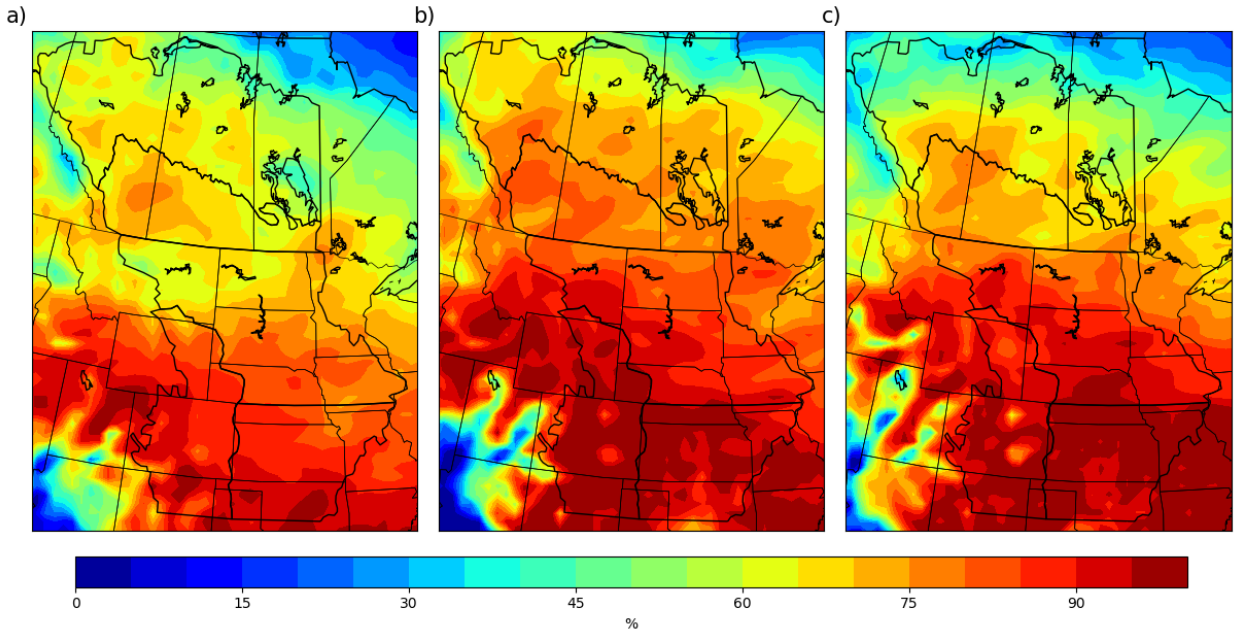

Figure A.17 Convective precipitation as a percentage of total precipitation for the future period in summer (JJA) for MM5-CCSM for a) June b) July and c) August.

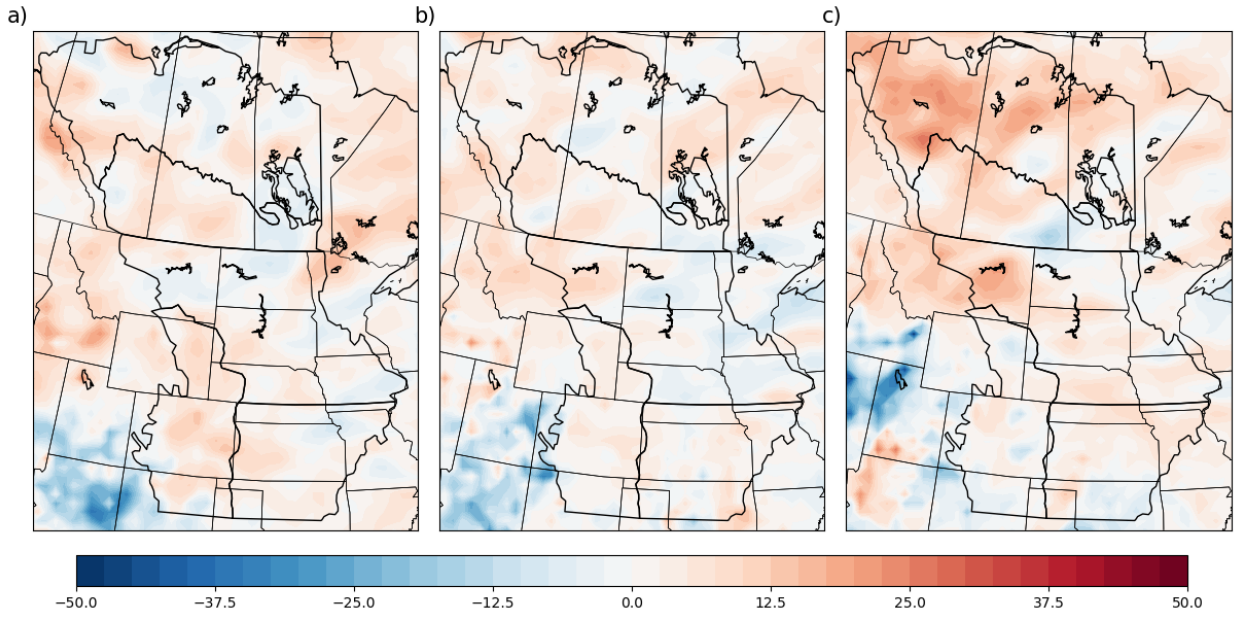

Figure A.18 Difference (future – current) in convective precipitation as a percentage of total precipitation in summer (JJA) for MM5-CCSM for a) June b) July and c) August.

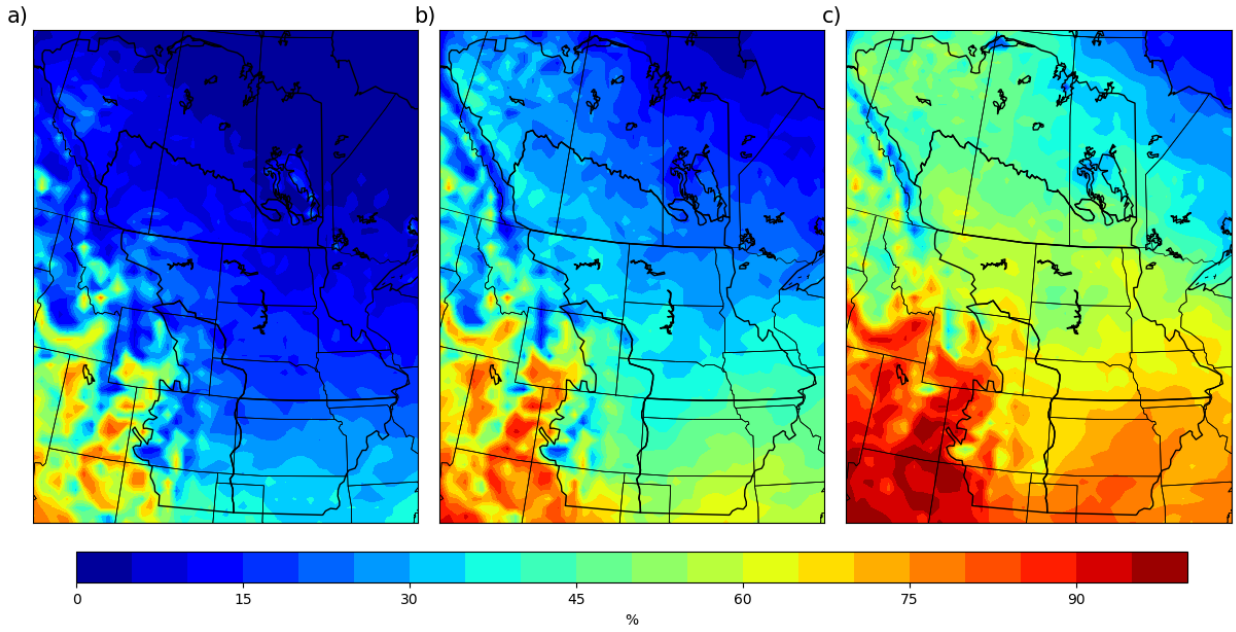

Figure A.19 Convective precipitation as a percentage of total precipitation for the current period in spring (MAM) for HRM3-HadCM3 for a) March b) April and c) May.

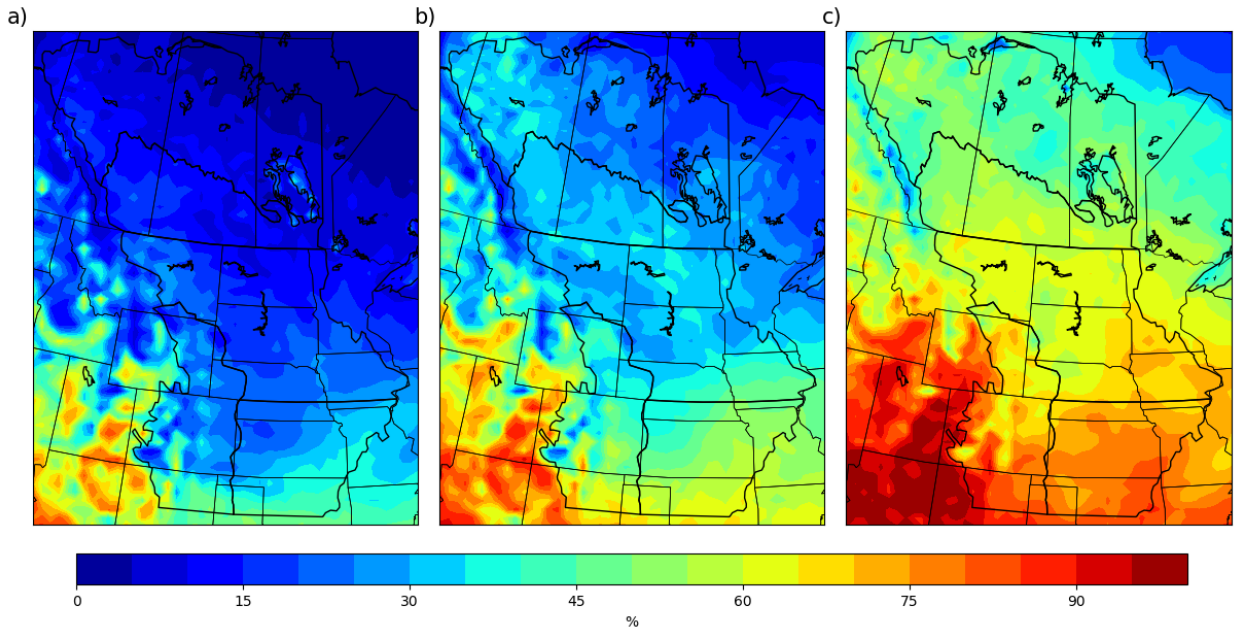

Figure A.20 Convective precipitation as a percentage of total precipitation for the future period in spring (MAM) for HRM3-HadCM3 for a) March b) April and c) May.

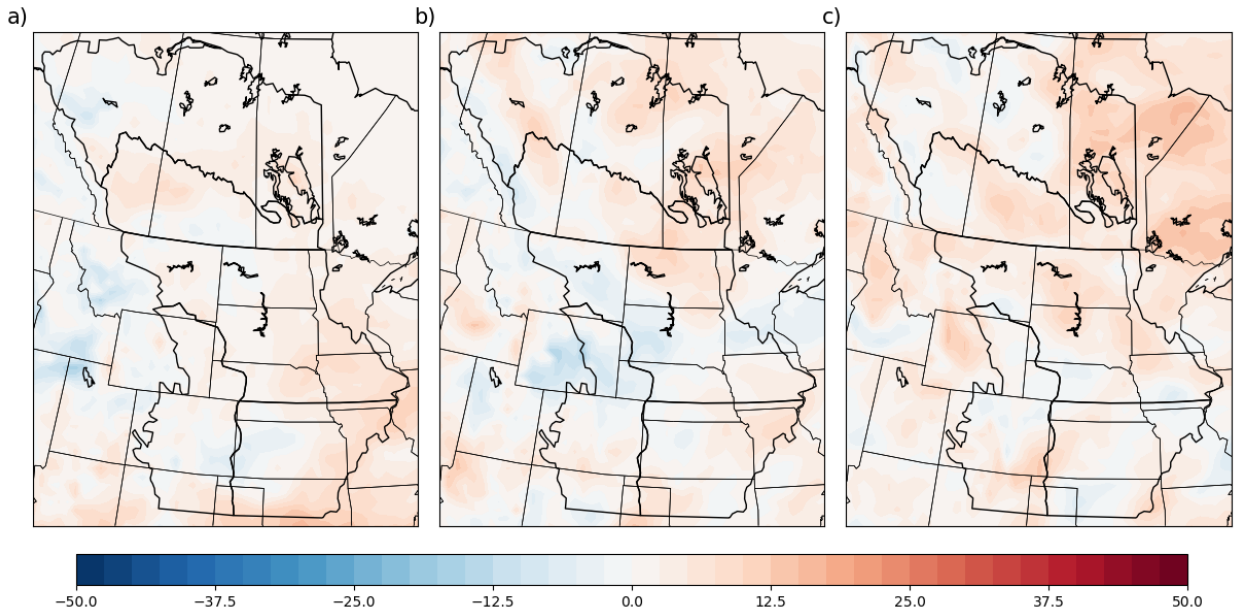

Figure A.21 Difference (future – current) in convective precipitation as a percentage of total precipitation in spring (MAM) for HRM3-HadCM3 for a) March b) April and c) May.

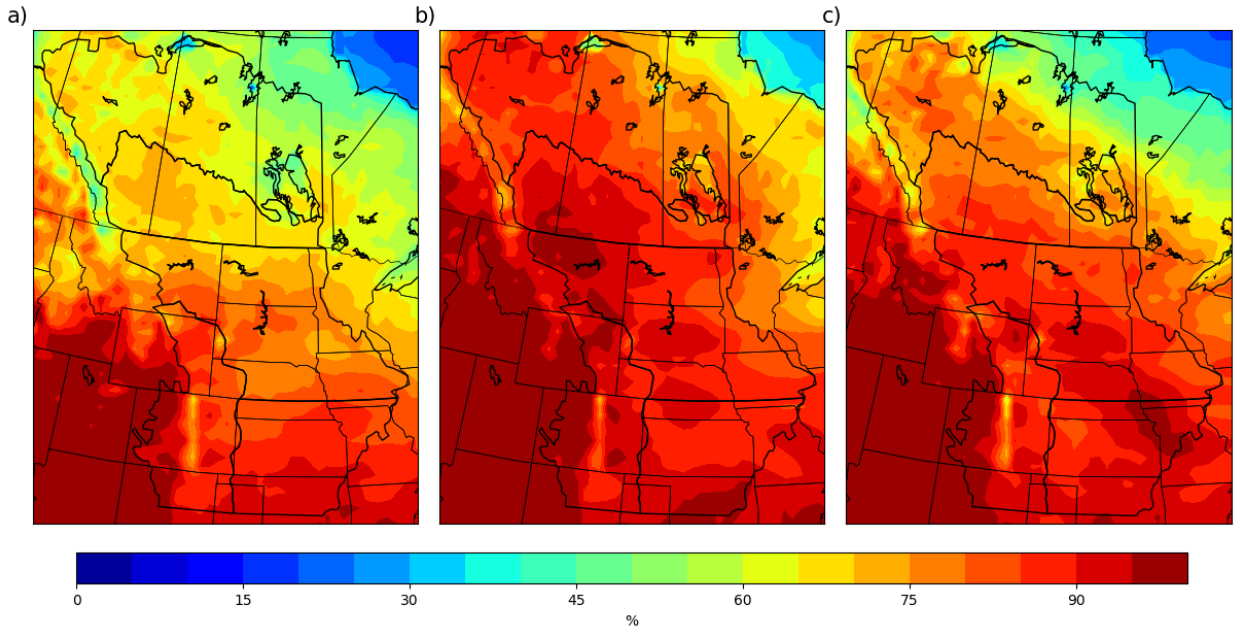

Figure A.22 Convective precipitation as a percentage of total precipitation for the current period in summer (JJA) for HRM3-HadCM3 for a) June b) July and c) August.

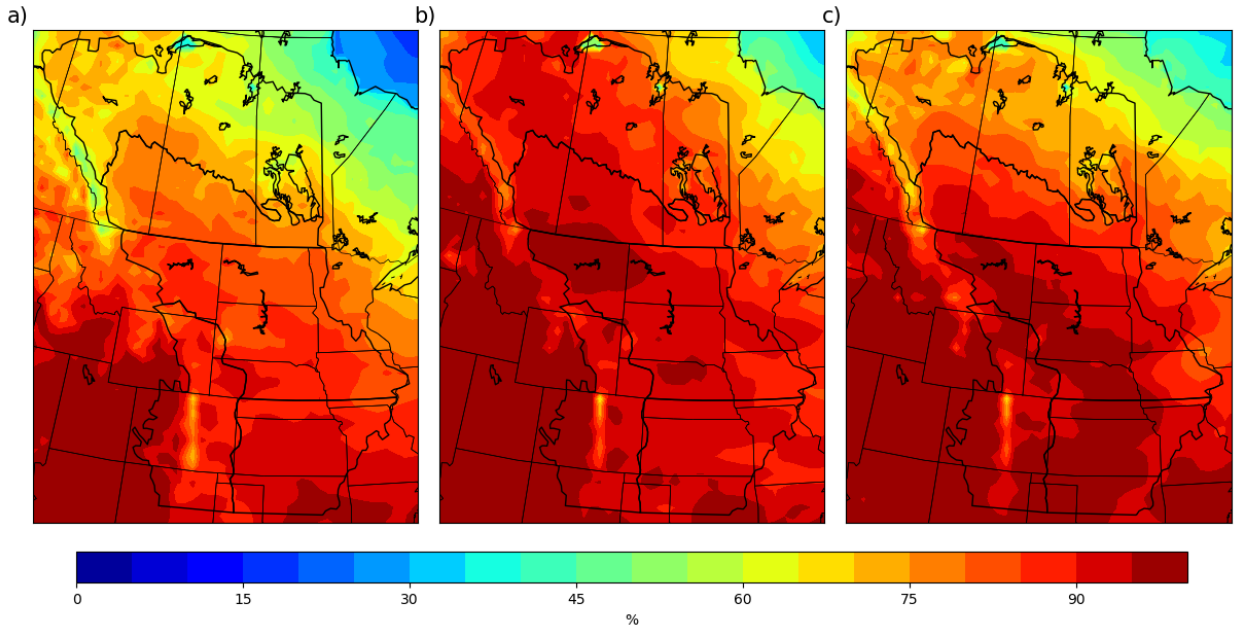

Figure A.23 Convective precipitation as a percentage of total precipitation for the future period in summer (JJA) for HRM3-HadCM3 for a) June b) July and c) August.

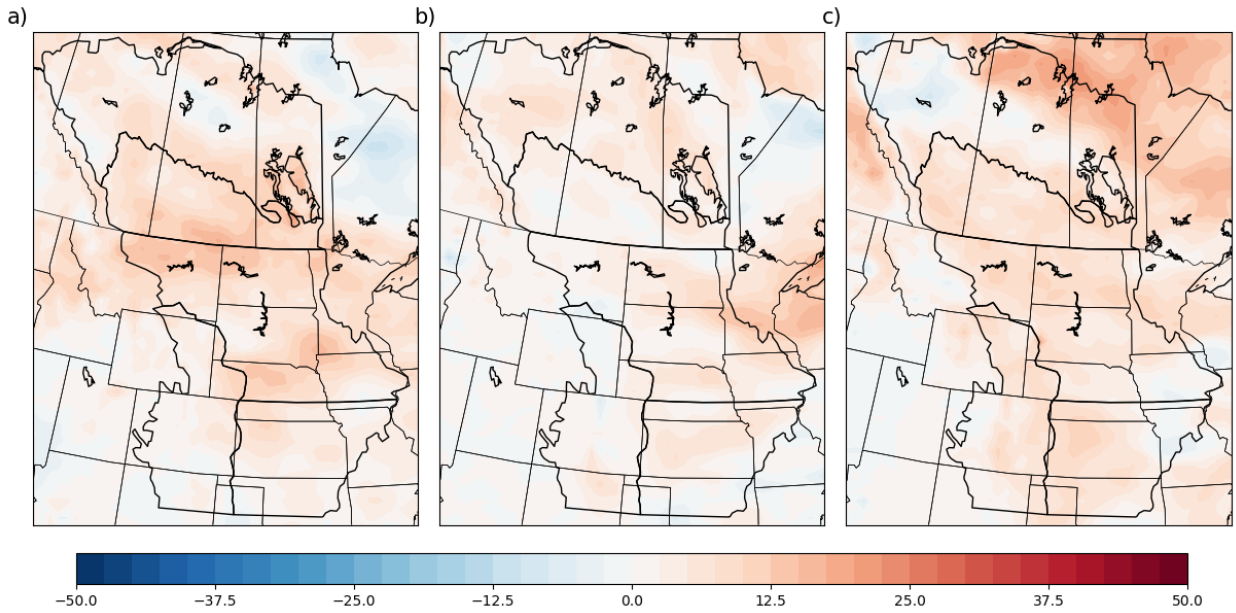

Figure A.24 Difference (future – current) in convective precipitation as a percentage of total precipitation in summer (JJA) for HRM3-HadCM3 for a) June b) July and c) August.

Appendix B: Mean Precipitation

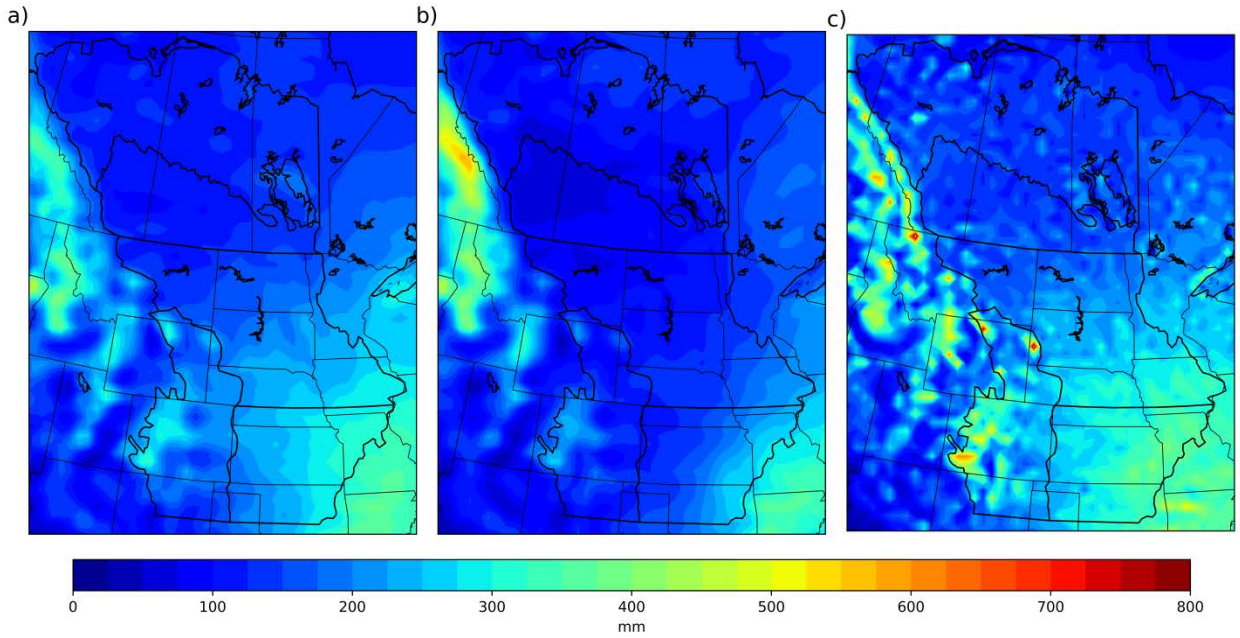

Figure B.1 Average spring (MAM) precipitation for the current period for MM5-HadCM3 (b) MM5-CCSM (c) HRM3-HadCM3.

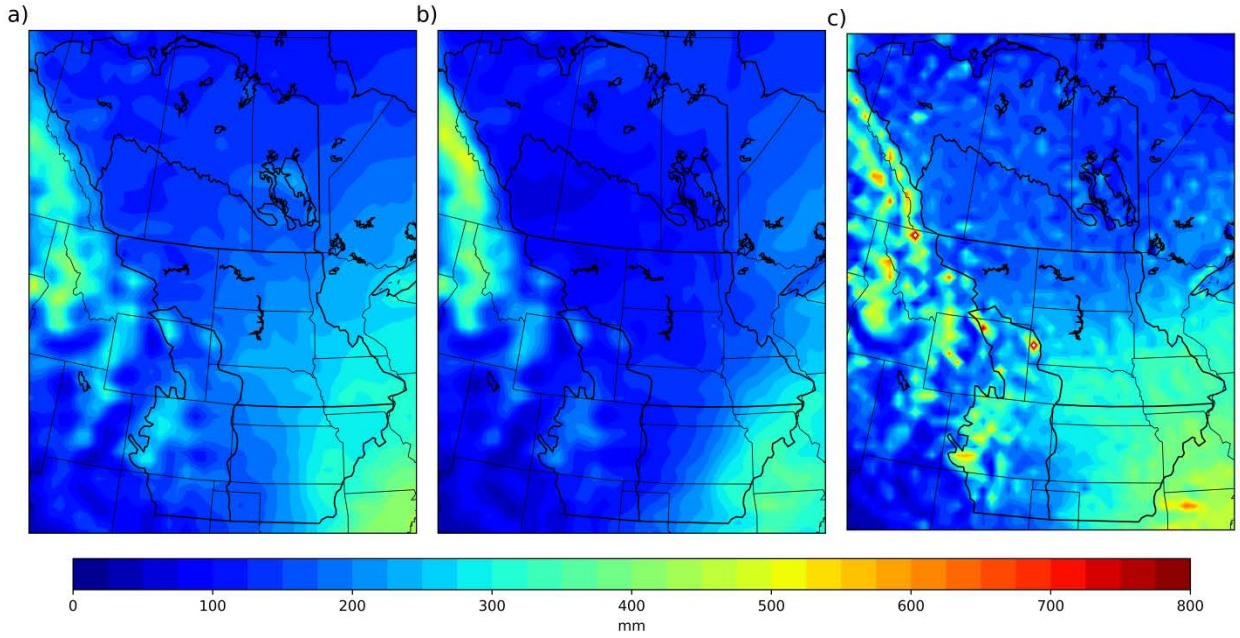

Figure B.2 Average spring (MAM) precipitation for the future period MM5-HadCM3 (b) MM5-CCSM (c) HRM3-HadCM3.

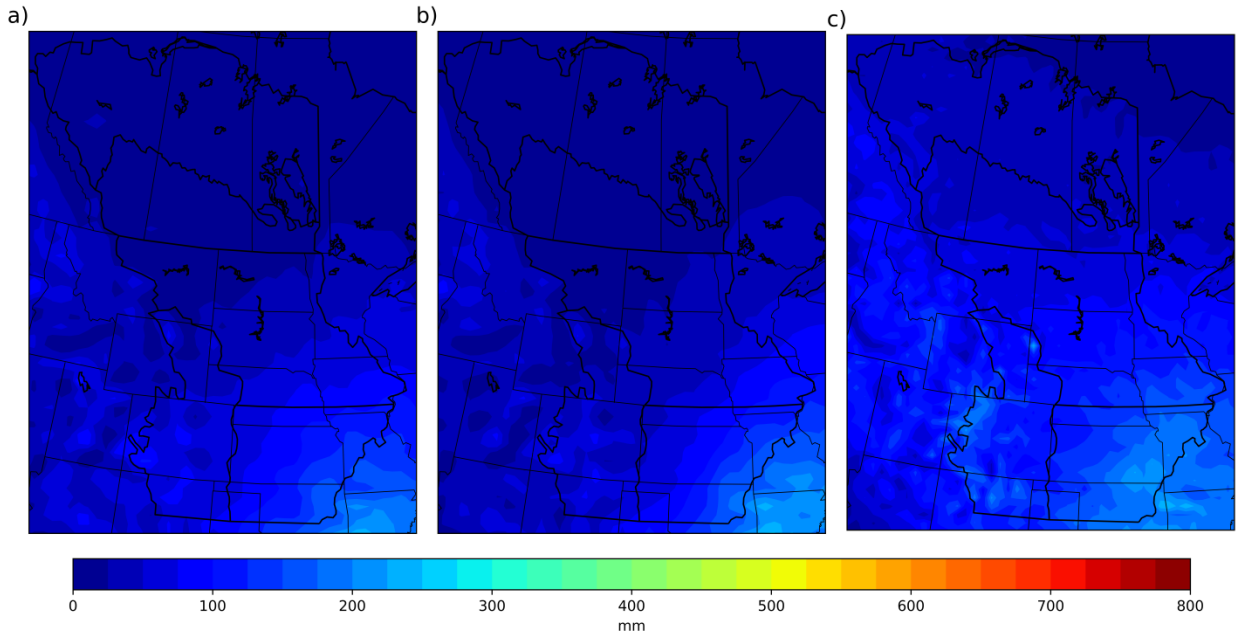

Figure B.3 Average spring (MAM) convective precipitation for the current period for MM5-HadCM3 (b) MM5-CCSM (c) HRM3-HadCM3.

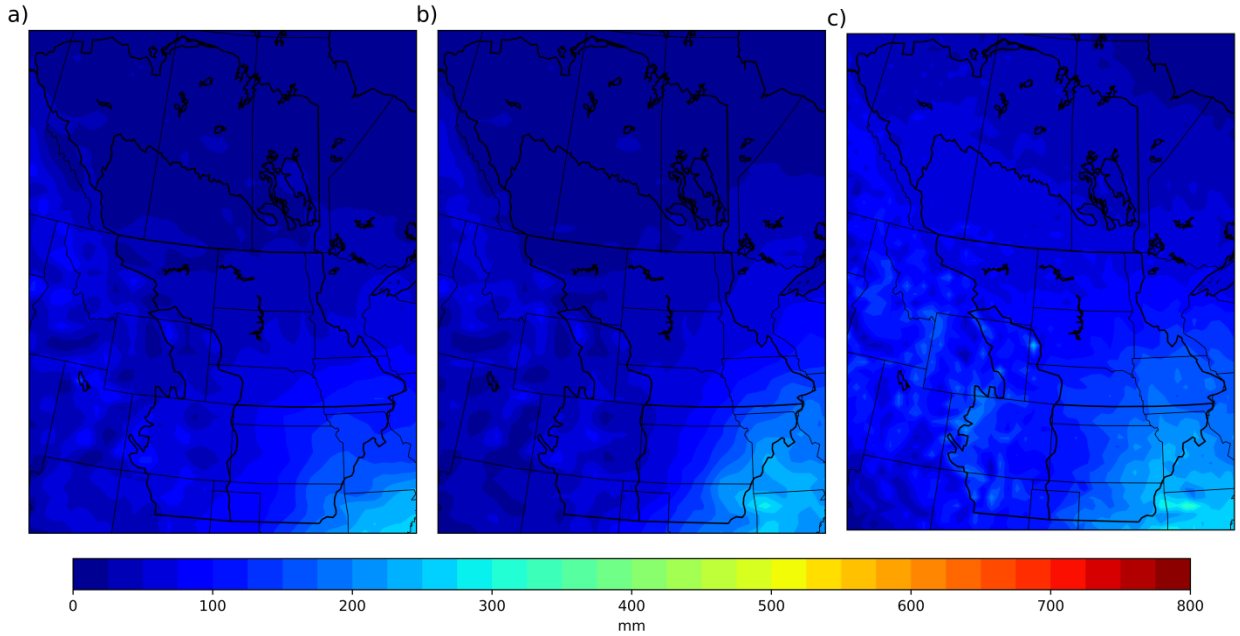

Figure B.4 Average spring (MAM) convective precipitation for the future period for MM5-HadCM3 (b) MM5-CCSM (c) HRM3-HadCM3.

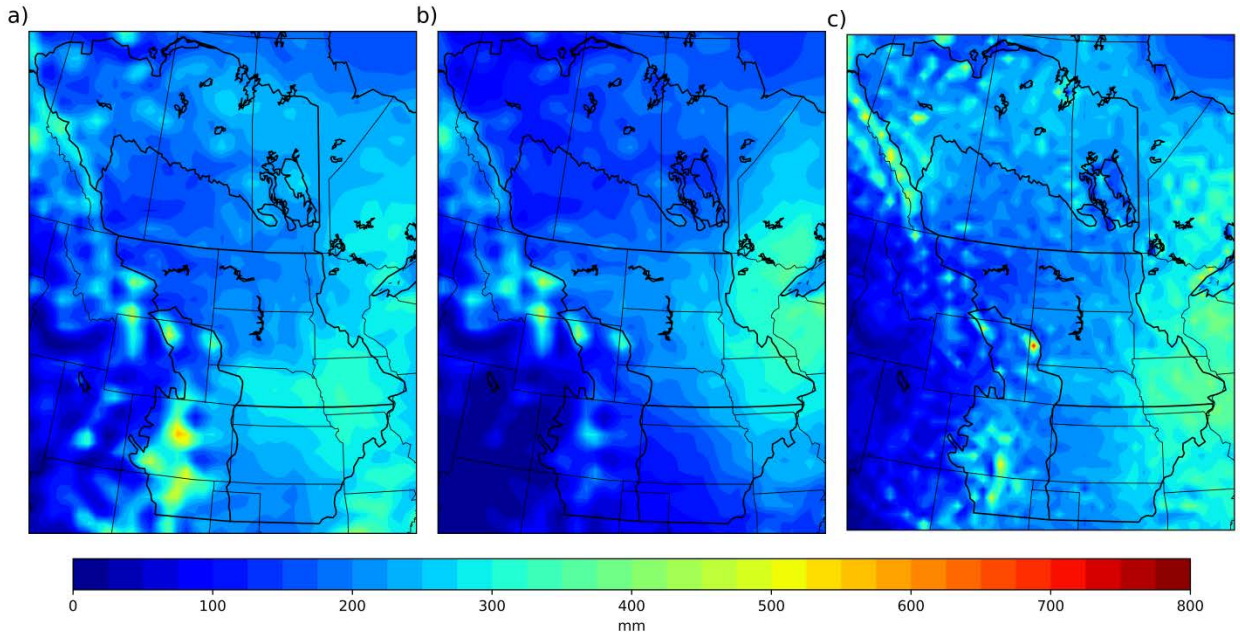

Figure B.5 Average summer (JJA) precipitation for the current period for MM5-HadCM3 (b) MM5-CCSM (c) HRM3-HadCM3.

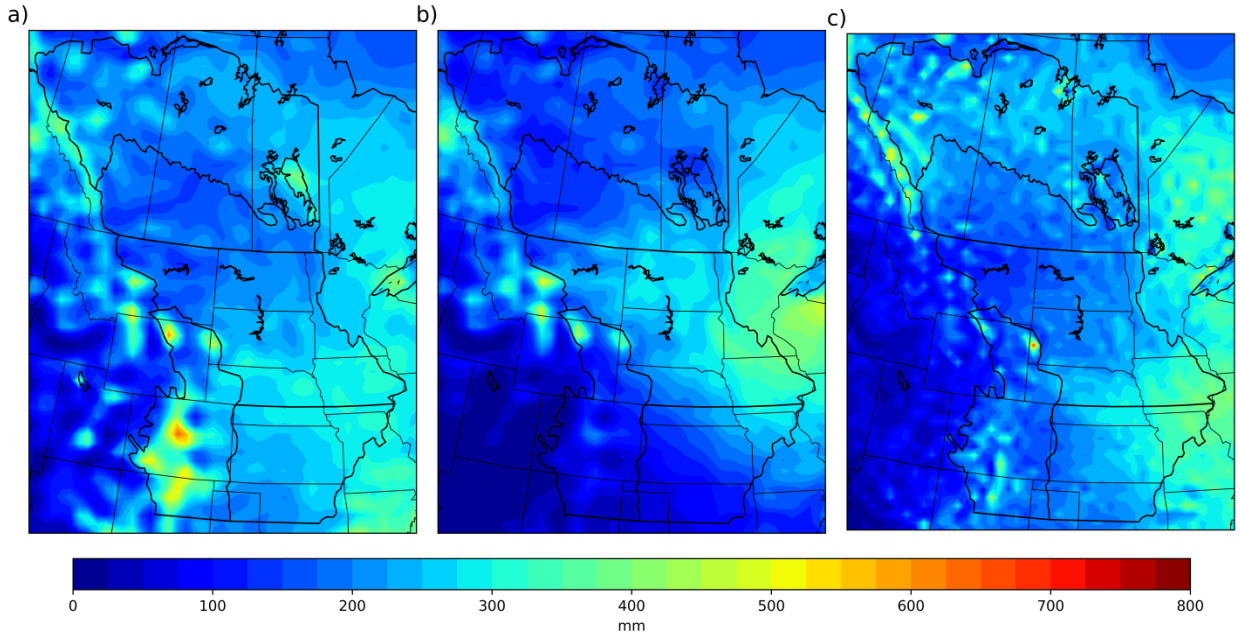

Figure B.6 Average summer (JJA) precipitation for the future period for MM5-HadCM3 (b) MM5-CCSM (c) HRM3-HadCM3.

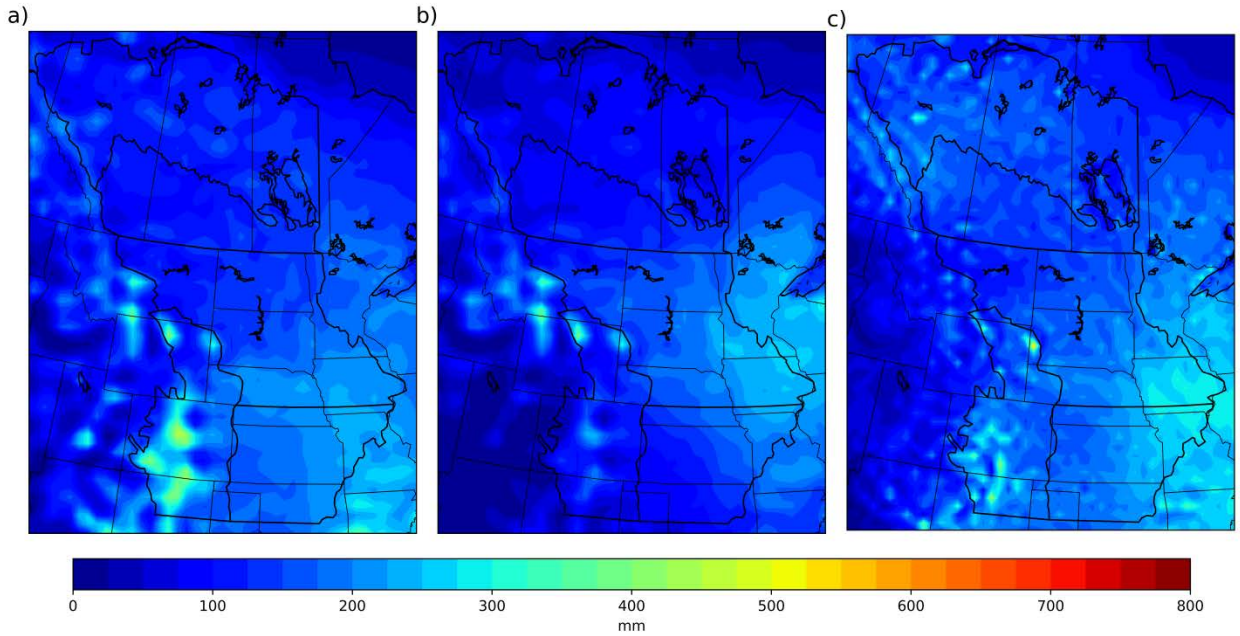

Figure B.7 Average summer (JJA) convective precipitation for the current period for MM5-HadCM3 (b) MM5-CCSM (c) HRM3-HadCM3.

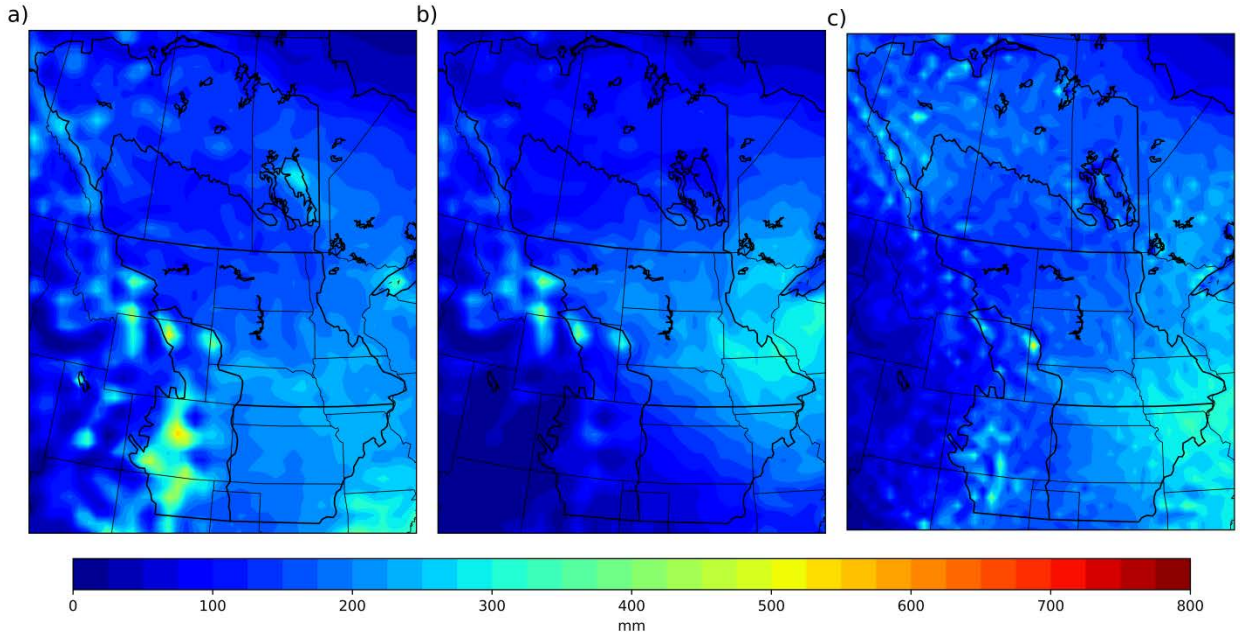

Figure B.8 Average summer (JJA) convective precipitation for the future period for MM5-HadCM3 (b) MM5-CCSM (c) HRM3-HadCM3.

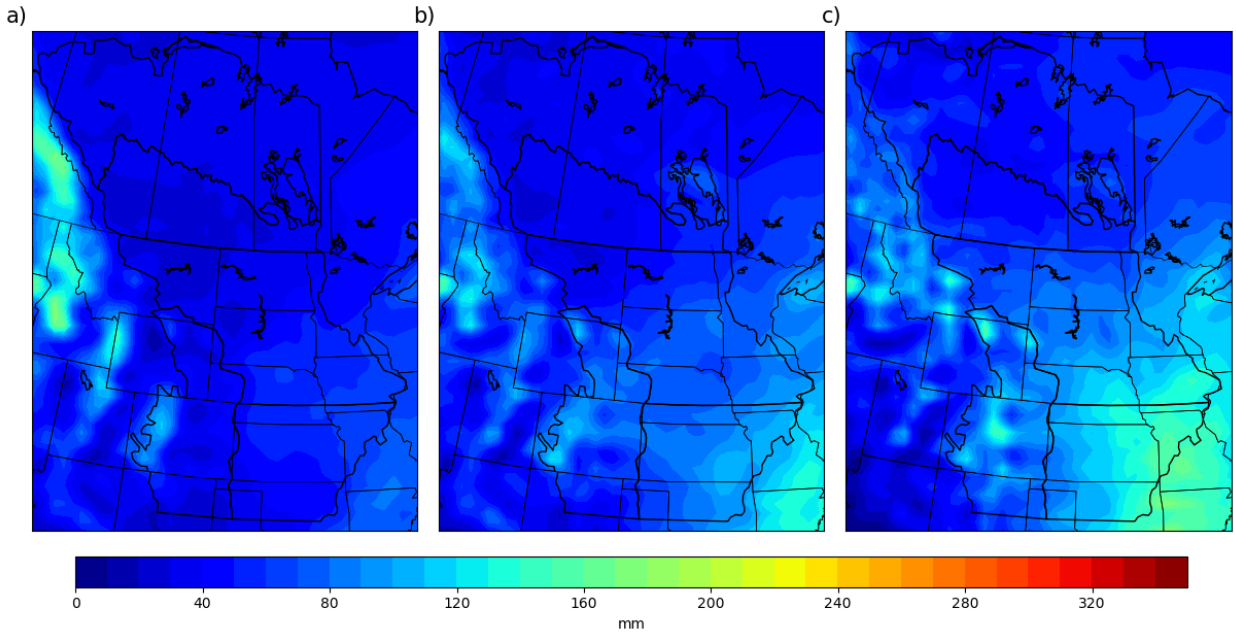

Figure B.9 Average precipitation for the current period for MM5-HadCM3 for a) March (b) April and c) May.

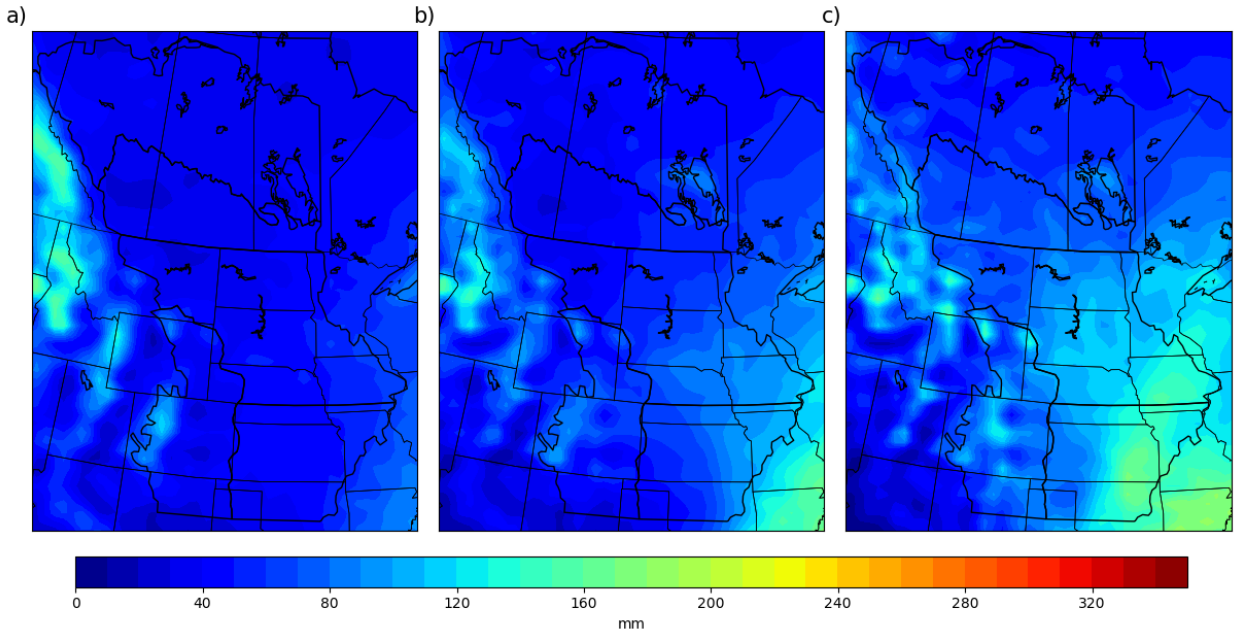

Figure B.10 Average precipitation for the future period for MM5-HadCM3 for a) March (b) April and c) May.

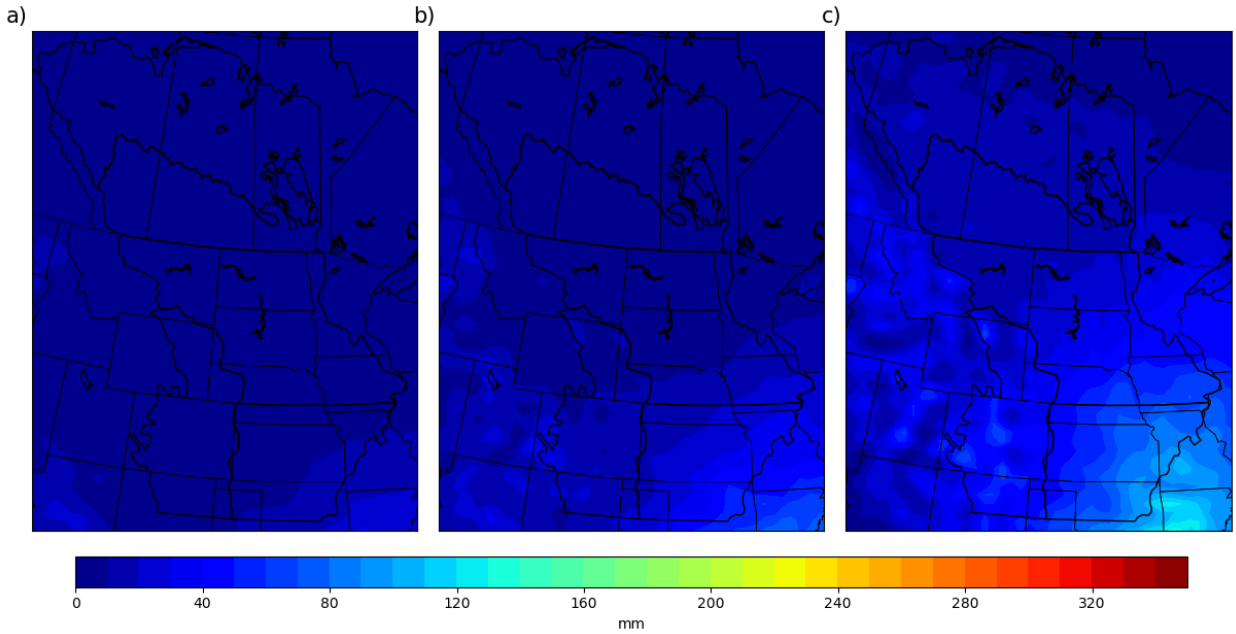

Figure B.11 Average convective precipitation for the current period for MM5-HadCM3 for a) March (b) April and c) May.

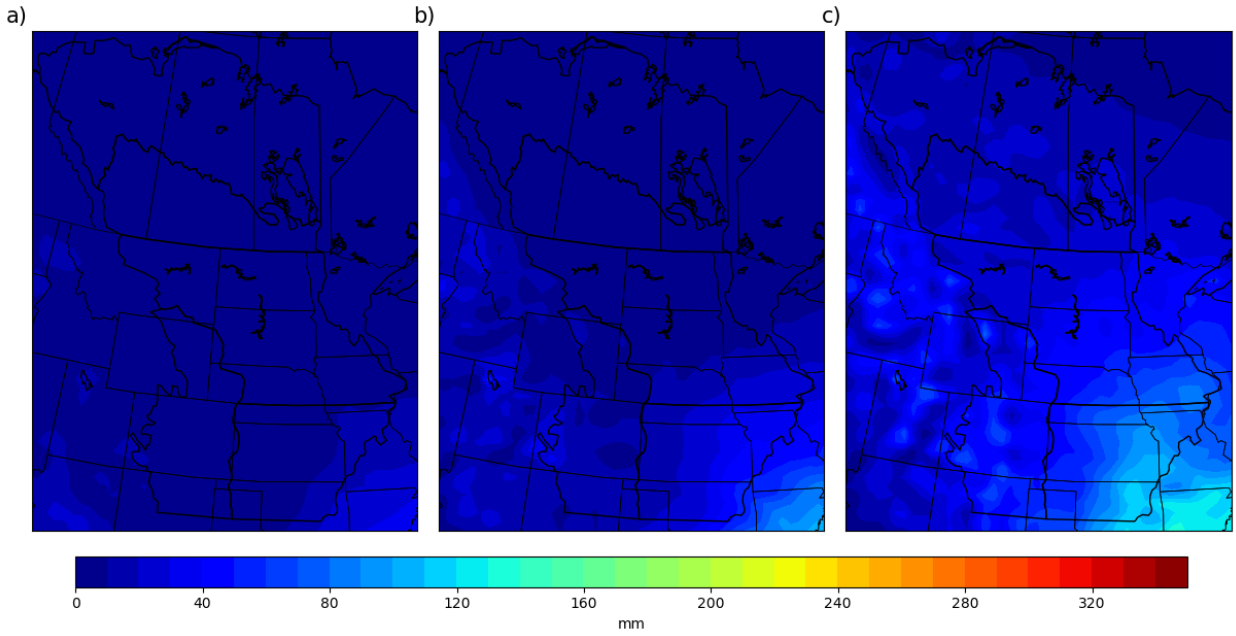

Figure B.12 Average convective precipitation for the future period for MM5-HadCM3 for a) March (b) April and c) May.

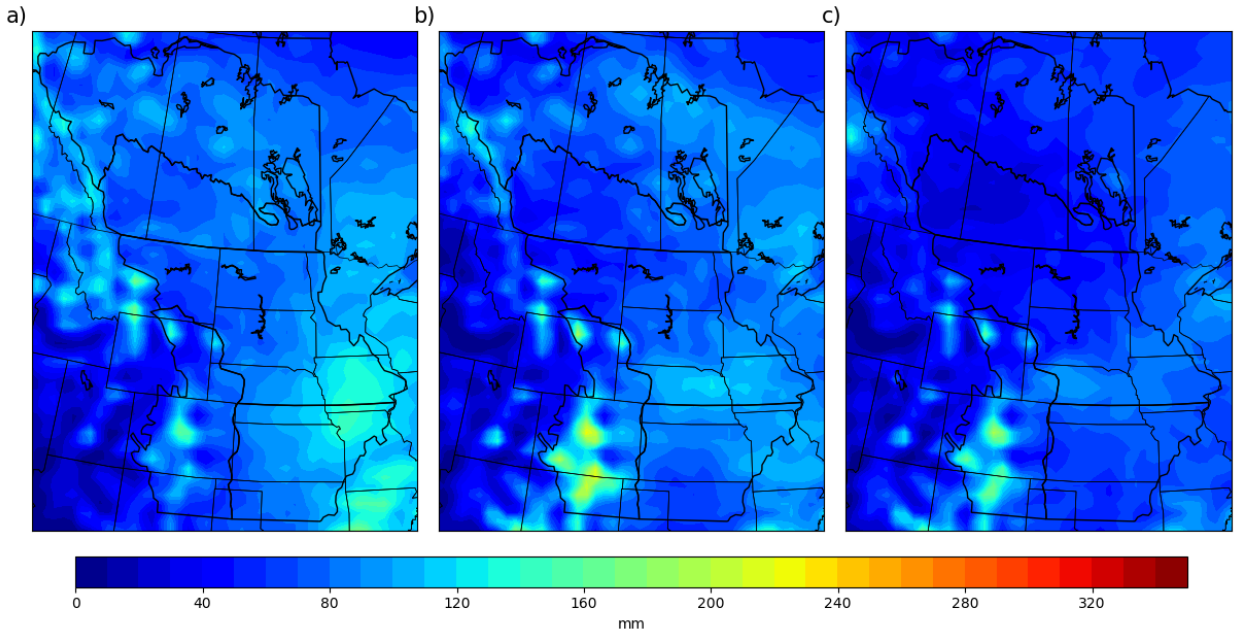

Figure B.13 Average precipitation for the current period for MM5-HadCM3 for a) June b) July and c) August.

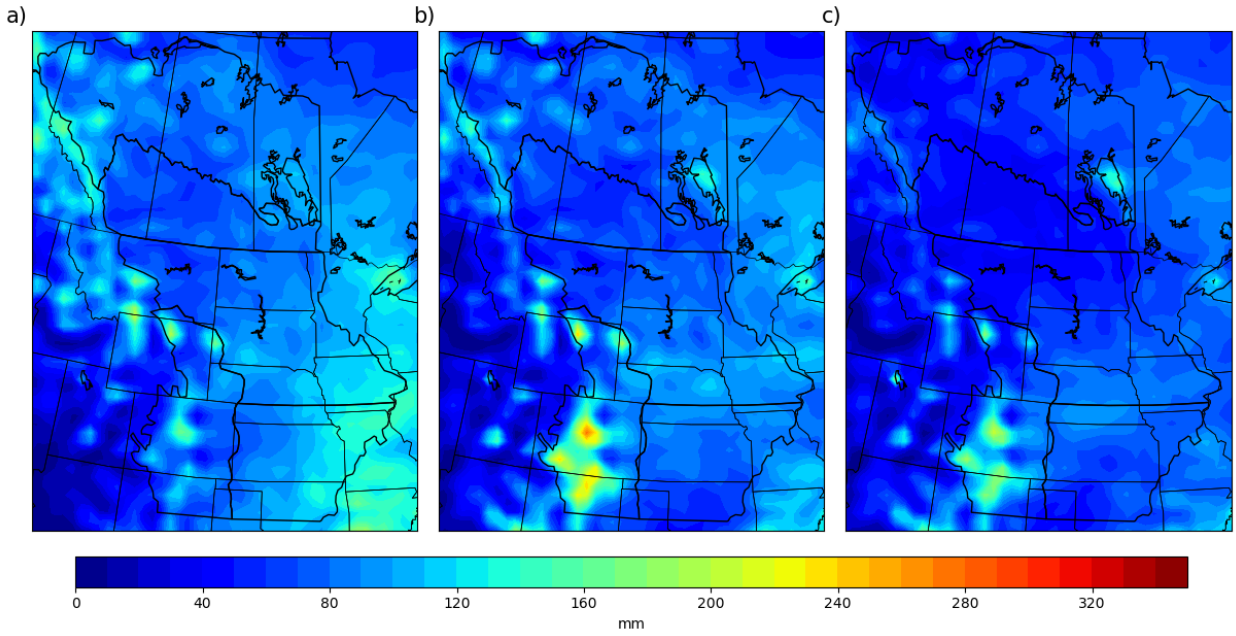

Figure B.14 Average precipitation for the future period for MM5-HadCM3 for a) June b) July and c) August.

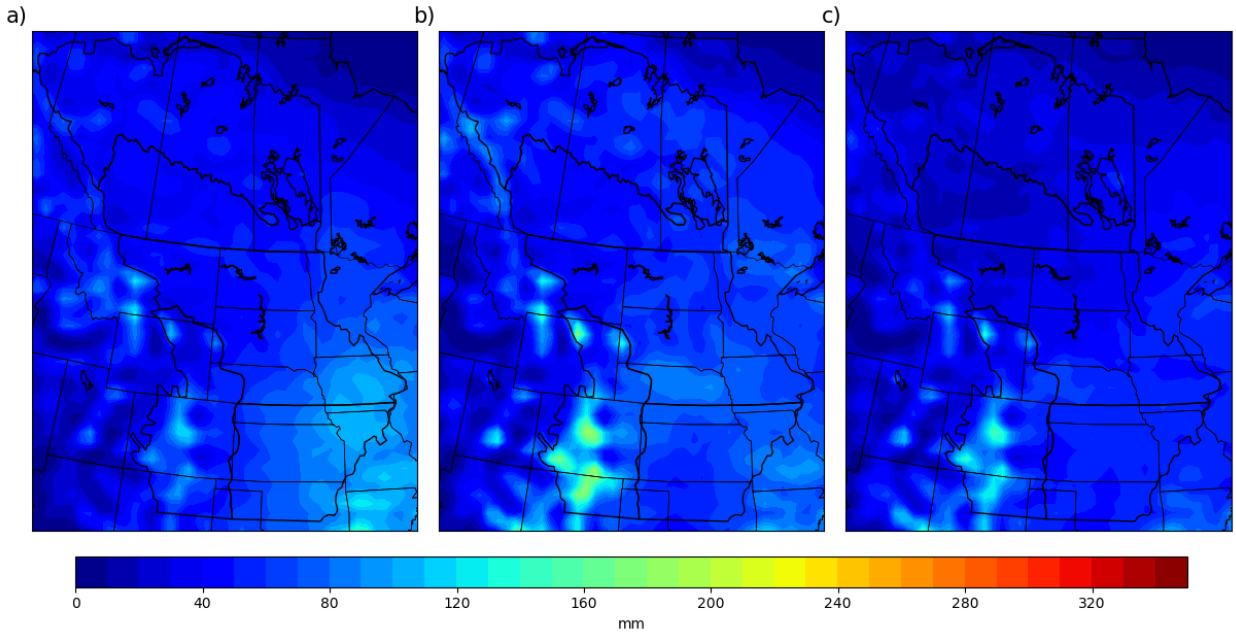

Figure B.15 Average convective precipitation for the current period for MM5-HadCM3 for a) June b) July and c) August.

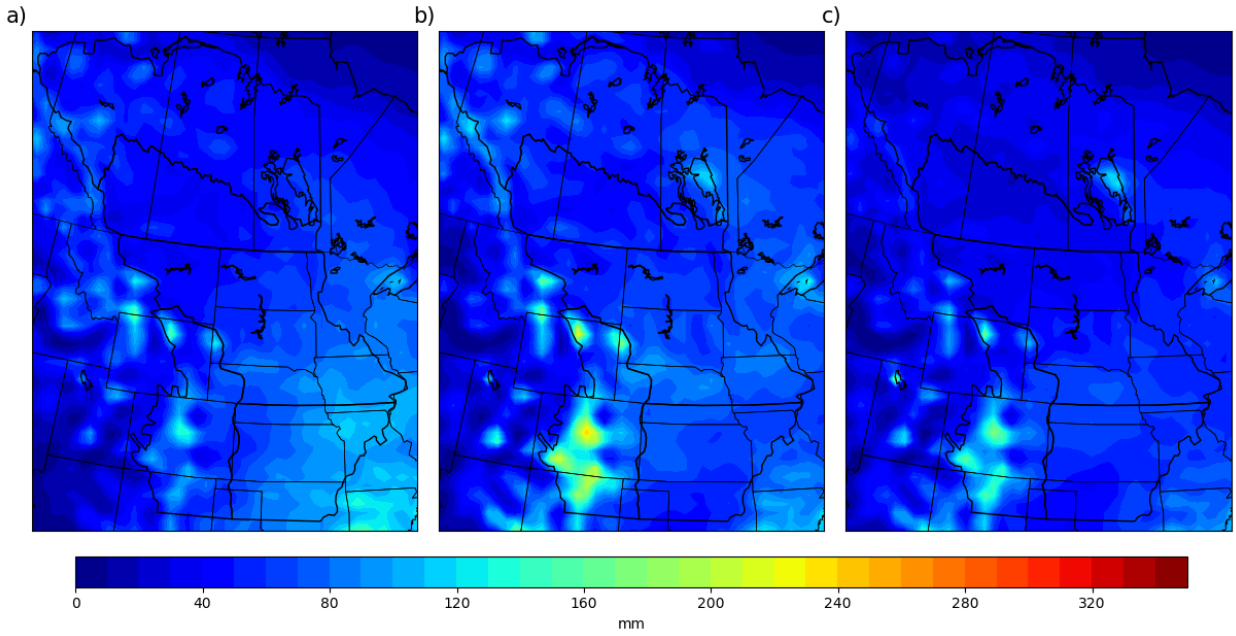

Figure B.16 Average convective precipitation for the future period for MM5-HadCM3 for a) June b) July and c) August.

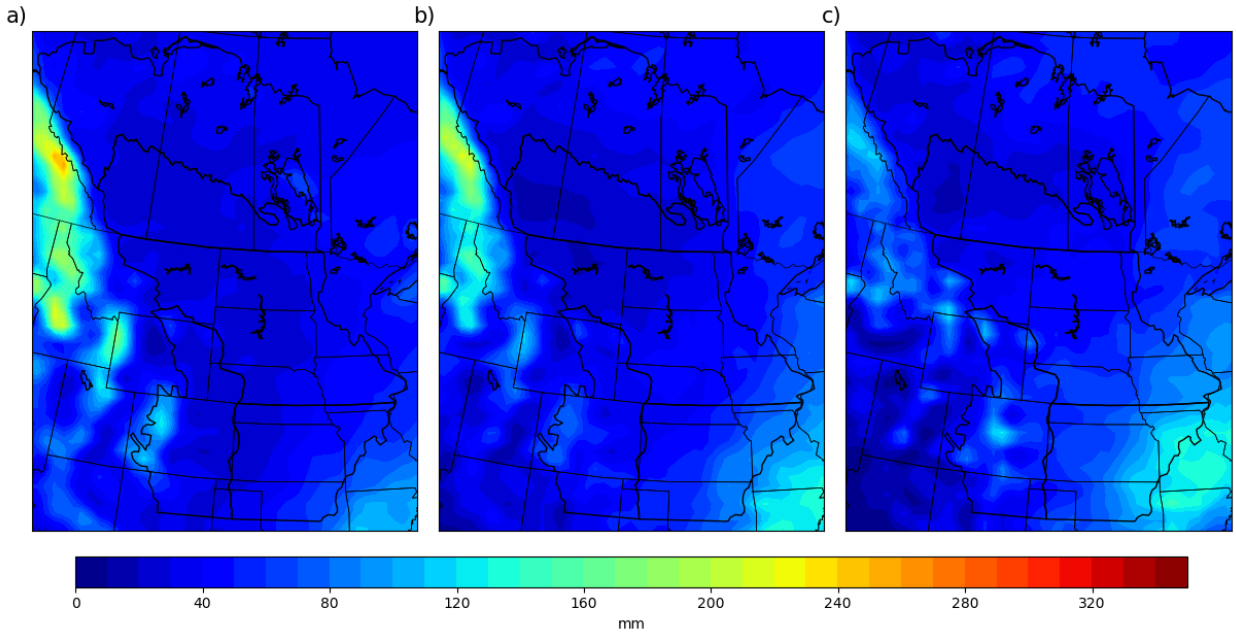

Figure B.17 Average precipitation for the current period for MM5-CCSM for a) March (b) April and c) May.

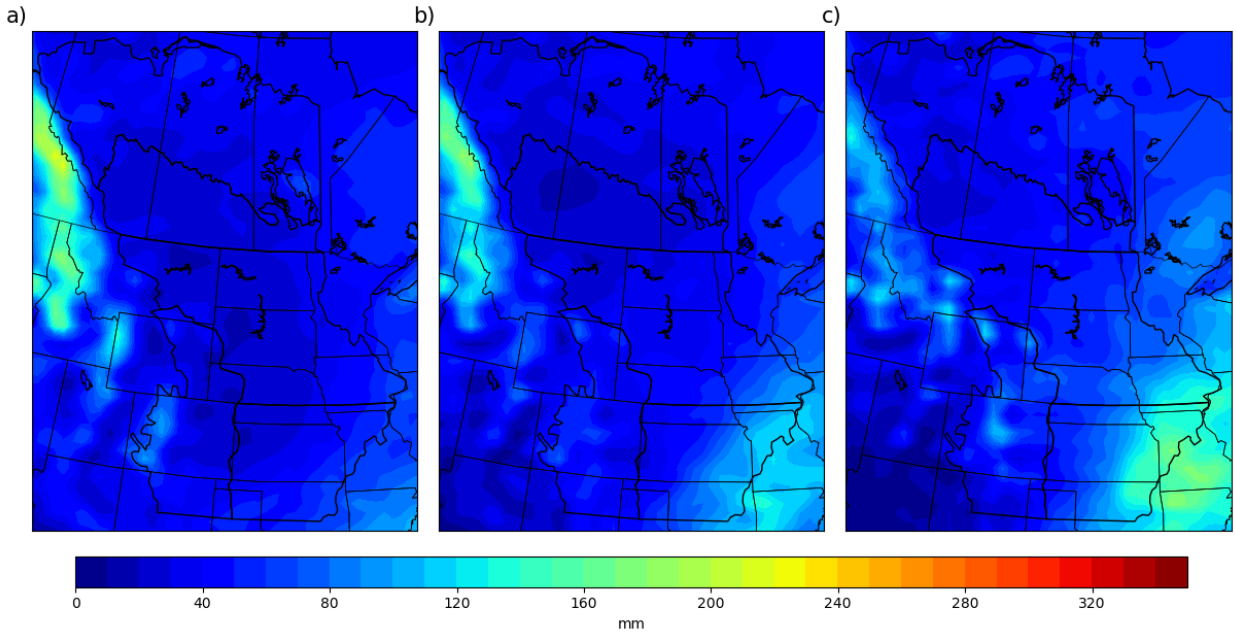

Figure B.18 Average precipitation for the future period for MM5-CCSM for a) March (b) April and c) May.

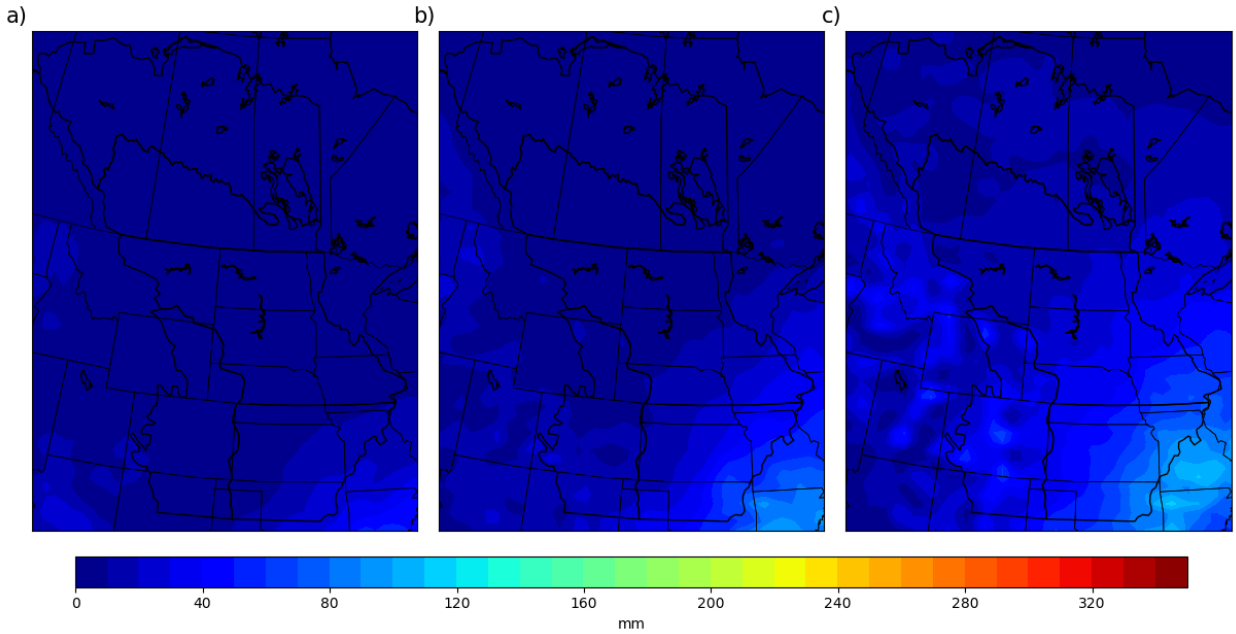

Figure B.19 Average convective precipitation for the current period for MM5-CCSM for a) March (b) April and c) May.

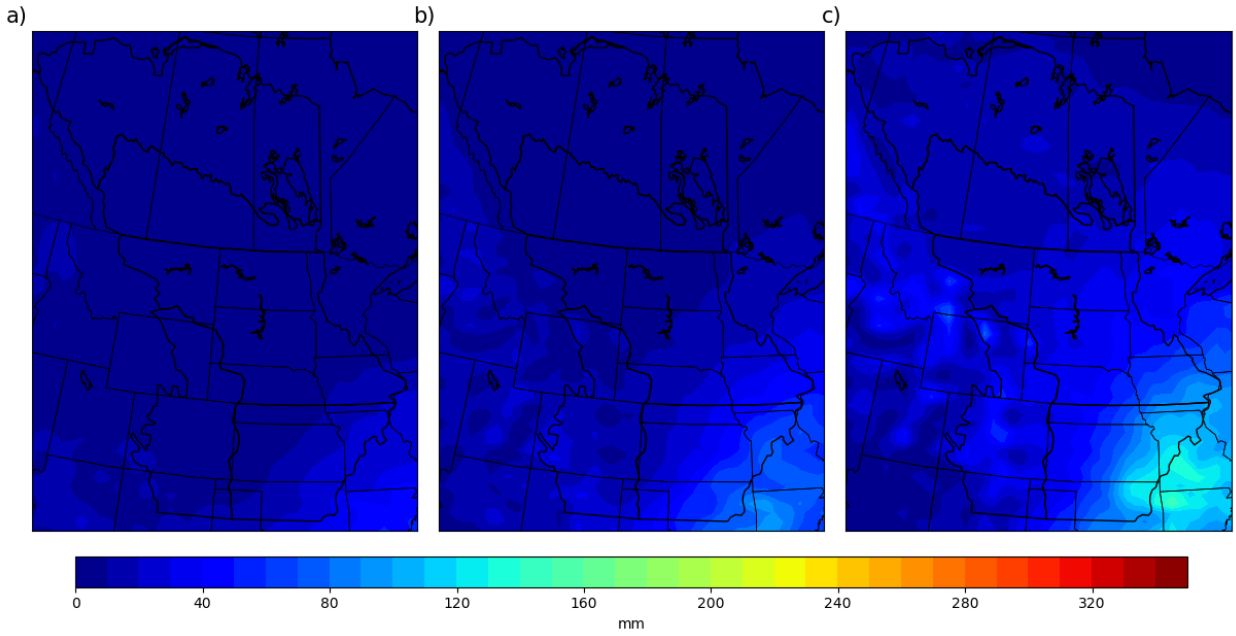

Figure B.20 Average convective precipitation for the future period for MM5-CCSM for a) March (b) April and c) May.

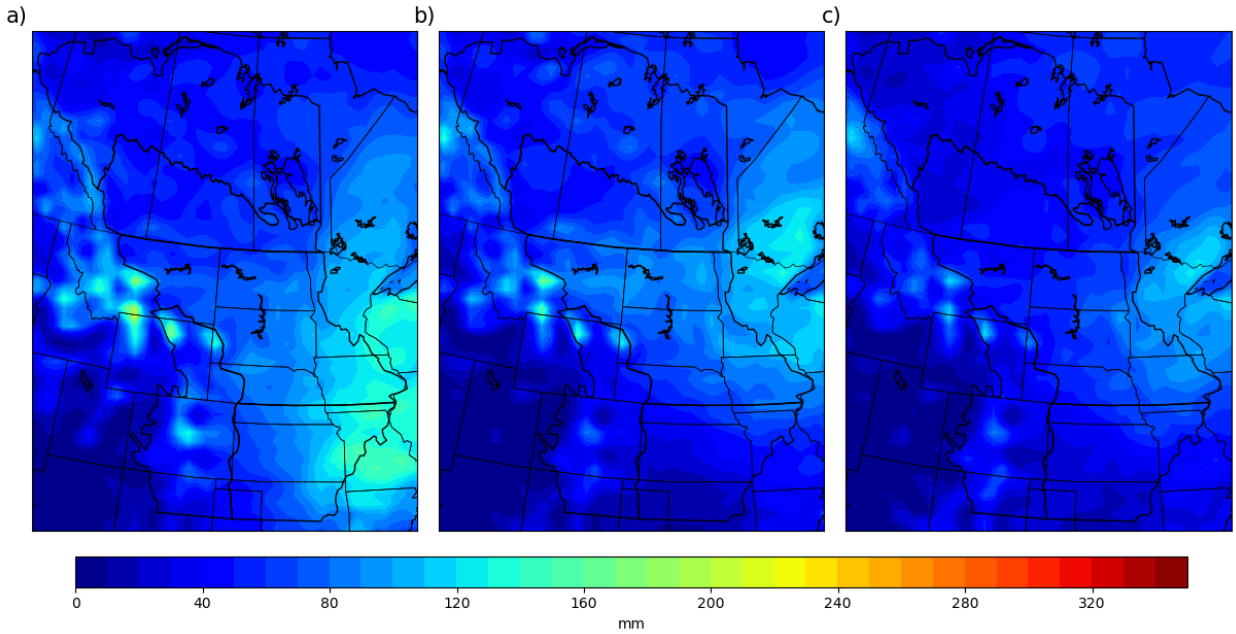

Figure B.21 Average precipitation for the current period for MM5-CCSM for a) June b) July and c) August.

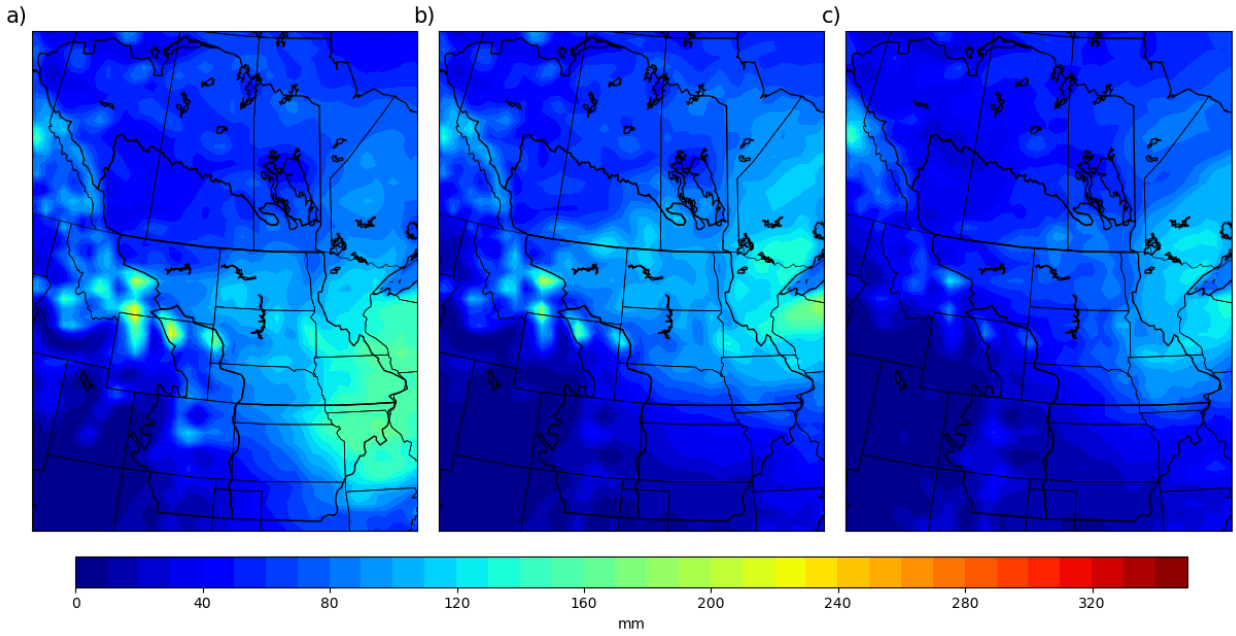

Figure B.22 Average precipitation for the future period for MM5-CCSM for a) June b) July and c) August.

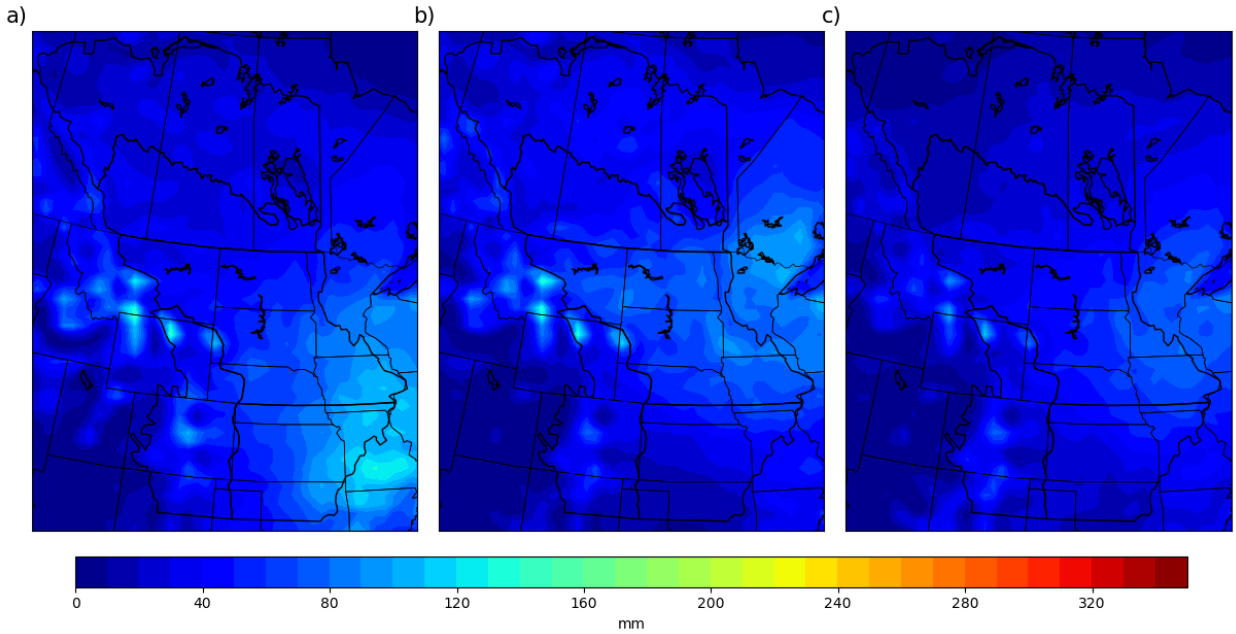

Figure B.23 Average convective precipitation for the current period for MM5-CCSM for a) June b) July and c) August.

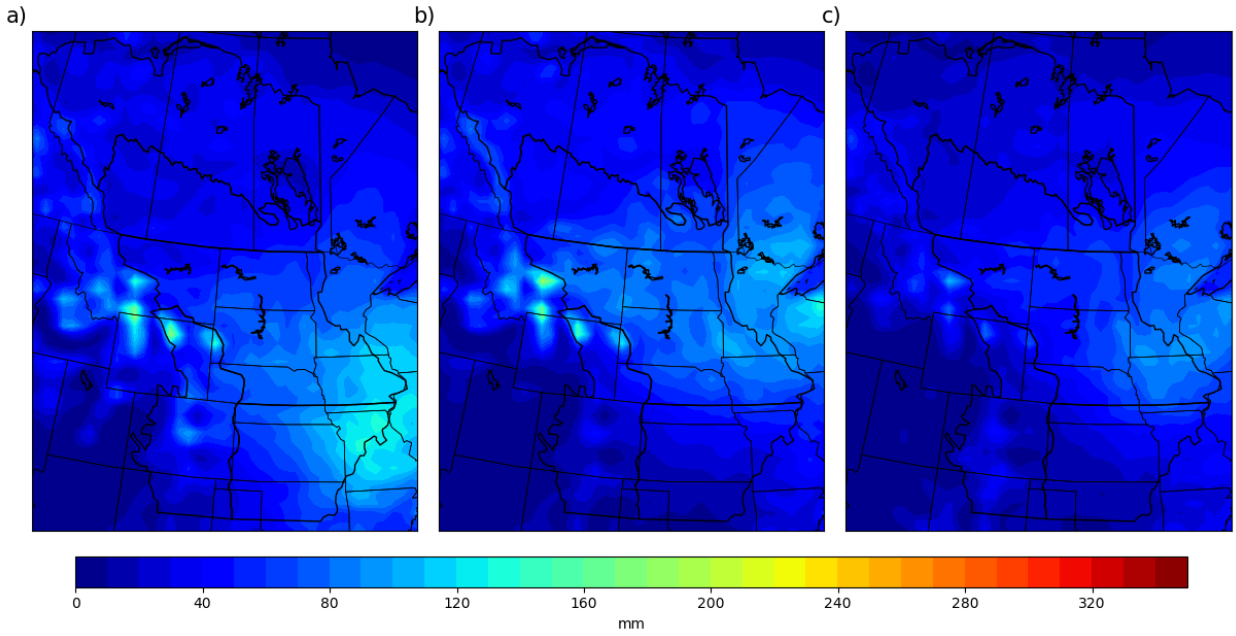

Figure B.24 Average convective precipitation for the future period for MM5-CCSM for a) June b) July and c) August.

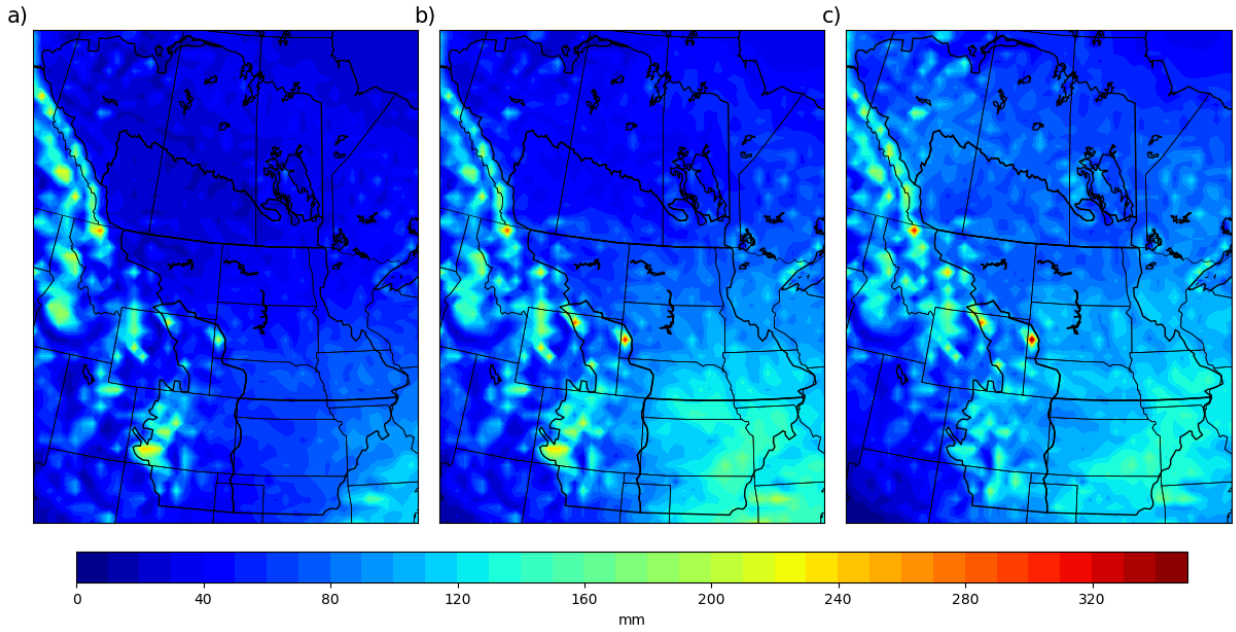

Figure B.25 Average precipitation for the current period for HRM3-HadCM3 for a) March b) April and c) May.

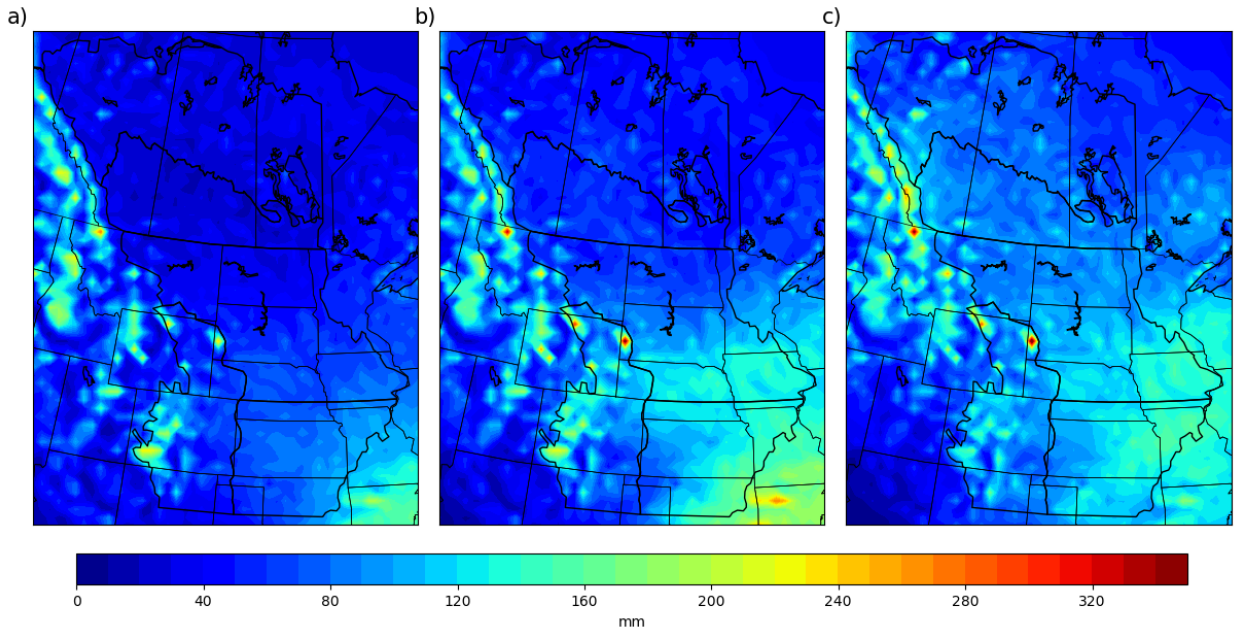

Figure B.26 Average precipitation for the future period for HRM3-HadCM3 for a) March b) April and c) May.

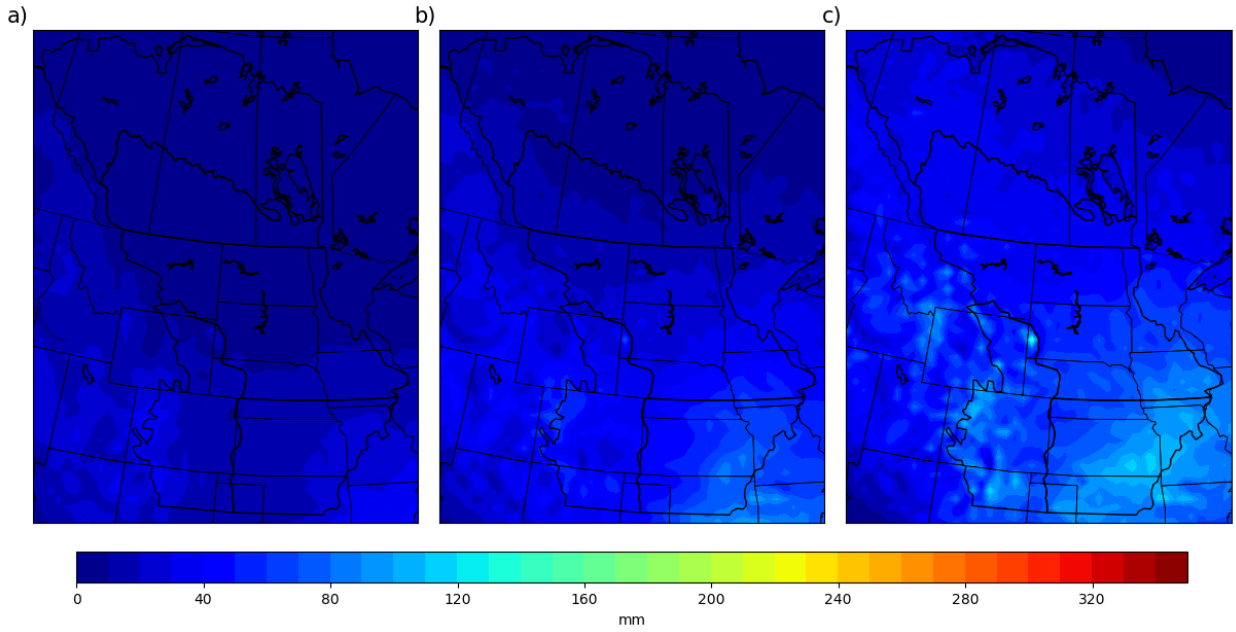

Figure B.27 Average convective precipitation for the current period for HRM3-HadCM3 for a) March b) April and c) May.

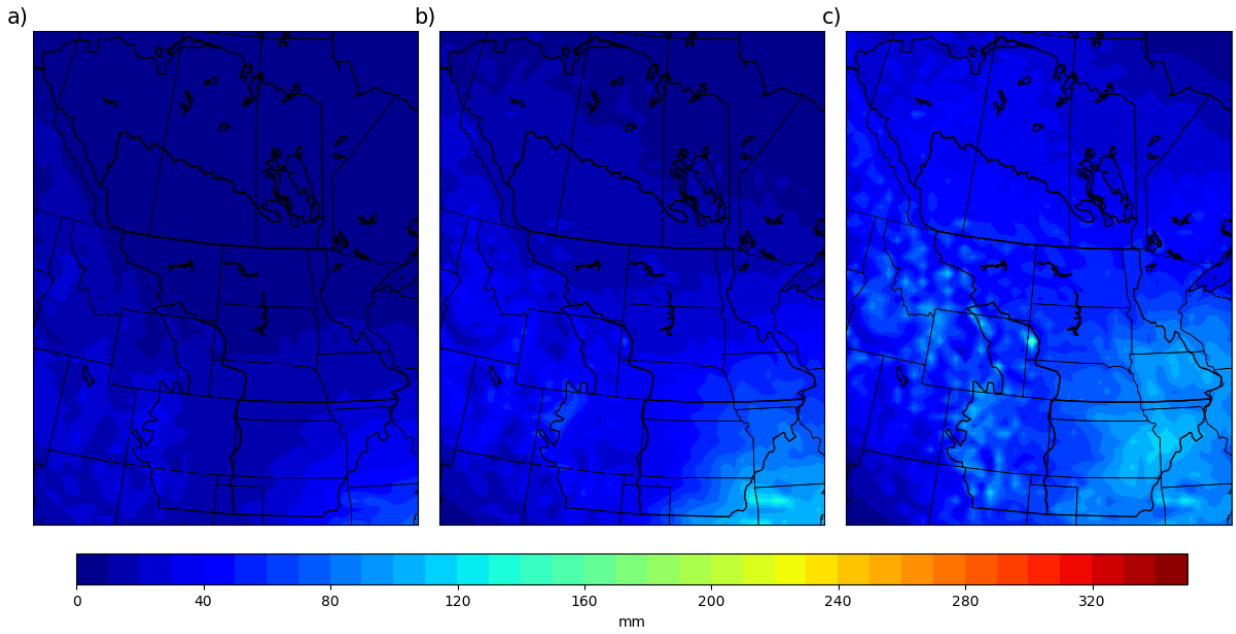

Figure B.28 Average convective precipitation for the future period for HRM3-HadCM3 for a) March b) April and c) May.

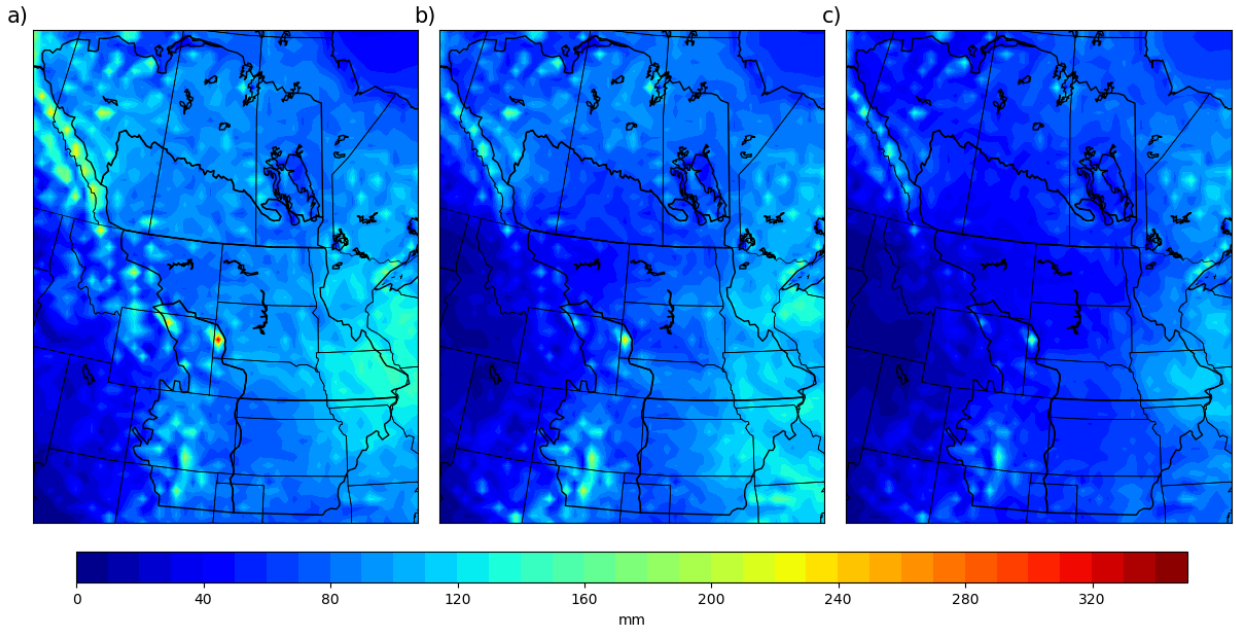

Figure B.29 Average precipitation for the current period for HRM3-HadCM3 for a) June b) July and c) August.

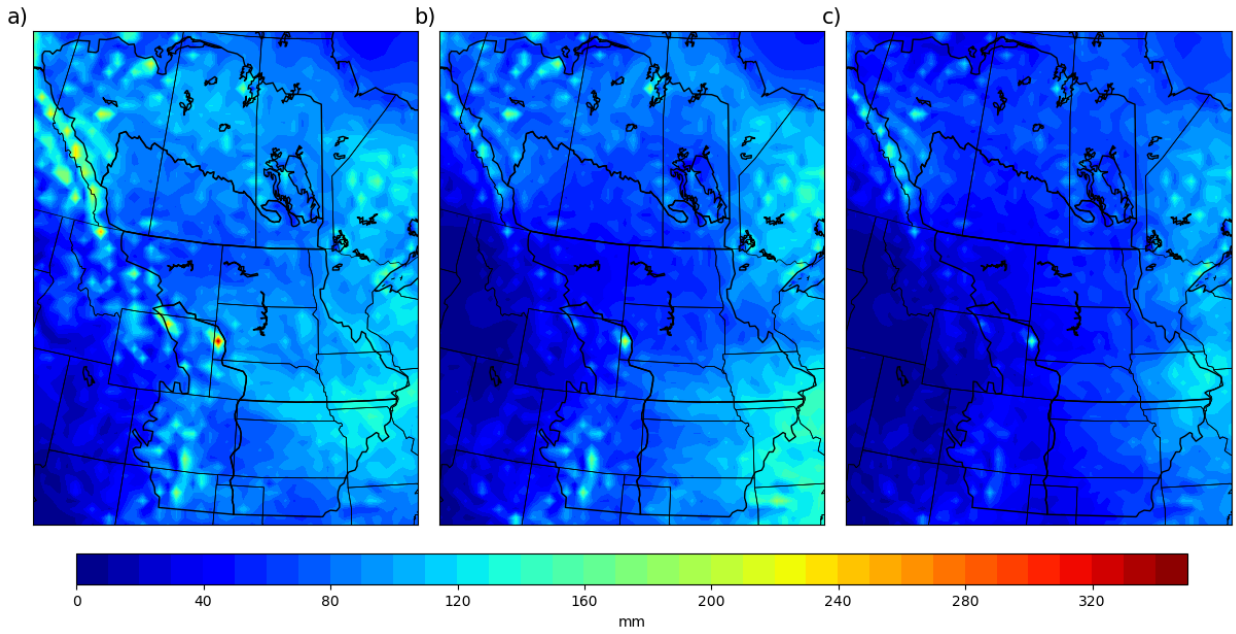

Figure B.30 Average precipitation for the future period for HRM3-HadCM3 for a) June b) July and c) August.

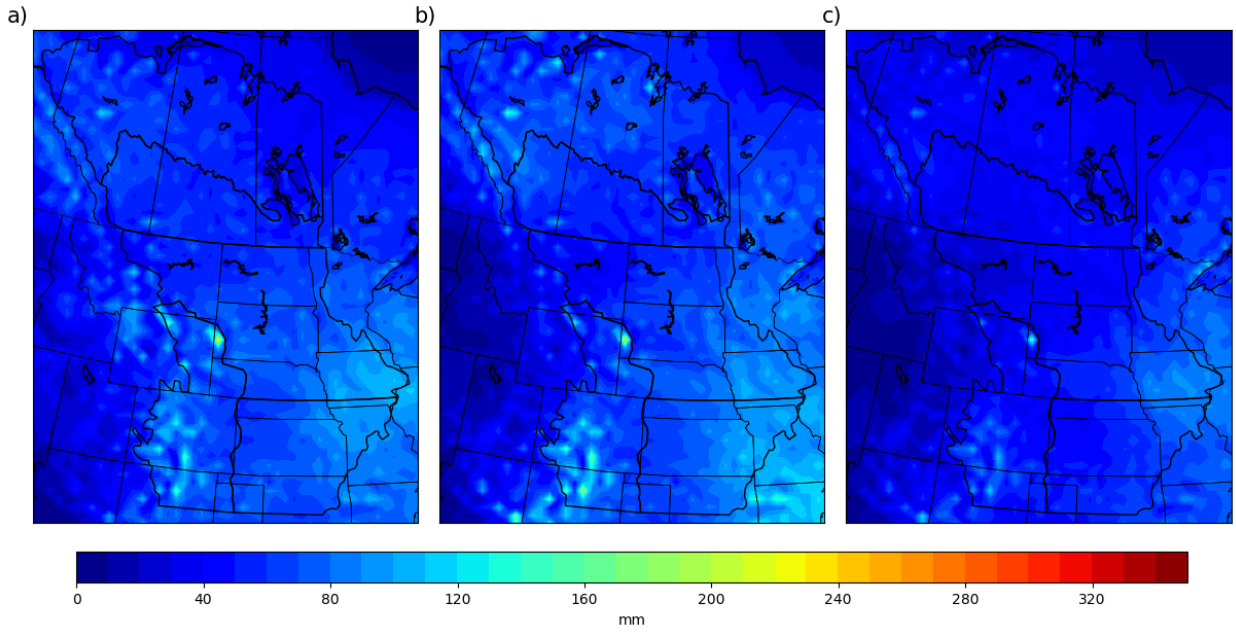

Figure B.31 Average convective precipitation for the current period for HRM3-HadCM3 for a) June b) July and c) August.

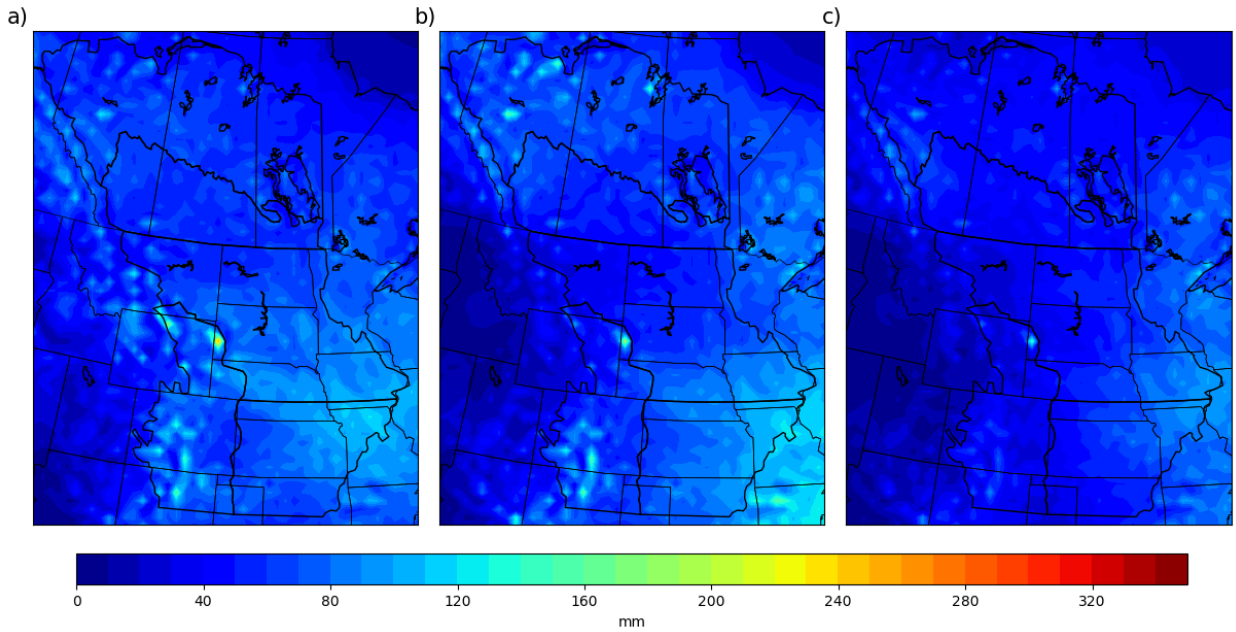

Figure B.32 Average convective precipitation for the future period for HRM3-HadCM3 for a) June b) July and c) August.